

University of Windsor

## Scholarship at UWindor

---

Electronic Theses and Dissertations

Theses, Dissertations, and Major Papers

---

2010

### MEMS based radar sensor for automotive collision avoidance

Ahmad Sinjari

*University of Windsor*

Follow this and additional works at: <https://scholar.uwindsor.ca/etd>

---

#### Recommended Citation

Sinjari, Ahmad, "MEMS based radar sensor for automotive collision avoidance" (2010). *Electronic Theses and Dissertations*. 7873.

<https://scholar.uwindsor.ca/etd/7873>

This online database contains the full-text of PhD dissertations and Masters' theses of University of Windsor students from 1954 forward. These documents are made available for personal study and research purposes only, in accordance with the Canadian Copyright Act and the Creative Commons license—CC BY-NC-ND (Attribution, Non-Commercial, No Derivative Works). Under this license, works must always be attributed to the copyright holder (original author), cannot be used for any commercial purposes, and may not be altered. Any other use would require the permission of the copyright holder. Students may inquire about withdrawing their dissertation and/or thesis from this database. For additional inquiries, please contact the repository administrator via email ([scholarship@uwindsor.ca](mailto:scholarship@uwindsor.ca)) or by telephone at 519-253-3000ext. 3208.

# **MEMS BASED RADAR SENSOR FOR AUTOMOTIVE COLLISION AVOIDANCE**

By  
Ahmad Sinjari

A Dissertation  
Submitted to the Faculty of Graduate Studies  
Through Electrical and Computer Engineering  
In Partial Fulfillment of the Requirements for  
The Degree of Doctor of Philosophy at the  
University of Windsor

Windsor, Ontario, Canada

2010

© 2010 Ahmad Sinjari



Library and Archives  
Canada

Published Heritage  
Branch

395 Wellington Street  
Ottawa ON K1A 0N4  
Canada

Bibliothèque et  
Archives Canada

Direction du  
Patrimoine de l'édition

395, rue Wellington  
Ottawa ON K1A 0N4  
Canada

*Your file Votre référence*  
ISBN: 978-0-494-81734-6  
*Our file Notre référence*  
ISBN: 978-0-494-81734-6

#### NOTICE:

The author has granted a non-exclusive license allowing Library and Archives Canada to reproduce, publish, archive, preserve, conserve, communicate to the public by telecommunication or on the Internet, loan, distribute and sell theses worldwide, for commercial or non-commercial purposes, in microform, paper, electronic and/or any other formats.

The author retains copyright ownership and moral rights in this thesis. Neither the thesis nor substantial extracts from it may be printed or otherwise reproduced without the author's permission.

#### AVIS:

L'auteur a accordé une licence non exclusive permettant à la Bibliothèque et Archives Canada de reproduire, publier, archiver, sauvegarder, conserver, transmettre au public par télécommunication ou par l'Internet, prêter, distribuer et vendre des thèses partout dans le monde, à des fins commerciales ou autres, sur support microforme, papier, électronique et/ou autres formats.

L'auteur conserve la propriété du droit d'auteur et des droits moraux qui protège cette thèse. Ni la thèse ni des extraits substantiels de celle-ci ne doivent être imprimés ou autrement reproduits sans son autorisation.

---

In compliance with the Canadian Privacy Act some supporting forms may have been removed from this thesis.

While these forms may be included in the document page count, their removal does not represent any loss of content from the thesis.

---

Conformément à la loi canadienne sur la protection de la vie privée, quelques formulaires secondaires ont été enlevés de cette thèse.

Bien que ces formulaires aient inclus dans la pagination, il n'y aura aucun contenu manquant.

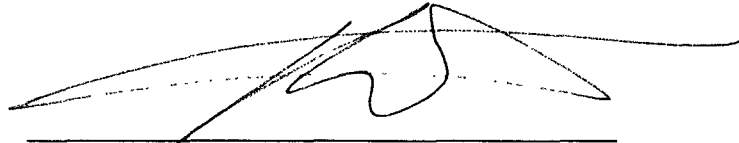
  
**Canada**

# A MEMs Based Radar Sensor For Automotive Collision Avoidance

by

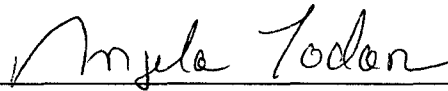
Ahmad Sinjari

APPROVED BY:

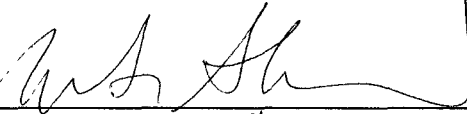


R. Mansour, External Examiner

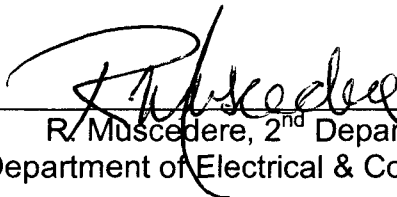
NSERC/IRC – University of Waterloo – Dept of Electrical & Computer Engineering



A. Sodan, Outside Department Reader  
School of Computer Science



E. Abdel-Raheem, 1<sup>st</sup> Departmental Reader  
Department of Electrical & Computer Engineering



R. Muscedere, 2<sup>nd</sup> Departmental Reader  
Department of Electrical & Computer Engineering



S. Chowdhury, Advisor  
Department of Electrical & Computer Engineering



S. Xu, Chair of Defense  
Faculty of Education

October 8, 2010

## **Author's Declaration of Originality**

I hereby certify that I am the sole author of this thesis and that no part of this thesis has been published or submitted for publication.

I certify that, to the best of my knowledge, my thesis does not infringe upon anyone's copyright nor violate any proprietary rights and that any ideas, techniques, quotations, or any other material from the work of other people included in my thesis, published or otherwise, are fully acknowledged in accordance with the standard referencing practices. Furthermore, to the extent that I have included copyrighted material that surpasses the bounds of fair dealing within the meaning of the Canada Copyright Act, I certify that I have obtained a written permission from the copyright owner(s) to include such material(s) in my thesis and have included copies of such copyright clearances to my appendix.

I declare that this is a true copy of my thesis, including any final revisions, as approved by my thesis committee and the Graduate Studies office, and that this thesis has not been submitted for a higher degree to any other University or Institution.

## Abstract

This dissertation presents the architecture of a new MEMS based 77 GHz frequency modulated continuous wave (FMCW) automotive long range radar sensor. The design, modeling, and fabrication of a novel MEMS based  $TE_{10}$  mode Rotman lens. MEMS based Single-pole-triple-throw (SP3T) RF switches and an inset feed type microstrip antenna array that form the core components of the newly developed radar sensor. The novel silicon based Rotman lens exploits the principle of a  $TE_{10}$  mode rectangular waveguide that enabled to realize the lens in silicon using conventional microfabrication technique with a cavity depth of 50  $\mu\text{m}$  and a footprint area to 27 mm x 36.2 mm for 77 GHz operation. The microfabricated Rotman lens replaces the conventional microelectronics based analog or digital beamformers as used in state-of-the-art automotive long range radars to results in a smaller form-factor superior performance less complex low cost radar sensor. The developed Rotman lens has 3 beam ports, 5 array ports, 6 dummy ports and HFSS simulation exhibits better than -2 dB insertion loss and better than -20 dB return loss between the beam ports and the array ports. A MEMS based 77 GHz SP3T cantilever type RF switch with conventional ground connecting bridges (GCB) has been designed, modelled, and fabricated to sequentially switch the FMCW signal among the beam ports of the Rotman lens. A new continuous ground (CG) SP3T switch has been designed and modeled that shows a 4 dB improvement in return loss, 0.5 dB improvement in insertion loss and an isolation improvement of 3.5 dB over the conventional GCB type switch. The fabrication of the CG type switch is in progress. Both the switches have a footprint area of 500  $\mu\text{m}$  x 500  $\mu\text{m}$ . An inset feed type 77 GHz microstrip antenna array has been designed, modelled, and fabricated on a Duroid 5880 substrate using a laser ablation technique. The 12 mm x 35 mm footprint area antenna array consists of 5 sub-arrays with 12 microstrip patches in each of the sub-arrays. HFSS simulation result shows a gain of 18.3 dB, efficiency of 77% and half power beam width of  $9^\circ$ .

To my parents, my wife, and my kids

## **Acknowledgements**

First and foremost I thank Allah subhanahu wa taala for his almighty support and blessing without whom this work would not have completed. I would like to acknowledge the aid and support provided by individuals and organizations. First I want to express my sincere gratitude to my supervisor, professor Sazzadur Chowdhury for his invaluable technical support, financial support, guidance, and encouragement. His appreciation of my progress was a source of continuous inspiration that helped me to make a steady progress towards the completion of this work. His encouragement to break-through the limits rather than bypass and to take care of all minute phenomenal possibilities in the design methodology, played the most significant role throughout this research work.

I would like to acknowledge the financial support and encouragement provided by the Ontario Centre of Excellence (OCE), whose interest in this research work formed the major financial support of this project. I would like to acknowledge the financial support provided by the Natural Sciences and Engineering Research Council of Canada (NSERC).

I would like to thank Ansoft Corporation of Pittsburgh PA, for the collaborative partnership that has enabled me to have access to their outstanding MEMS design environment. Thanks for the customer supporting team for their timely response in solving software related problems.

I would like to thank the crews at (CIRFE) Centre for Integrated RF engineering at the university of Waterloo and university of Western Ontario during the fabrication



process of the system, for many technical discussions and interactions that have made significant contributions in this research work.

I would like to express my deepest gratitude to my friends, peers and co-workers associated with in the MEMS group for providing a friendly, helpful and enlightened learning atmosphere.

Finally, special thanks to my wife, whose encouragement, support, and patience over the past four years are just beyond words.

# Table of Contents

Author's Declaration of Originality.....	iii
Abstract.....	iv
Dedication.....	v
Acknowledgements.....	vi
List of Tables.....	xi
List of Figures.....	xii
List of Symbols and Abbreviations.....	xv

## 1. Introduction

1.1. Goal.....	1
1.2. Research Methodolgy.....	6
1.3. Principal Results.....	7
1.4. Dissertation organization.....	9

## 2. Research Perspective

2.1. Background.....	10
2.2. Radar Basics.....	11
2.3. Pulse-Doppler vs FMCW Radar.....	16
2.4. Automotive Radar.....	17
2.5. State-of-the-Art in Automotive Radars.....	18
2.6. Beamforming in Automotive Radars.....	22
2.6.1 Analog Beamforming.....	23
2.6.2 Digital Beamforming.....	24
2.7 Rotman Lens Beamformer.....	26
2.7.1 Microstrip Rotman Lens.....	27
2.7.2 Synthesized Rotman Lens.....	28
2.7.3 Dielectric Rotman Lens.....	28
2.8 RF Switching.....	30
2.9 Antenna System.....	32
2.10The MEMS Radar.....	34

### **3. New Radar Architecture and MEMS Rotman Lens**

3.1	Architecture of MEMS Radar.....	36
3.1.1	Radar type selection.....	36
3.1.2	Frequency Selection.....	37
3.1.3.	Beamformer selection.....	38
3.1.4	Switch selection.....	38
3.1.5	Antenna Selection.....	38
3.1.6	Signal processor selection.....	38
3.1.7	New Radar Sensor Architecture.....	39
3.2	Rotman Lens Design Principles.....	40
3.3	Rotman Lens Design for Automotive Radar.....	43
3.3.1	Rotman Lens Design Methodology.....	44
3.3.2	New Approach of Rotman Lens Design.....	45
3.4	Fabrication.....	55
3.5	Conclusions.....	60

### **4 MEMS SP3T RF Switch**

4.1	MEMS RF Switch Overview.....	61
4.2	Cantilever MEMS RF Switches.....	62
4.3	Bridge MEMS RF Switches.....	63
4.4	Design of SP3T MEMS RF Switch for 77 GHz Radar.....	64
4.5	CG MEMS SP3T RF Switch.....	66
4.6	Material Selection.....	66
4.7	Mathematical Modeling.....	67
4.8	HFSS and IntelliSuite Simulation Results for Both Types of RF Switches.....	69
4.9	Fabrication.....	75
4.10	Conclusions.....	79

### **5. Microstrip Patch Antenna**

5.1	Microstrip Antenna Overview.....	80
5.2	Microstrip Antenna.....	80
5.3	Microstrip Single Patch Design.....	84

5.4 Design Requirements for Target Automotive Radar Antenna.....	88
5.5 Microstrip Antenna Array Design Considerations.....	88
5.5.1 Microstrip Antenna array Design.....	88
5.6 Microstrip Antenna Simulation Results.....	92
5.7 Microstrip Antenna Fabrication.....	94
5.7.1 Microstrip Antenna Array Fabrication Steps.....	96
5.8 Conclusions.....	98

## 6 Conclusions and Future Work

6.1 Conclusions.....	99
6.2 Future work.....	101
References.....	103
Appendices	
Appendix A: Program code for Rotman lens design.....	109
Appendix B: Program code for (SP3T) switch design .....	143
Appendix C: Release recipe for the Single pole triple through (SP3T) switch..	180
Appendix D: Program code for microstrip antenna design.....	181
VITA AUCTORIS.....	216

## **List of Tables**

Table 2.1 Road fatalities per 100,000 inhabitants.....	10
Table 2.2 Rank change order of the global burden of disease.....	11
Table 2.3 Commercially available new generation of automotive radar systems.....	20
Table 2.4 Bosch LLR3 Radar sensor features.....	20
Table 2.5 Requirements for Future Radar Systems.....	21
Table 3.1 Rotman Lens Final Design Specifications.....	55
Table 4.1 Layer Names, Thickness and Mask Level.....	67
Table 4.2 SP3T Design Specifications.....	69
Table 4.3 SP3T RF performance summar.....	74
Table 5.1 RT 5880 Specifications.....	84
Table 5.2 Microstrip Antenna Array Specifications.....	92

## List of Figures

Figure 1.1 Phased array based automotive radar.....	4
Figure 1.2 Improved version of the phased array based automotive radar.....	5
Figure 2.1 Pulse characteristics in a pulsed-radar.....	12
Figure 2.2: Transmit signal frequency for FSK-CW radar.....	13
Figure 2.3 Up sweep and down sweep signal characteristics in a FMCW radar.....	14
Figure 2.4 A car fitted with radar.....	17
Figure 2.5 Different range radar system in a vehicle.....	18
Figure 2.6 Analog beamformer with power and phase adjustment to rotate the beam....	23
Figure 2.7 Bosch LLR automotive radar.....	24
Figure 2.8 Toyota CRDL 77 GHz LRR radar sensor.....	25
Figure 2.9 Schematic of the intrinsic beamforming capability of the Rotman lens.....	26
Figure 2.10 Microstrip Rotman lens.....	27
Figure 2.11 Synthesized Rotman lens.....	28
Figure 2.12 Dielectric Rotman lens.....	29
Figure 2.13 RF-MEMS-based automotive radar front-end.....	30
Figure 2.14 MEMS cantilever type RF.....	31
Figure 2.15 Microstrip patch antenna.....	33
Figure 2.16 Microstrip antenna array.....	33
Figure 3.1 Block diagram of the new MEMS based radar sensor.....	39
Figure 3.2 Rotman lens schematic diagram.....	41
Figure 3.3 Target scanning angle.....	44
Figure 3.4 design methodology of the Rotman lens.....	45
Figure 3.5 TE <sub>10</sub> propagation mode in a rectangular waveguide.....	48
Figure 3.6 Lens contour for $\alpha=1$ , $g=1$ .....	49
Figure 3.7 Lens contour for $\alpha=2$ , $g=1$ .....	50
Figure 3.8 Lens contour for $\alpha=3$ , $g=1$ .....	50
Figure 3.9 Lens contour for $\alpha=4$ , $g=1$ .....	50
Figure 3.10 Rotman lens of 2.5 $\mu\text{m}$ thickness.....	51
Figure 3.11 Rotman lens of 10 $\mu\text{m}$ thickness.....	51
Figure 3.12 (a) Rotman lens of 50 $\mu\text{m}$ thickness excited from beam port 1.....	52

Figure 3.12 (b) Rotman lens of 50 $\mu\text{m}$ thickness excited from beam port 2.....	52
Figure 3.12 (c) Rotman lens of 50 $\mu\text{m}$ thickness excited from beam port 3.....	52
Figure 3.13 characteristic impedance of the Rotman lens.....	53
Figure 3.14 Return loss of the Rotman lens.....	53
Figure 3.15 Insertion loss between beam port 1 and array port 2.....	53
Figure 3.16 Insertion loss between beam port 1 and array port 3.....	53
Figure 3.17 Insertion loss between beam port 1 and array port 4.....	54
Figure 3.18 Insertion loss between beam port 1 and array port 5.....	54
Figure 3.19 Insertion loss between beam port 1 and array port 6.....	54
Figure 3.20 Silicon wafers immersed in the RCA solution.....	56
Figure 3.21 Rotman lens mask.....	56
Figure 3.22 Alcatel 601E Deep Silicon Etch.....	57
Figure 3.23 SEM profiles of the silicon wafers.....	57
Figure 3.24 Rotman lens Fabrication process diagram.....	58
Figure 3.25 Fabricated Rotman lens and the cap.....	59
Figure 3.26 Fabricated Rotman lens after bonding process.....	59
Figure 4.1 Cantilever MEMS RF switch.....	63
Figure 4.2 Bridge MEMS RF switch.....	63
Figure 4.3 Bias tee.....	64
Figure 4.4 Conventional MEMS SP3T RF GCB switch.....	65
Figure 4.5 HFSS simulation shows the coupling capacitance between the GCB and a CPW line of a conventional MEMS SP3T RF operating at 77 GHz.....	65
Figure 4.6 CG MEMS SP3T RF switch.....	66
Figure 4.7 Characteristic impedance (Both GCB and CG type switches).....	70
Figure 4.8 Return loss between ports 1 and 2.....	71
Figure 4.9 Insertion loss between ports 1 and 2.....	72
Figure 4.10 Isolation between ports 1 and 3.....	72
Figure 4.11 Isolation between ports 1 and 4.....	73
Figure 4.12 Cantilever collapsing simulation.....	73
Figure 4.13 Cantilever displacement simulation.....	74
Figure 4.14 Cantilever pull-in voltage simulation.....	74

Figure 4.15 Chromium deposition and patterning.....	75
Figure 4.16 Silicon Nitride deposition and patterning.....	76
Figure 4.17 Chromium and Gold deposition.....	76
Figure 4.18 Gold and chromium patterning.....	76
Figure 4.19 Anchor and dimple patterning.....	77
Figure 4.20 G2 deposition using Electron Beam Evaporation method.....	77
Figure 4.21 Pattern of the top gold G2.....	77
Figure 4.22 SP3T MEMS RF switch release.....	78
Figure 4.23 SEM pictures of the RF switch before and after release.....	78
Figure 5.1 Microstrip patch antenna.....	80
Figure 5.2 Electric field along the patch length.....	81
Figure 5.3 Microstrip patch equivalent circuit.....	83
Figure 5.4 Physical and effective length of microstrip patch.....	86
Figure 5.5 Microstrip antenna array.....	91
Figure 5.6 Microstrip antenna array return loss.....	93
Figure 5.7 Microstrip antenna array gain and half power beam width (HPBW).....	93
Figure 5.8 Antenna array gain versus frequency.....	94
Figure 5.9 Antenna array efficiency.....	94
Figure 5.10 Ultrafast laser pulses.....	95
Figure 5.11 Microstrip antenna array fabrication zones.....	96
Figure 5.12 Fabricated microstrip antenna array.....	97
Figure 5.13 SEM figures of the fabricated microstrip antenna array.....	97
Figure 6.1 MEMS Multimode radar block diagram.....	101
Figure 6.2 FPGA Reconfigurable microstrip antenna array.....	102
Figure 6.3 Operation modes of the MEMS based automotive radar.....	102



## List of Symbols and Abbreviations

$G$	On-axis focal length
$F$	Off-axis focal length
$W$	Off-axis length of the transmission path
$W_0$	On-axis length of the transmission path
$\alpha$	Scanning angle
$\eta$	Lens numerical aperture
$\lambda_0$	Wavelength of the operating frequency $f$
$c$	Velocity of light
$\varepsilon_r$	Dielectric constant
$\lambda_m$	Modified wavelength
$P_r$	Received power
$P_t$	Transmitted power
$l_a$	Array port length
$l_b$	Beam port length
$\theta_a$	Array port angle
$\theta_b$	Beam port angle
$PZT$	Lead zirconium titanium
$TE_{10}$	Transverse electric mode 10
HFSS	High frequency structure simulator
RF	Radio frequency
DRIE	Deep reactive ion etching
$E_x, E_y, E_z$	Electric field components
$H_x, H_y, H_z$	Magnetic field components
$\lambda_c$	Cut-off wavelength
$f_c$	Cut-off frequency
$Z_{TE}$	$TE_{10}$ wave characteristic impedance

$V_p$	Phase velocity
$V_g$	Group velocity
$k_c$	Propagation constant
CIRFE	Center for integrated RF engineering
UWMEMS	University of Waterloo MEMS process
SP3T	Single-Pole-Triple-Throw
FET	Field effect transistor
SPST	Single-pole-single-throw
CPW	Coplanar waveguide
$C$	Capacitance
$A$	Area
$d$	Distance
$Q$	Charge
$V$	Voltage
$k$	Beam stiffness
$E$	Young's modulus
$w$	Beam width
$t$	Beam thickness
$l$	Length of the beam
$V_p$	Pull-in voltage of the cantilever
$g_0$	zero bias gap
$\epsilon_0$	Permittivity of free space
$W$	Length of the DC pad
$C_r$	Chromium
Au	Gold
$\text{SiO}_x$	Silicon oxide
HPBW	Half power beam width
MIC's	microwave integrated circuits
FEA	Finite Element Analysis

$\tan \delta$	Dissipation factor
$f_r$	Resonance frequency
$h$	Substrate height
$L$	Patch length
$\mu_0$	Permittivity of the air
$c$	Velocity of the light
$\varepsilon_{\text{reff}}$	The effective dielectric constant
$Z_0$	Resonant input impedance
ADS	Advanced Design System
$\lambda_g$	Guided wave length

# **Chapter 1**

## **Introduction**

### **1.1 Goal**

A significant research effort is going on worldwide to develop a system that can provide collision warning to a driver, act to avoid collisions and to provide pre-crash warning to a driver in case a collision is unavoidable [1-5]. Realization of such systems requires sensors, which are able to observe the complete surrounding of cars and sophisticated signal processing algorithm to evaluate the sensor data fast and reliably. Current vehicle mounted proximity detection systems employ sensors like electromagnetic radars (short, medium and long range), lasers, vision-based sensors like video cameras; GPS based systems, and ultrasonic sensors. Out of all these systems, radar based systems offer superior performance compared to others as they work under nearly all weather conditions whereas the performance of other systems are compromised in bad weather situations [1,3]. Additionally radars are able to provide information about location (distance and angular direction) and relative velocity of objects.

However, due to high cost of stand-alone manufacturing and GaAs technology, current radar based automotive collision avoidance systems are too expensive and automakers are reluctant to incorporate these solutions in low-end vehicles. As a result the overall highway safety situation remains almost the same even if some of the vehicles are equipped with advanced radar systems. To put the problem in perspective, less than 1% of vehicles running in Canadian highways are equipped with radar sensors.

MEMS technology enables to create high performance microscale devices that could be batch fabricated using microfabrication techniques like conventional VLSI chips. The resulting microscale devices exhibit superior performance compared to their counterparts in terms of performance, reliability, system level integration, and overall cost. The advantage of higher performance and miniaturization coupled with low cost batch fabrication will enable to use these devices to realize an affordable but superior small form-factor radar sensor that can be used in collision avoidance and pre-crash warning systems. Instead of using electronically scanning phased array principle as employed by

state-of-the-art automotive radars, MEMS based radio frequency (RF) components such as Rotman lens, RF switches, antennas, filters, etc. can be used to realize a high performance smaller size radar that can be mass produced cost-effectively due to the batch fabrication capability. As the Rotman lens that exploits the physical geometry of a cavity to realize a directional beam without any signal processing, a microfabricated Rotman lens can eliminate the use of conventional microelectronic beamforming to minimize the latency time and integration issues while improving system reliability and thermal management situations. Similarly, MEMS based RF switches can be used to route the signal among different components of the radar sensor with a much superior performance in terms of return loss, insertion loss and isolation compared to microelectronic microwave switches.

The basic idea is to minimize and replace conventional microelectronic components in a typical radar sensor by superior performance but low cost MEMS based components to realize a compact small form-factor cost effective high performance radar sensor that will have much higher penetration rate in the automotive market, and consequently will help to minimize life losses and property damage due to automotive collisions. Consequently, the overall highway safety situation will be dramatically improved. In this context, the overall goal of this dissertation is to develop a radar architecture using MEMS based Rotman lens and RF switches and design and fabricate the MEMS based RF components and a microstrip antenna array that can be used to realize the developed radar architecture.

Market research firm Strategy Analytics predicts that over the period 2006 to 2011, the use of long-range distance warning systems in cars could increase by more than 65 percent annually, with demand reaching 3 million units in 2011, with 2.3 million of them using radar sensors. By 2014, 7 percent of all new cars will include a distance warning system, primarily in Europe and in Japan [6].

Global auto industries and governments are extensively pursuing radar based proximity detection systems for 1) ACC support with Stop & Go functionality, (2) collision warning, (3) pre-crash warning, (4) blind spot monitoring, (5) parking aid (forward and reverse), (6) lane change assistant, and (7) rear crash collision warning. The European Commission (EC) has set an ambitious target to reduce road deaths by 50% by

the end of 2010. German government formed a consortium called KOKON (which is a consortium of semiconductor manufacturers Infineon and Atmel, the automotive sensor suppliers Bosch and Continental Automotive Systems, and the car manufacturer Daimler-Chrysler that are supported by several universities and institutes) to develop 77/79 GHz radar systems and their components for automotive safety applications. The objective of the project is to develop cost effective short range radar (SRR) and long range radars (LRR) in order to achieve a higher market penetration of life-saving safety systems. Similar research initiative like IVBSS, VII, VSC-2 are being pursued vigorously in the US by the Department of transportation (DOT) and in Japan where forward collision warning system for vehicles using a long range radar has been identified as a most critical component for highway safety. However, due to the high price of the radar sensor based ranging systems, only the expensive vehicles (less than 1%) in Canadian highways are equipped with long range radars. As an outcome of the KOKON project, Infineon developed a SiGe based 77 GHz radar chip set and is expecting that the new SiGe based chip will be able to lower the price tag of automotive long range radar.

The development of both European and North American automotive radar technology is relying on the 76-81 GHz frequency range as this range of frequency enables to fabricate smaller radars and offers better performance compared to 24 GHz solutions.

The general trend of all these automotive radar systems is that 76-81 GHz frequency modulated continuous wave (FMCW) radars based on phased array principle with beamforming and beam steering capability are replacing the pulsed-Doppler radars that were first introduced in vehicles in the 90s. Another trend is to develop SiGe based chipsets to realize radar front end (transceiver, receiver and mixers) that will be cost effective as compared to GaAs based discrete or integrated components. Though, a SiGe based radar front-end chipset will lower the price of automotive radars to some degree, the price reduction isn't sufficient to enable a radar in all the vehicles as a standard item like the air-conditioner, the antenna system is still discrete, and resolution range and distance measurement isn't adequate for some cases [7]. Additionally, though the phased array based radar has become the current technology of choice, the time necessary to form a beam using analog or digital microelectronics based beamforming engines becomes a critical issue if real-time implementation is necessary.

The basic architecture of automotive radar working on the phased array principle is shown in figure 1.1.

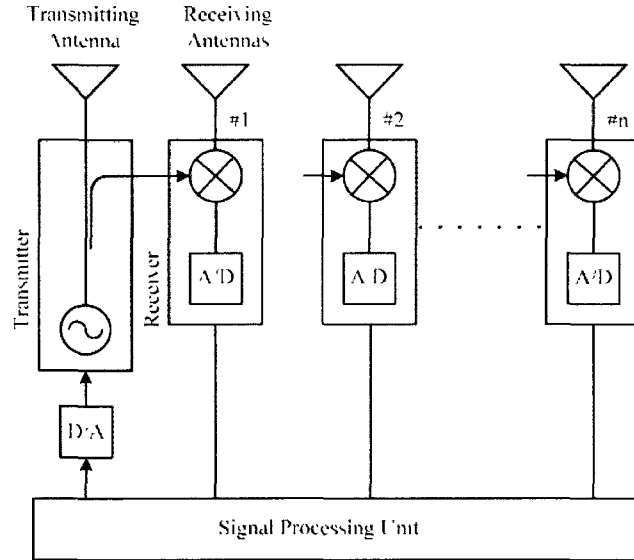


Figure 1.1 Phased array based automotive radar

This system consists of a transmitting antenna and several receiving antennas placed along a line at equal intervals. Each receiving antenna is connected to an independent receiver. To these receivers, a local signal separated from the transmitter signal is supplied. The transmitted wave reflected by the object is received by the receiving antennas. The receiver produces a baseband signal generated by synchronous detection. After A-D conversion, the baseband signal is input to the signal processing unit, where the direction of arrival of the received wave is estimated. Based on this configuration, the direction resolution obtained by ESPRIT is evaluated by numerical simulation. An implementation of such radar uses 9 receiving antennas. The problem with this implementation is if the phase delay of one of the receivers is different from those in the other receivers, the accuracy and resolution of angle detection by the super resolution method are degraded. Also there is a risk that the phase delays of nine receivers may fluctuate as a result of temperature variations. Further, the cost is increased because the feed network of the local signal and nine receivers are needed.

An improved version of the basic architecture is shown in figure 1.2 where two single-pole-triple-throw (SP3T) switches have been used to multiplex three transmit and three receive channels to minimize the number of antennas from 10 to 6 and the number of receivers from 9 to 1. A control circuit switches the 3 equal transmitting antennas and 3 receiving Antennas using the SP3T switches to result in one base band channel, and, after demultiplexing in the digital domain, nine digital receiver channels are obtained for digital beamforming. However, due to the transmission loss in the switches, the SNR is degraded and the angular resolution may be decreased.

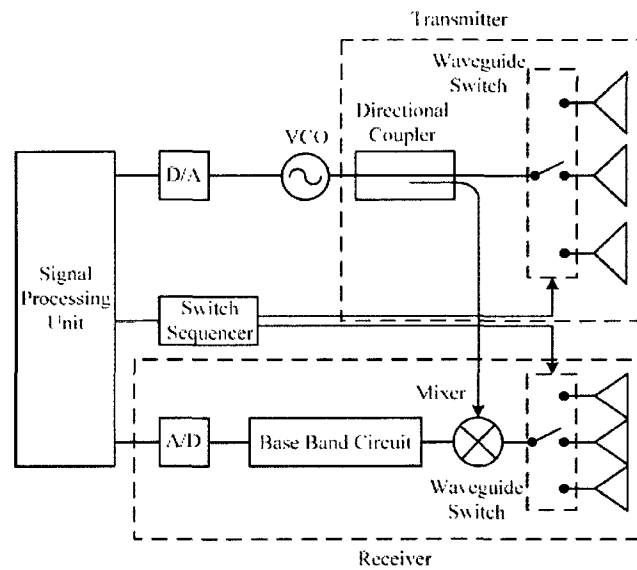


Figure 1.2 Improved version of the phased array based automotive radar

Investigation shows that the limitations associated with both the systems can be overcome or minimized if the beamforming operation is shifted from electronic domain to a passive microfabricated Rotman lens beamformer. This will drastically reduce the system complexity, processing time, system integration, and thermal drift issues. Additionally, if the waveguide switches are being replaced by MEMS based RF switches that exhibit superior performance as compared to the waveguide ones, a highly improved radar sensor can be realized. The MEMS based radar sensor can be commercialized at a much lower cost due to the batch fabrication capability of the MEMS components.

Obviously, the current microstrip or dielectric waveguide based Rotman lens are large enough to be fabricated using the microfabrication technology and not suitable to realize the target small form-factor 77 GHz radar. Design of MEMS RF switches are also



needs to be optimized for 77 GHz to minimize the losses. As the radiating elements, high performance microstrip antenna arrays are also needed to be designed.

In summary this dissertation investigates the development of a MEMS based radar. The specific goals of this research are thus summarized as:

1. Develop the architecture of a MEMS based 77 GHz FMCW long range radar sensor for automotive collision avoidance application. Due to the passive nature, true time delay, and high reliability characteristics of the target MEMS Rotman lens, high performance MEMS RF switches and a high gain high efficiency microstrip patch antenna array, a relatively enhanced cycle time can be achieved as compared to current state-of-the-art systems, and with appropriate off-the-shelf radar front end, the target system would offer a highly compact higher performance small form factor radar solution for automotive applications.
2. Investigate to develop a small size Rotman lens for the target radar sensor that can be microfabricated using standard microfabrication techniques such as deep reactive ion etching (DRIE). Carry out the design and simulation of the developed Rotman lens for performance evaluation using industry standard software such as HFSS, ADS, and Intellisuite.
3. Develop and realize a fabrication process sequence to fabricate the Rotman lens.
4. Design, simulate and fabricate a MEMS based SP3T switch operating in the 77 GHz range for use in the target radar sensor.
5. Design, simulate and fabricate a 77 GHz microstrip antenna array for use in the target radar sensor

It is to be mentioned here that two other groups of students in the University of Windsor MEMS lab are working on the packaging and FPGA implementation of the signal processing algorithm to realize the complete radar sensor.

## **1.2 Research Methodology**

The course of developing a MEMS-based 77 GHz radar sensor involves the following steps:

1. An extensive review of existing automotive radar sensors will be performed to determine the state-of-the-art in automotive radar sensors and industry set specifications of the future long range radars.

2. Develop the architecture of a new MEMS based radar sensor to meet or overcome the industry set specifications for a future automotive long range radar.
3. Investigate the state-of-the-art in Rotman lens technology to design and develop a new 77 GHz MEMS based Rotman lens.
4. Investigate the state-of-the-art in MEMS based RF switches and microstrip antenna arrays to develop and design MEMS switches and an antenna array suitable for use in the target radar sensor.
5. Simulation of the designed MEMS devices using HFSS, ADS and IntelliSuite software for performance evaluation.
6. Optimization of the devices to yield maximum performance considering the design constraints.
7. Devices fabrication.

### **1.3 Principal Results**

The principle results of this research work are summarized as follows:

1. The architecture of new MEMS based 77 GHz long range radar has been developed for automotive collision avoidance application. A provisional patent (US 61/282,595, March 5, 2010) has been filed in the US patent Office. The radar has a form factor of 40 mm x 30 mm x 10 mm after packaging, which is smaller than the state-of-the-art Bosch 3rd generation long range radar LRR3 that has dimensions of 77 mm x 74 mm x 58 mm. The new radar architecture has been evaluated by Keith Warble, an industry expert in radar technology who commented that “The device is superior in architecture and can out-perform the current industry leading state-of-the-art Bosch/Infineon LRR3 (3rd generation long range radar) in performance and cost”.
2. Novel MEMS based TE<sub>10</sub> mode 77 GHz Rotman lens has been designed and fabricated using deep reactive ion etching and thermo-compression bonding of two 500  $\mu$ m thick silicon wafers. The lens has 3 beam ports, 5 array ports, 6 dummy ports, and has a footprint area of 27 mm x 36.2 mm. The Rotman lens has

a cavity depth of 50  $\mu\text{m}$  with a footprint area of 11 mm x 14 mm. The lens has been simulated using HFSS and exhibits better than -2 dB insertion loss and better than -20 dB return loss between the beam ports and the array ports. The lens can steer a beam by  $\pm 4$  degrees.

3. Two types of MEMS based single-pole-triple-throw (SP3T) cantilever type RF switches were designed and fabricated. One of them uses ground connecting bridges (GCB) to connect the ground associated with different ports while the other uses a novel continuous ground (CG) geometry. The CG configuration SP3T switch has improved the switch performance by eliminating the coupling capacitance between the ports and ground connecting bridges. Both the switches have a footprint area of 500  $\mu\text{m}$  x 500  $\mu\text{m}$ . The GCB type switch has been fabricated using the UWMEMS process in the University of Waterloo while the fabrication of the CG type switch is in progress. The GCB type switch exhibits a return loss of -16 dB. Insertion loss of -1.1 dB and maximum isolation of -13 dB between input and the non-actuated output ports. The CG type switch exhibits a return loss of -20 dB. Insertion loss of -0.65 dB and maximum isolation of -16.5 dB between input and the non-actuated output ports. The S-parameter values are better than the measured values of a cantilever type MEMS RF switch published in [36]. This validates the design of both types of switches. In summary, the CG configuration has improved the return loss by 4 dB compared with the GCB version of the switch. The insertion loss has improved by 0.5 dB and the isolation has been improved by 3.5 dB.
4. An inset feed type 77 GHz microstrip antenna array has been designed and fabricated on a Duroid RT5880 substrate. The 12 mm x 35 mm footprint area antenna array consists of 5 sub-arrays with 12 microstrip patches in each of the sub-arrays. HFSS simulation result shows a gain of 18.3 dB, efficiency of 77% and half power beam width of  $9^\circ$ . The antenna array has been fabricated in the Clark MXR facilities in Dexter Michigan using the PCB and laser ablation techniques.

## 1.4 Dissertation organization

Chapter 2 of this dissertation will cover the literature review of the automotive radar.

Chapter 3 presents the architecture of the new MEMS based 77 GHz FMCW radar sensor and design, simulation and fabrication of a novel MEMS Rotman lens, that propagate  $TE_{10}$  mode only. The air-cavity Rotman lens forms the core beamforming and beam steering component of the new radar sensor.

Chapter 4 will cover design and fabrication of a MEMS Single-Pole-Triple-Throw (SP3T) RF switch to sequentially feed the FMCW signal among the beam ports of a microfabricated Rotman lens that forms an integral part of a MEMS based 77 GHz automotive radar sensor. The series type MEMS RF switch relies on electrostatic actuation of a microfabricated cantilever beam and incorporates 1 input port and 3 output ports. Two different versions of the MEMS RF switch have been designed: a ground connecting bridge (GCB) conventional geometry where microfabricated bridges have been used to provide the ground connectivity and a new continuous ground (CG) without any bridge. Both the switches have been optimized for operation in the 77 GHz; however, the CG version provides improved performance as it eliminates the effects of coupling capacitance between the ports and the ground.

Chapter 5 describe the design, simulation and fabrication of a microstrip antenna array that forms an integral part of a MEMS based radar working in the 77 GHz range. The microstrip antenna array incorporates 5 sub-arrays and 12 patches in each sub-array. The design is based on a serial array inset fed method.

Chapter 6 outline the conclusions and elaborate the future research work that could be carried out.

## Chapter 2

### Research Perspective

#### 2.1 Background

Car accidents claim the lives of 1.2 million annually and 52 million injuries globally up to the (WHO) world health organization latest statistics. Car accidents claim a life every 15 minutes in the U.S. Nevertheless, one-third of all accidental deaths in the U.S. per year still involve cars. In North America alone the rate of fatalities related to road accidents has been stagnant at approximately 43,000 per year, which sums to a huge annual loss of life and property [8]. Table 2.1 shows the road fatality rates in selected countries or areas

Table 2.1 Road fatalities per 100,000 inhabitants

Country or area	Per 100,000 inhabitants
Australia	9.5
European Union	11.0
Great Britain	5.9
Japan	8.2
Netherlands	6.8
Sweden	6.7
United States of America	15.2

Table 2.2 [8] shows the change in rank order for the 10 leading causes of the global burden of disease for the years of 1990 and 2020. It shows the rank of the road traffic injuries has been changed from 9 to 3, which means a serious research have to be done to make the roads more safe.

Table 2.2 Rank change order of the global burden of disease

1990		2020	
Rank	Disease or injury	Rank	Disease or injury
1	Lower respiratory infections	1	Ischemic heart disease
2	Diarrheal diseases	2	Unipolar major depression
3	Prenatal conditions	3	<b>Road traffic injuries</b>
4	Unipolar major depression	4	Cerebrovascular disease
5	Ischemic heart disease	5	Chronic obstructive pulmonary disease
6	Cerebrovascular disease	6	Lower respiratory infections
7	Tuberculosis	7	Tuberculosis
8	Measles	8	War
9	<b>Road traffic injuries</b>	9	Diarrheal diseases
10	Congenital abnormalities	10	HIV

Canada and USA have set a target to reduce road traffic fatalities by 30% and 20% respectively by the end of 2010. The use of Forward Collision Warning long range radar and Lane Departure Warning camera-based sensor among other security features will become very effective to reduce road fatality rates.

## 2.2 Radar Basics

The history of radar starts with experiments by Heinrich Hertz in the late 19th century that showed that radio waves were reflected by metallic objects. This possibility was suggested in James Clerk Maxwell's seminar work on electromagnetism [8]. However, it was not until the early 20th century that systems able to use these principles were becoming widely available, and it was German engineer Christian Huelsmeyer who first used them to build simple ship detection device intended to help avoid collisions in fog [8].

The name radar comes from the acronym RADAR (Radio Detection and Ranging), coined in 1940 by the U.S. Navy for public reference to their highly classified work in Radio Detection and Ranging [9]. Thus, a true radar system must both detect and provide

range (distance) information for a target. Before 1934, no single system gave this performance; some systems were Omni-directional and provided ranging information, while others provided rough directional information but not range. A key development was the use of pulses that were timed to provide ranging, which were sent from large antennas that provided accurate directional information. Combining the two allowed for accurate plotting of targets.

Radar systems can be classified by two major types: Pulsed and Continuous Wave [10]. Both implementations have distinct operating principle, transmit signal generation, receive signal conditioning and processing, control and synchronization issues, and power requirements.

**Pulsed Radar:** Pulsed radars send short-duration in the range of a few hundred nanoseconds, high-power (typically in kilowatts range) pulses which illuminate a target in the line-of-sight. A pulse is essentially a sinusoid (carrier wave) at the chosen operating frequency as shown in figure 2.1.

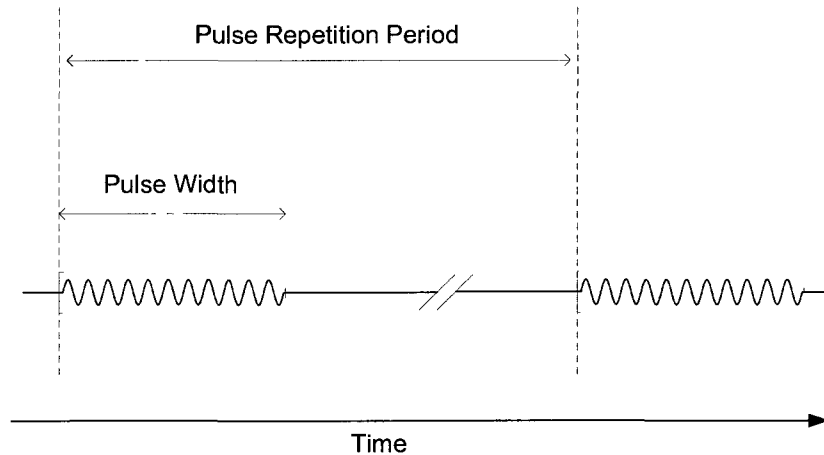


Figure 2.1 Pulse characteristics in a pulsed-radar.

In Pulsed radar the range and relative velocity of the target are determined as follows:

Range, 
$$r = \frac{c \times T_{\text{two-way}}}{2} \quad (2.1)$$

Relative velocity, 
$$v_{\text{rel}} = \frac{-f_d \times \lambda_0}{2} \quad (2.2)$$

Here,  $c$  is the speed of electromagnetic radiation in air,  $T_{\text{two-way}}$  is the two-way travel time for a pulse reflected from the target to return to the source,  $f_d$  is the Doppler shift and  $\lambda_0$  is the operating wavelength.

The Doppler shift in the carrier wave frequency within the pulse corresponds to the relative velocity of the target, and the time taken for the radar to detect a return of the pulse determines the range of the target.

**Continuous Wave Radar:** Continuous Wave (CW) radars continuously transmit the RF wave at a pre-specified frequency at a lower power level (typically less than 50mW). The CW radar systems continuously receive the echo from a target over a period of time, commonly called the Coherent Processing Interval (CPI). During the CPI, the instantaneous transmit and receive signals are mixed, and the resultant intermediate frequency (IF) signal is assessed over the CPI for valid targets. The CW radar technology is still under constant refinement with new strategies related to both hardware and signal processing algorithms being developed. There are two prime implementations of CW radar, FSK-CW (Frequency Shift Keying) radar and FMCW (Frequency Modulated) radar. In FSK-CW the RF frequency jumps between multiple frequencies over a CPI, whereas FMCW makes use of a frequency chirp in a sine, saw-tooth or triangular fashion [66]. The transmit waveforms for both CW radar types are shown in Figure 2.2.

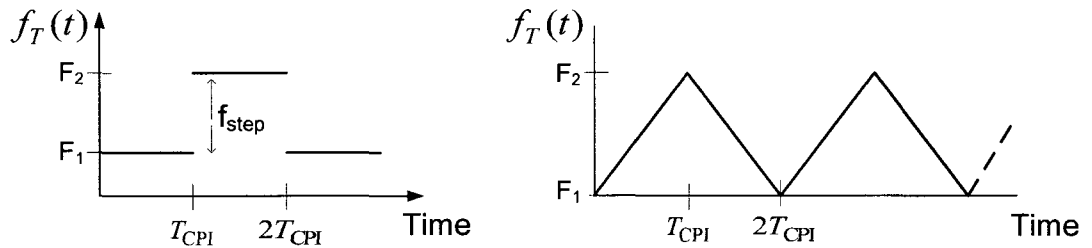


Figure 2.2: Transmit signal frequency for FSK-CW radar (left) and triangular FMCW radar (right) linear frequency up and down sweeps (or chirps).

The target range in FSK-CW radar can be determined as following:

$$r = \frac{c\Delta\Phi}{4\pi(F_2 - F_1)} \quad (2.3)$$

And, the relative velocity can be determined following



$$v_{\text{rel}} = \frac{-f_d \times \lambda_0}{2} \quad (2.4)$$

Where,  $c$  is the speed of electromagnetic radiation in air,  $\Delta\Phi$  is the difference in phase shift at the two frequencies  $F_1$  and  $F_2$ ,  $f_d$  is the Doppler shift and  $\lambda_0$  is the operating wavelength. The main disadvantage of the FSK-CW radar is that it can not detect targets in the direct path of the radar.

The up sweep and down sweep signal characteristics in a FMCW radar is shown in figure 2.3, the beat frequency for the up and down sweeps is different due to a change in range of a moving target. If the target is stationary relative to the radar, both up and down sweep beat frequencies will be the same. In the figure 2.3,  $B$  is the chirp bandwidth and  $T$  is the chirp duration.

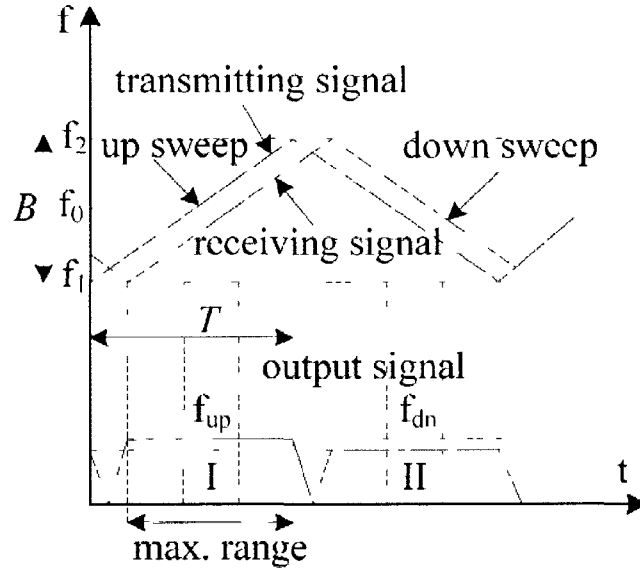


Figure 2.3 Up sweep and down sweep signal characteristics in a FMCW radar.

The range and velocity in FMCW radar can be calculated in the following manner:

For relatively stationary target, transmitted radar signal:

$$s(t) = \exp\left(j2\pi\left(f_T t + \frac{1}{2}kt^2\right)\right) \quad (2.5)$$

Where  $\tau$  = Round trip delay time =  $2R/c$

$k$ =Rate of change of frequency= $B/T$

Received signal:

$$r(t) = \exp\left(j2\pi\left(f_r(t-\tau) + \frac{1}{2}k(t-\tau)^2\right)\right) \quad (2.6)$$

Mixing (2.5) and (2.6) results in:

$$IF(t) = \exp\left(j2\pi\left(f_r\tau + kt\tau - \frac{1}{2}k\tau^2\right)\right) \quad (2.7)$$

Differentiate the phase in (2.7) with respect to time to get instantaneous frequency:

$$f_{up} = k\tau = k(2R/c) \quad (2.8)$$

For a moving target, with velocity  $v_r$  relative to the radar and assuming  $\tau_0$  is round trip time, following the same methodology as the stationary target, after mixing:

$$IF(t) = \exp\left(j2\pi\left(f_r\tau_0 + \left(k\tau_0 + 2f_r\frac{v_r}{c} - 2k\tau_0\frac{v_r}{c}\right)t - \frac{1}{2}k\tau_0^2 + 2\frac{k}{c}\left(v_r - \frac{v_r^2}{c}\right)t^2\right)\right) \quad (2.9)$$

Differentiate the phase of (2.9) signal with respect to time:

$$f_{up} = k\tau_0 + 2f_r\frac{v_r}{c} = k\tau_0 + f_d \quad (2.10)$$

Similar analysis with the “down sweep” gives the result:

$$f_{down} = k\tau_0 - f_d \quad (2.11)$$

Combining (2.9) and (2.10), we can extract the Doppler frequency shift and the frequency shift due to distance to the target as:

$$f_d = \frac{f_{up} - f_{down}}{2} \quad (2.12)$$

$$f_r = \frac{f_{up} + f_{down}}{2} \quad (2.13)$$

From  $f_r$  the range  $R$  can be estimated as

$$R = \frac{cT}{4} \left( \frac{f_{up} + f_{down}}{B} \right) \quad (2.14)$$

And from  $f_d$  the relative velocity  $v_r$  can be obtained as

$$v_r = \frac{c}{2} \left( \frac{f_{up} - f_{down}}{f_0} \right) \quad (2.15)$$

### 2.3 Pulse-Doppler vs FMCW Radar

FMCW radar can provide an accurate range measurement. It is also possible to measure the range of a single target by comparing the phase difference between two or more FMCW frequencies [9]. Range measurement with FMCW waveforms has been widely employed, as in aircraft radar altimeters and surveying instruments. Weather robustness of the FMCW radar options versus the mass, volume, power, and heat shield blowout the Doppler radar features. The FMCW Radar is the lowest risk option based on a better technological understanding of the design and its shorter development timeline. Furthermore, it provides the weather robustness of a radar

Low cost and short range detection/localization of the FMCW radars arouse a growing interest for civil and military applications such as automotive anti-collision radars or target detection devices [10]. This field of application is principally devoted to FMCW radars, which allow a direct range measurement, but are less expensive.

Some of the earlier automotive radar applications relied on a high-power Pulsed Doppler radar technique, but the suitability of the technique came under criticism after the televised failure of the Mercedes-Benz pulsed radar assisted Distronic cruise control system on Stern TV in 2005 [11]. This has instigated the industry to study and use the FMCW radar technique for modern radar systems. FMCW radar in automotive applications is still a developing field of study, with on-going research at all system levels including signal processing and RF hardware design.

The advantages of the FMCW radar can be summarized as:

- No lower theoretical limit to range resolution.
- Less affected by clutter.

- Lower power rating than Pulse radar; e.g. 100ns pulse width with 2kW peak power, whereas 77 GHz continuous wave can operate with as low as 20mW to same range.
- Typically, energy used by Pulse radar systems is 2.0-4.0J, whereas for CW radar it is 1.2J-2.0J.

## 2.4 Automotive Radar

The first patent of radar application on car was claimed by Christian Huelsmeyer in a German Patent on April 30, 1904. In the 70's, more intensive automotive radar developments started at microwave frequencies. A car fitted with radar in 1974 is shown in figure 2.4.

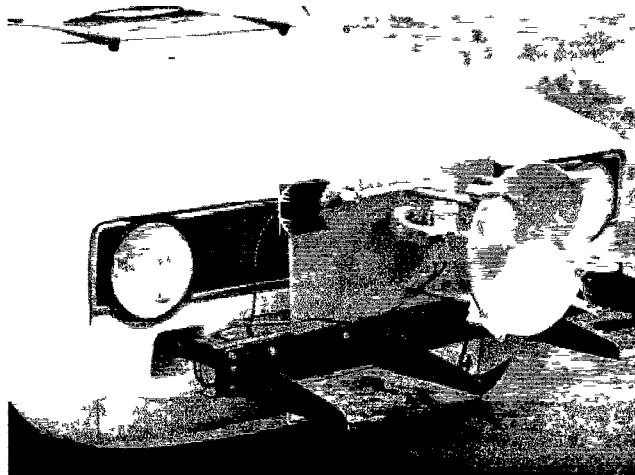


Figure 2.4 A car fitted with radar [54].

The activities of the following decades were mainly concentrated on developments at 24 GHz, 49 GHz, 60 GHz, and 77 GHz [8]. The key driver of all these investigations has been the idea of collision avoidance to save lives and minimize property damage. This motivated for many engineers and scientists all over the world to develop smart vehicular radar units. During this quite long period a lot of know-how has been gained in the field of microwaves and in radar signal processing. Following the course, the commercialization of automotive radar became feasible in the 90's.

Competing technologies in vehicular surround sensing and surveillance are ultrasonic's, lasers and video cameras. Car manufacturers and suppliers are developing optimized sensor configurations for comfort and safety functions with respect to functionality, robustness, reliability and dependence on adverse weather conditions. The total system costs have to meet the marketing targets to be attractive for the end customers. First applications with surround sensing technologies were parking aid (based on ultrasonic's), collision warning, and Adaptive Cruise Control (ACC).

## 2.5 State-of-the-Art in Automotive Radars

First commercialization of the automotive radars started at late 90's. European and US companies have been focused mainly on radar based ACC. Figure 2.5 shows the automotive radar application portfolio, which has set an industry-wide standard for radar systems. It has been identified that different capability radar technology can be used for Long range radar (LRR) for ACC, medium range (MRR), short range (SRR) for stop and go, parking aid, blind spot detection, back up, and lane change support to realize a comprehensive collision avoidance, pre-crash warning, and collision mitigation system by establishing a safety shell around the vehicle as shown in Figure 2.5 below.

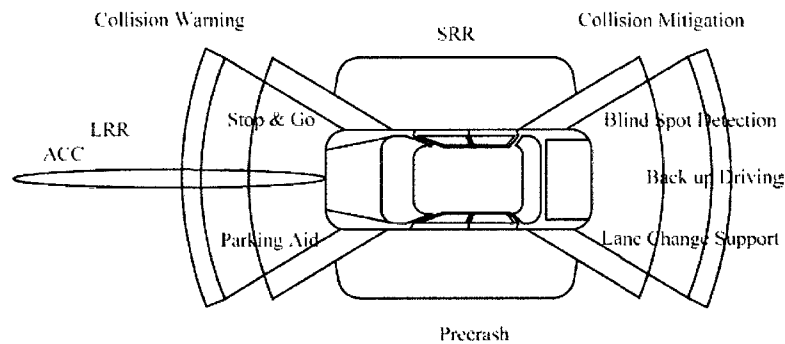


Figure 2.5 Different range radar system in a vehicle [53].

In 1999, Mercedes introduced the 77 GHz “Distronic” into the S class (500 and up) [12]. Other premium models equipped optionally with an ACC, such as BMW 7 series, Jaguar (XKR, XK6), Cadillac (STS, XLR), Audi A8, and VW Phaeton. ACC is also available in Mercedes E, CL, CLK, SL class, BMW 5 and 6 series, Audi A6, Nissan (Cima, Primera), Toyota (Harrier, Celsior), Lexus (LS, GS), and Honda (Accord, Inspire, Odyssey) [13]. European car manufacturers offer 77 GHz systems for ACC systems, their

Japanese competitors Honda and Toyota introduced an active brake assist for collision mitigation (additionally to ACC) in 2003 based on 77 GHz long range radar (LRR) technology [14]. In contrast to the only smooth deceleration capability of an ACC system (because ACC is only marketed as a comfort feature), the active brake assist provides much higher braking forces for deceleration, when a threatening situation is identified and the driver starts braking, but maybe not as strong as it would be necessary to avoid a crash.

A joint research project on “Automotive high frequency electronics – KOKON” was started in September 2004, funded by the German Ministry of Education and Research (BMBF) [15]. The consortium consists of two semiconductor companies (Atmel and Infineon), two automotive radar sensor manufacturers (Bosch and ContiTemic), and one automotive company (DaimlerChrysler) supported by institutes and universities. Silicon Germanium (SiGe) has been identified as the chip technology which may fulfill the technological requirements and the cost constraints and which might be an alternative to already existing GaAs solutions used in 77 GHz LRR systems [16]. Within the KOKON project the development of both 77 GHz LRR and 79 GHz SRR radar chip technology is investigated. As spin-off cost reduction and performance improvement of 77 GHz LRR sensors were expected.

The ROCC project essays a study of automotive radar vehicular integration and live testing, investigation of complete sensor packaging including DSP unit(s), evaluation of automotive radar beyond 100 GHz, SMD packaging of RF MMICs, feasibility study for 500 GHz UWB automotive radar based on LFM CW technique, improvement of energy efficiency and multi-mode multi-range self-calibrating sensors. The lattermost objective is currently one of the most pursued topics in automotive radar; recent self-calibrating dual-band MMICs such as those presented in [17] and [18] propose the capability of switching between 24 GHz and 77 GHz SRR, MRR and LRR using the same MMIC RF radar frontend.

Table 2.3 lists some of the commercially available automotive radar systems by different developers and their operating specifications. The AC3 by TRW Automotive is a third-generation adaptive cruise control radar operating at 77 GHz, capable of scanning targets at a distance up to 250 meters [19].

Table 2.3 Commercially available new generation of automotive radar systems [19].

Developer	Operation Frequency	Radar Type	Range (m)	Relative Velocity (km/h) <sup>1</sup>	Field of View	Refresh Time (ms) <sup>2</sup>
<b>TRW Automotive</b>	77 GHz	Pulsed Doppler	1 - 250	±220	±8°	50
<b>Delphi</b>	76 GHz	Pulsed Doppler	1 - 174	-360 to +90	±10°	50
<b>Denso</b>	77 GHz	FMCW	2 - 150	±200	±20°	50
<b>Bosch</b>	77 GHz	FMCW	0.5 - 250	-500 to +250	±30°	50

One of the most recent systems from Table 2.3 is the Bosch LRR3 which was launched in September 2009 on the Porsche Panamera 2010 model. One of the claims of Bosch LRR3 is being the world's smallest radar sensor package at 74mm x 77mm x 58mm, as it shown in tables 2.3 and 2.4.

Table 2.4 Bosch LLR3 Radar sensor features.

Frequency range	76...77 GHz
Distance	0.5...250 m
Accuracy	±0.1 m
Relative speed	-75 ...+60 m/s
Accuracy	±0.12 m/s
Vision range	
Horizontal opening angle	30 ° (-6 dB)
Vertical opening angle	5 ° (-6 dB)
Modulation	FMCW
Max. number of detected objects	32
Operating temperature	-40 °C...+85 °C
Vehicle connector	MQS 8 Pins
Cycle time (incl. auto diagnosis)	typically 80 ms
<b>Dimensions (H x W x D)</b>	<b>77 mm x 74 mm x 58 mm</b>
Weight	285 g
Power consumption typically	4 W
ISO certification	ISO 15622 Class IV sensor

The requirements for future radar systems to establish a safety shell around the vehicle as shown in figure 2.5 as identified by the industry are listed in Table 2.5. [14]

Table 2.5 Requirements for Future Radar Systems [14]

Function	Requirements Range/Velocity Field of view	Sensors, Category	Proposed Radar Principle	Proposed Carrier Frequency	Alternative Sensors	Remarks
Parking Aid	0.2...5m 0...±30km/h full vehicle width	2-4xSRR per bumper	UWB pulsed	24 GHz	Ultrasonic	100 ms cycle time
Blind Spot Surveillance	0.5...10m/0.5...40m reasonable velocity interval two lane beside vehicle	1-2xSRR or 1-2xMRR per side	FMCW/ FSK/ Pulsed	24 GHz	Video/ Laser	50ms cycle time
ACC	1m...150m reasonable velocity interval three lanes in front of vehicle in 65m	1xLRR	FMCW/ FSK/ Pulsed	77GHz	Laser	50ms cycle time
ACC plus	1m...150m/0.5...40m reasonable velocity interval three lanes in front of vehicle in 20m	1xLRR 1xMRR	FMCW/ FSK/ Pulsed	77GHz/ 24GHz	Laser	50ms cycle time Laser/Video sensor fusion reasonable
ACC plus Stop&Go	0.5m...150m/0.5...40m reasonable velocity interval three lanes in front of vehicle in 10m full vehicle width in 0.5m	1xLRR 2xMRR	FMCW/ FSK/ Pulsed	77GHz/ 24GHz	Laser	50ms cycle time Laser/Video sensor fusion reasonable
Closing Velocity Sensing	0.5m...10m/0.5...30m any velocity about 45°	1xLRR 1xMRR	FMCW/ FSK/	24GHz	None	10ms cycle time
Pre-Crash Reversible Restraints	0.5m...10m/0.5...30m any velocity full vehicle width in 0.5m	2xSRR 2xMRR	FMCW/ FSK/	24GHz	None	10ms cycle time function is add-on to line above very low false alarm rate
Pre-Crash Non-Rev. Restraints	0.5m...10m/0.5...30m any velocity full vehicle width in 0.5m	2xSRR 2xMRR	FMCW/ FSK/	24GHz	None	10ms cycle time function is add-on to line above ultra low false alarm rate laser/video sensor fusion requ.
Collision Mitigation	0.5m...150m/0.5...40m any velocity three lanes in front of vehicle in 10m full vehicle width in 0.5m	1xLRR 2xMRR	FMCW/ FSK/	77GHz/ 24GHz	None	10ms cycle time function is add-on to ACC plus ultra low false alarm rate laser/video sensor fusion requ
Collision Avoidance	0.5m...150m/0.5...40m any velocity three lanes in front of vehicle in 10m full vehicle width in 0.5m	1xLRR/ 2xMRR	FMCW/ FSK/	77GHz/ 24GHz	None	10ms cycle time function is add-on to line above ultra low false alarm rate laser/video sensor fusion requ



Though GaAs, or SiGe based MMIC are being pursued vigorously to minimize the cost and size while improving the performance of automotive radars, the auto industry is eyeing on to exploit the small cost, batch fabrication capability of the MEMS technology to realize more sophisticated radar system that can provide improved performance over the microelectronic based radars. The project goal of a European consortium SARFA has been set to utilize RF MEMS as an enabling technology for performance improvement and cost reduction of automotive radar front ends operating at 76-81 GHz. [20].

It has been determined that the radar sensors for automotive applications need to have a beamforming, and beamsteering capability to scan the target area to precisely determine the location of an obstacle, vehicle or a pedestrian, for example. Current systems employ analog or digital beamforming and beamsteering techniques that employ extensive microelectronic signal processing to realize a narrow beam that can be electronically steered to determine the position of a target.

## **2.6 Beamforming in Automotive Radars**

Beamforming is a signal processing technique used in sensor arrays for directional signal transmission or reception. Beamforming can be used for both radio and sound waves. It has found numerous applications in radar, sonar, wireless communications, radio astronomy, speech, acoustics, and biomedicine [21].

Beamforming takes advantage of interference to change the directionality of the array. When transmitting, a beamformer controls the phase and relative amplitude of the signal at each transmitter, in order to create a pattern of constructive and destructive interference in the wavefront.

When receiving, information from different sensors is combined in such a way that the expected pattern of radiation is preferentially observed. In automotive radar systems, beamforming allows a means of electronic steering of a narrow scanning beam to detect targets with higher angular resolution.

Beamforming involves both the generation of a directional pattern as well as steering of the main lobe over the azimuth and also the elevation angles. Microelectronic beamforming can be categorized into two main types:

- Analog Beamforming
- Digital Beamforming

### 2.6.1 Analog Beamforming

The general layout of an analog beamformer is illustrated in figure 2.6 that can be implemented using analog RF circuit components. A directional beam is formed at the radiating elements after the generated RF signal is phase shifted using tuned phase shifting elements and constant weights. An analog sine or triangle wave generator can be used to continuously vary the phase shifting elements, which effectively causes the beam to be steered [21].

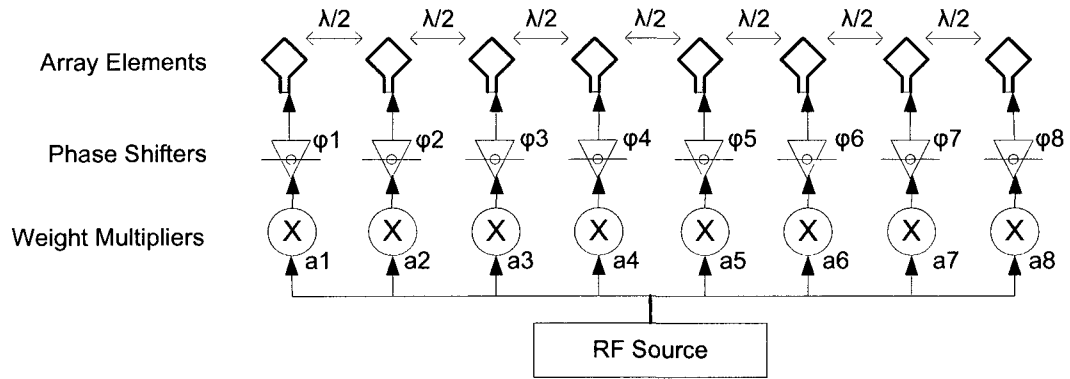


Figure 2.6 Analog beamformer with power and phase adjustment to rotate the beam.

Bosch 77 GHz LRR2 automotive radar has been developed to operate using this analog beamforming concept. Fig. 2.7 shows Bosch's LRR in its 2nd generation [13]. The system has a box size of only  $74 \times 70 \times 58 \text{ mm}^3$  (H x W x D) and contains all sensing and ACC functionality. The 77 GHz circuitry contains 4 feeding elements (polyrods) directly attached to 4 patch elements on the RF board, illuminating a dielectric lens, that results in a broad illuminating transmit beam and four single receiving beams which partially overlap in azimuth yielding a total azimuthal coverage of  $\pm 8$  degrees.

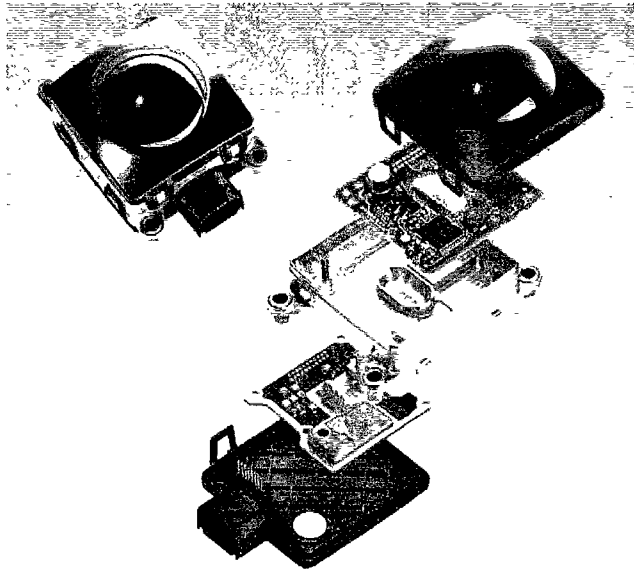


Figure 2.7 Bosch LLR automotive radar [13].

### 2.6.2 Digital Beamforming

77 GHz radar sensors with digital beamforming (DBF) front ends were introduced into the market by Toyota motor company in 2003. Denso built a bistatic LRR with planar patch antennas with a range capability up to 150m and a field of view of approx.  $\pm 10$  degrees [11].

The Toyota CRDL 77GHz LRR radar shown in Figure.2.8, switches 3 equal transmitting antennas and 3 receiving antennas resulting also in one base band channel, and, after demultiplexing in the digital domain, nine digital receiver channels for digital beamformer. Toyota claimed that they have developed a high-functionality, compact millimeter-wave radar sensor that is applicable to convenience systems and active safety systems simultaneously, but they claimed also that it will not be viable in mass production phase.

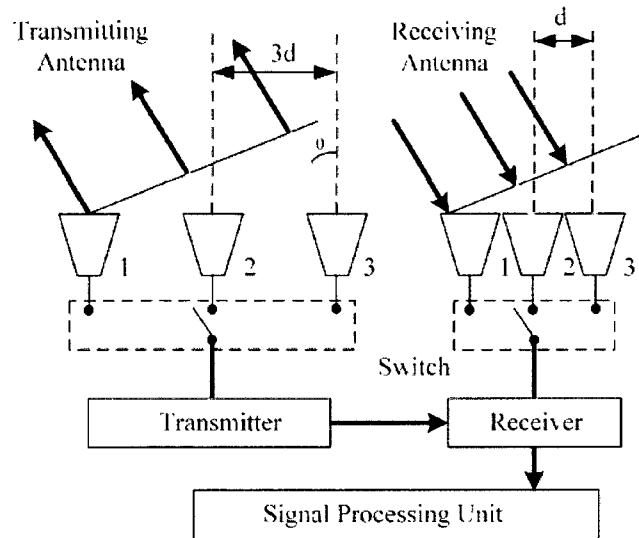


Figure 2.8 Toyota CRDL 77 GHz LRR radar sensor

Digital control circuits will replace the analog circuits to control the phase and power of the signal fed at every antenna patch, digital control offers the following advantages [21-22].

- Improved beamformer control: The phase at individual patch or sub-array level can be accurately controlled. The beam shape and size can be controlled electronically to any degree resulting in a more selective beamforming.
- Switching between multiple beams: Switching between beams of different widths by enabling or disabling array elements or generating distinct beams using separate sub-arrays.
- High precision control of phase shift and power: DSPs or FPGAs are powerful tools for high-resolution high-speed precise digital control of antenna components. These digital circuits can be used to drive high power antenna circuits with improved control and precision as compared to conventional analog implementations.

Digital beamformers require memory blocks, adders and multipliers as system building blocks. These digital components are available in high-speed on-chip resources in FPGAs which typically operate at clock frequencies of 550 MHz (e.g. Virtex 6 FPGA by Xilinx). This makes digital beamforming techniques more feasible and efficient.

Digital beamforming does require more signal conditioning prior to digital processing. If the signal frequency is too high (greater than 100 MHz, say) direct sampling is not possible. To overcome this issue, the signal needs to be down-converted to an intermediate frequency (IF) using an RF mixer which can be sampled. Various beamformer architectures are available in [21-22].

## 2.7 Rotman lens Beamformer

A Rotman lens [23] is a passive device that can enable a beamforming and beamsteering capability without any microelectronic signal processing as needed by analog or digital beamformers. During operation, the electromagnetic property of a dielectric cavity is exploited to realize a directional in-phase signal.

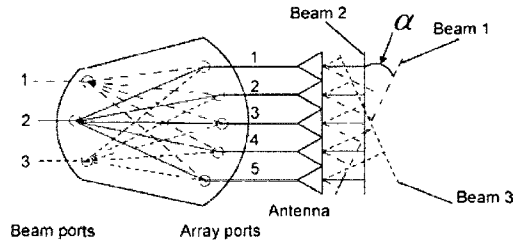


Figure 2.9 Schematic of the intrinsic beamforming capability of the Rotman lens [23].

A Rotman lens is a parallel plate architecture that has beam ports on one side and array ports on the opposite side of a dielectric material filled cavity as shown in Figure 2.9. An input signal fed at any of the beam ports travel different distances through the lens cavity to reach a pre-specified number of array ports positioned along the outer lens contour depending on the dimension of the lens cavity and the shape of the lens contours. By properly choosing the lens contours, lens cavity geometry, and the dielectric material filling the lens cavity, it is possible for the signals arriving at the array ports to add up in phase that in effect realizes a beam that is steered in a particular direction. The beam is then radiated through a suitable antenna system. For example, if a signal is incident at the beam port 2, it will produce a beam of  $0^\circ$  phase shift at the array ports (beam 2), while if a signal is incident at the port 1 or 3, it will produce a beam that is steered by an angle of  $\pm \alpha$  at the array ports shown beams 1 & 3 in the figure. Thus, by sequentially switching

the signal through the beam ports, the radiating beam from the array ports can be steered by an angle determined from the position of the beam ports. Detailed design methodology of a Rotman is presented in chapter 3. Typical Rotman lenses are large and are realized using microstrip geometries or dielectric material filled waveguides.

The Rotman Lens features a true time delay phase shift capability and removes the need for costly phase shifters to steer a beam over wide angles. The Rotman Lens has a long history in military radar, but it has also been used in communication systems. The United States Army use it in C band (4–8 GHz) up to Ka Band (27.5–31 GHz) [24], [25]. The broadband performance of Rotman Lenses meets a key need of allowing the same antenna system to serve multiple functions, thus further reducing cost, complexity, and weight. Detailed techniques to design a conventional Rotman lens are available in [24–27].

Rotman lens could be categorized as following:

### 2.7.1 Microstrip Rotman Lens

In a microstrip Rotman lens, the lens geometry is formed by etching the topside metal cladding of a wafer with a desired dielectric constant and the other side cladding serves as the ground plane. Representative designs of microstrip type Rotman lens are available in [4–7]. The layout of a 77 GHz microstrip Rotman lens that has been fabricated as a printed circuit on a dielectric substrate is shown in figure 2.10 [2].

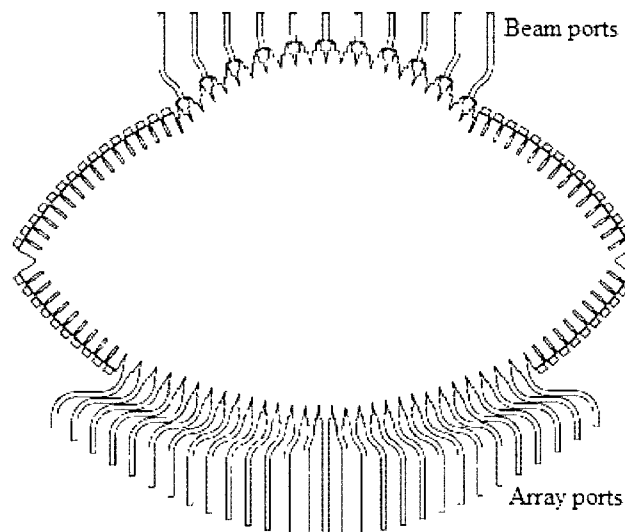


Figure 2.10 Microstrip Rotman lens [2].

Although the Rotman lens of this category has a conformal geometry, the lens suffers a high interference between the adjacent beam and array ports, mutual coupling, fringing field and is limited to low power and low beamwidth applications as only higher order modes can propagate through the lens. In this type of Rotman lens, the beamwidth usually is adjusted by combining adjacent beams to produce a broader beam with a lower gain that results in a high fabrication cost.

### 2.7.2 Synthesized Rotman Lens

In [27] a Rotman lens is presented that has dielectric contours of varying permittivity within the lens cavity. The varying permittivity is realized through a synthesized dielectric technique, where a periodic lattice of holes is formed within the dielectric substrate. The top side of the fabricated lens is shown in Figure 2.11 (a), while the bottom side is shown in Figure 2.11 (b). The region of synthesized dielectric material is placed upon a copper ground plane. The design improves the insertion loss by 1.2 dB and it is usable only up to 11 GHz. The frequency limit of 11 GHz makes this type of lens unsuitable for fabrication using typical micromachining techniques as the fabrication of the synthesized dielectric layer involves etching of quarter wavelength ( $\lambda/4$ ) deep holes of pre-specified diameters.

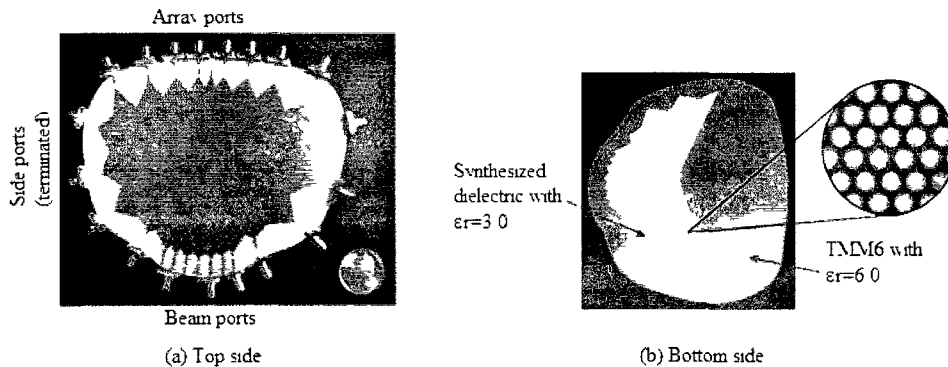


Figure 2.11 Synthesized Rotman lens.[27]

### 2.7.3 Dielectric Rotman Lens

The dielectric Rotman lens consists of a dielectric slab, tapered slot (TS) structure, and the transitions between the antipodal slots and microstrip lines [28]. The top and side views of the lens are shown in figures 2.12 (a) and (b) respectively.

The top conductor is shown in black in the lens geometry, and the bottom conductor is shown in hatched lines. A major drawback of this lens is the mutual

coupling between the adjacent ports that leads to change in the characteristic impedance seen at the port due to the presence of nearby elements which makes the impedance matching more difficult and a high drop in the power transferred from the beam ports to the array ports (lower efficiency).

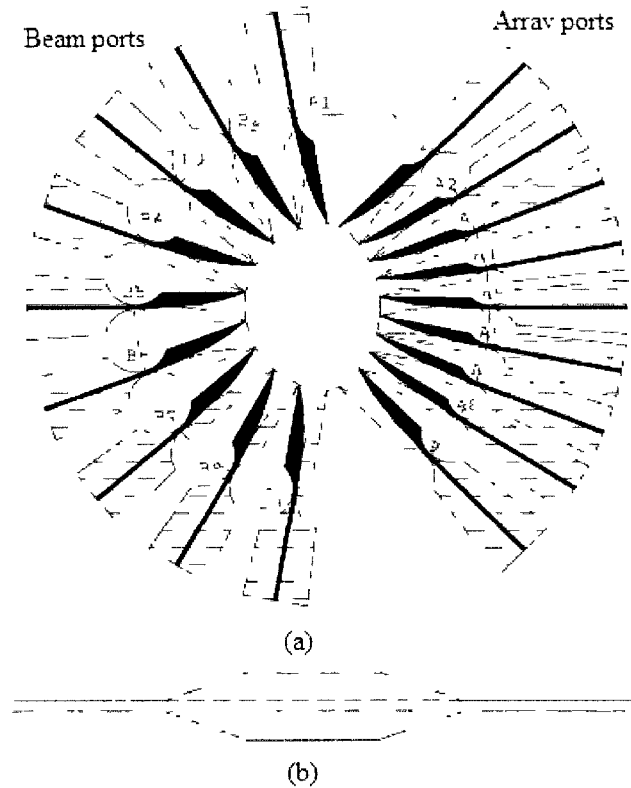


Figure 2.12 Dielectric Rotman lens (a) top view (b) side view.[28]

The above mentioned three categories of Rotman lens can't be realized using microfabrication technology to fabricate them at 77 GHz, either due to their lower efficiency and poor performance (due to interference, mutual coupling, fringing field, low beamwidth, attenuation and impedance matching) or the availability of such high thickness wafers.

The design of RF-MEMS-based automotive radar front-end based on phase shifters and Rotman lens as shown in Figure 2.13 has been presented in [29]. In the design, the beam and array ports of the low power microstrip type Rotman lens suffers a high interference due to the small distance between the ports in the operating frequency of 77 GHz.



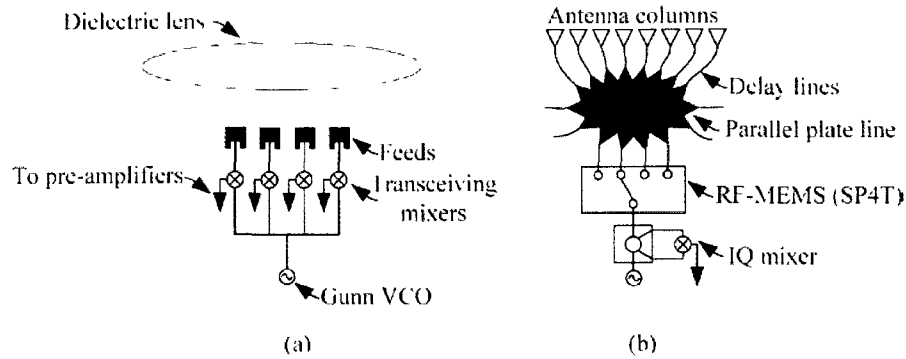


Figure 2.13 RF-MEMS-based automotive radar front-end.[29]

## 2.8 RF Switching

Switching signals between ports is a critical function in many microwave systems such as radars, communications links, and electronically scanned antennas. In a radar, the RF signal (pulse, FSK-CW or FMCW) needs to be fed to a beamforming and beamsteering networks and the output of the beamforming and beamsteering networking needs to be fed to an antenna system to radiate the signal. Similarly, the echoed RF signal reflected back from the target also needs to be switched to generate a signal that can be processed using microelectronic signal processing techniques to obtain the range, angle, and velocity information of the target. In such an operation, the switch's insertion loss adds directly to receiver noise figure and reduces transmitter power. Thus, low insertion loss is an important requirement for switches to be used in a radar system. Isolation is another very important parameter that quantifies the leakage from an "ON" to an "OFF" port.

Advances in silicon-based processing technology in the last few decades resulted in a rapid improvement in semiconductor based solid-state microwave switches. However, for high frequency RF applications, these fast-acting solid-state switches continue to have disadvantages such as low power handling capacity, high resistive losses, higher insertion loss, relatively higher DC power consumption, and poor isolation. Electromechanical switches, in contrast, are high power devices, but useful only at lower RF frequencies, and operate at a much slower speed. On the other hand, heavy and bulky waveguide type switches are not attractive to realize compact small form-factor switches to realize low cost high performance automotive radars.

Advances in MEMS technology enabled to realize low cost high performance micromechanical RF switches that exhibit low resistive loss, negligible power consumption, good isolation and high power handling capability compared with semiconductor switches. Additionally MEMS RF switches can be batch fabricated and easily integrated with the semiconductor drive and control circuits. Furthermore, being smaller, lighter, faster and less power consuming, the MEMS RF switches and relays have a high off-state to on-state impedance ratio. These improved performance characteristics of MEMS RF switches can be exploited to route signals among different components of a highly compact small form-factor low cost high performance radar sensor for automotive applications.

Typical operation of a MEMS cantilever type RF switch is shown in figure 2.14. A bias voltage across the beam and the DC pad causes an electrostatic attraction force between the beam and the DC pad that pulls the beam down towards the DC pad. At a certain voltage, the electrostatic force overcomes the elastic restoring force of the beam and the beam collapses on the DC pad to establish the connectivity (ON state). When the bias voltage is withdrawn, the beam moves back to its rest position due to inertia (OFF state). A detailed review of MEMS RF switches is presented in chapter 4.

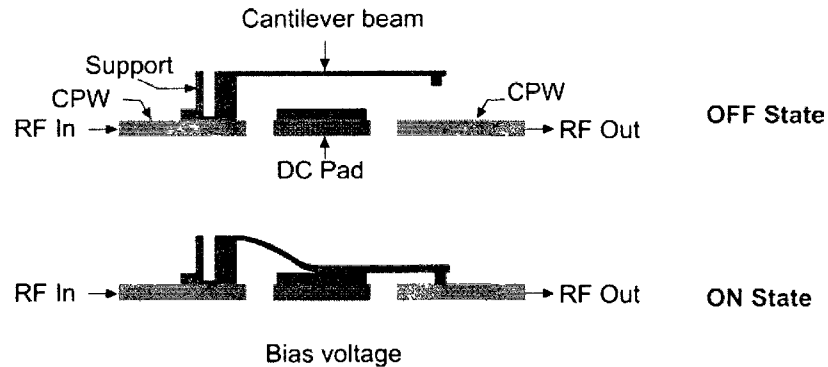


Figure 2.14 MEMS cantilever type RF.

A cantilever type MEMS switch was presented in [30] to be used in the range of 9.5-13 GHz; it is  $(600 \times 600) \mu\text{m}^2$  in size. It exhibits a return loss of -20 dB, insertion loss of -1 dB, isolation of -28 dB and actuation voltage of 65 V.

In [31] a capacitive type RF MEMS switch was presented to be used at 60 GHz, it has a membrane size of  $(10 \times 240) \mu\text{m}^2$ . It exhibits a return loss of -25 dB, insertion loss of -0.2 dB, isolation of -15 dB and actuation voltage of 10 V.

The performance of a cantilever MEMS RF switch was reported in [32]. It has been designed to operate at 40 GHz and it exhibits a return loss of -27 dB, insertion loss of -0.7 dB.

The goal of this research work is to design and fabricate a high performance MEMS based RF switch to be used as an integral part of the system.

## 2.9 Antenna System

The Antenna subsystem forms an integral part of a radar sensor to radiate and receive the signal (pulse, FSK-CW or FMCW) that enables to determine the range, velocity, or location of the target. There are different kinds of antennas used in automotive radars like horn antenna, reflector antenna, dual reflector antenna, and microstrip antenna. Out of different types of antennae, microstrip antennas have become the technology of choice for automotive radars for their simple and inexpensive manufacturing using modern printed-circuit technology. They are mechanically robust when mounted on rigid surfaces, compatible with MMIC designs, and when the particular patch shape and mode are selected, they are very versatile in terms of resonant frequency, polarization, pattern, and impedance.

Microstrip antennas are planar resonant cavities that utilize the fringing fields along the edges of a microstrip patch to radiate electromagnetic energy. A typical microstrip patch antenna consists of a very thin metallic strip (patch) of thickness  $t$  placed on a dielectric substrate of thickness  $h$  and of dielectric constant of  $\epsilon_r$  above a ground plane as shown in figure 2.15.

The metallic patch can take many different configurations. The rectangular and circular patches are the most popular because of ease of analysis and fabrication, and their attractive radiation characteristics, especially low cross-polarization radiation.

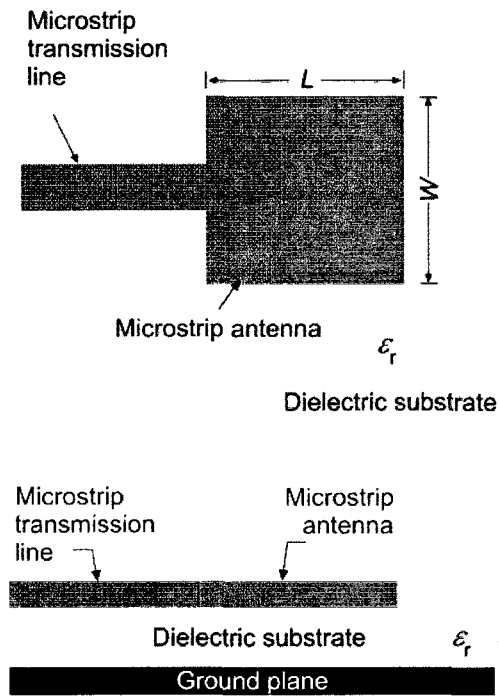


Figure 2.15 Microstrip patch antenna.

An array of patches has to be used to get certain gain, directivity and efficiency required by the application to be performed using the microstrip antenna array. Figure 2.16 shows a microstrip antenna array.

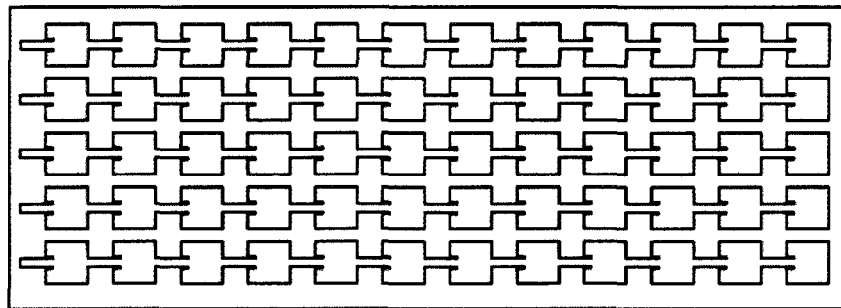


Figure 2.16 Microstrip antenna array.

Recent microstrip antenna arrays are using different ways to feed the patch, number of patches required by the specific application to get the gain and directivity required [33-40]. Detailed analysis of microstrip antenna arrays is providing in chapter 5.

A microstrip antenna array was presented in [40] in which corporate feed was used to feed the array in the 77 GHz range. It has a gain of 17.5 dB, return loss of -7 dB, efficiency of 69% and half power beamwidth of 12°.

In [41] a corporate feed microstrip antenna array was presented to be operated in the range of (32-36) GHz. It has a HPBW of 27°, gain of 16 dB.

A 2x8 microstrip corporate feed antenna array is presented in [42] to be used in 12 GHz, it exhibit a return loss of -15 dB, gain of 20 dB and half power beamwidth of 10°.

All above mentioned designs are using corporate feed which suffers high RF losses due to the feed line lengths. They also use a normal rectangular patch that lead to a lower gain microstrip antenna array.

## **2.10 The MEMS Radar**

The MEMS technology will have a great impact in automotive radar sensors by introducing electronically scanned arrays (ESA) using recent UWB antenna array developments, true-time-delay beamformers, transmit/receive (T/R) switches and tuneable matching networks [43]. The integration of RF MEMS radar components in automotive radar subsystems will make the new generation of automotive radars more efficient, reliable and cost effective. It incorporate passive electronically scanned arrays (lens arrays, and beamformers), passive subarrays, and T/R modules for active electronically scanned arrays [44]

The application of an automotive radar system is classified according to the range it covers. Long range radar (LRR) and medium range radar (MRR) are used in cruise control and collision avoidance, and short range radar (SRR) is used in collision avoidance, crash-prevention and parking-assist systems.

Having established that automotive radar can be very helpful in reducing the number of fatal accidents, it is essential that low cost and reliable radar systems be made to improve road safety globally. Lower cost (compared to \$3000-\$5000 approx. for current systems) will enable even lower-end vehicles to be equipped with safety options, boosting road safety. MEMS technology offers the advantage of realizing low cost batch

fabrication of high performance RF components like Rotman lens, RF switches that can be used to realize compact high performance lightweight radar in a small form factor.

# Chapter 3

## New Radar Architecture and MEMS Rotman Lens

This chapter presents the architecture of the new MEMS based 77 GHz FMCW radar sensor and design, simulation and fabrication of a novel MEMS Rotman lens. The  $TE_{10}$  mode air-cavity Rotman lens forms the core beamforming and beam steering component of the new radar sensor. The Rotman lens has a footprint area of 27 mm x 36.2 mm including the transmission lines, incorporates 3 beam ports, 5 array ports, and 6 dummy ports. The Rotman lens has a cavity depth of 50  $\mu\text{m}$  with a cavity footprint area of 11 mm x 14 mm. The lens has been designed to steer a beam by  $\pm 4$  degrees. HFSS simulation shows that the designed Rotman lens has an insertion loss of -2 dB, return loss of -20 dB and characteristic impedance of  $50\Omega$ . The lens has been fabricated using deep reactive ion etching and thermo-compression bonding of two 500  $\mu\text{m}$  thick silicon wafers.

### 3.1 Architecture of MEMS Radar

Following the review of the state-of-the-art in automotive radars and requirements set by the auto industry for long range radar as listed in table 2.5, a decision can be made to select the radar type that can provide the best performance while addressing the design constraints.

#### 3.1.1 Radar type selection

The visible disadvantages of the 3 main radar types, pulsed, FSK-CW and FMCW can be summarized as:

Pulsed Doppler disadvantages:

- Velocity measurement limited by *blind speed* when  $f_d$  is a multiple of the PRF.
- Maximum measurable Doppler shift has to be less than PRF to avoid ISI among different pulses and target returns.
- To reduce the above velocity ambiguity the PRF can be increased, however increasing the PRF creates range ambiguity.

- Relatively high power requirements in the automotive scenario.
- Greater risk of jamming or confusion due to high-power pulses from other Pulsed radars.

FSK-CW disadvantages:

- Invisible targets in the direct path of the radar.
- Target range is computed based on the difference in phase shift for two consecutive frequency hops. This makes the system subject to phase noise.
- The CPI needs to be large enough to avoid range ambiguity.

FMCW radar overcomes these disadvantages with:

- No theoretical limit to range resolution and better short range detection.
- Reduced effects of clutter and atmospheric noise.
- Lower power rating than Pulsed radar.
- Less effects of phase noise.
- More resistance to interference from other similar radars in the vicinity.
- No theoretical blind spots.
- Resistance to jamming (frequency modulation is a common tool in ECCM – Electronic Counter-Countermeasures to overcome jamming effects)

This qualitative comparison warrants the use of FMCW for the new MEMS radar sensor for long range radar (LRR) application.

### **3.1.2 Frequency Selection**

The 76–77 GHz band was regulated in the 90's followed by a standardization in Europe (ETSI EN 301 091). Now, this band is allocated for Intelligent Transport Services (ITS) in Europe, North America, and Japan [13]. In March 2004 the European commission allocated the frequency range 77 – 81 GHz for UWB SRR with permitted usage from 2005 onwards. In the USA and Canada, 77 GHz has been specified for automotive radar applications.



With regard to the automotive long range radar, the maximum range (150 meters following Table 2.5) is proportional to the effective antenna aperture size and to the square root of the frequency. Therefore, highest frequencies should be preferred to get smaller radar size. It will be also a cost saving approach.

#### **3.1.3. Beamformer selection:**

To eliminate the need for microelectronic based analog or digital beamforming engine, a Rotman lens has been adopted to perform the operation of beamforming and beamsteering.

#### **3.1.4 Switch selection:**

Instead of non-MEMS waveguide type switches, MEMS based RF switches have been selected to feed the FMCW signal to the beam ports of the Rotman lens.

#### **3.1.5 Antenna Selection**

Microstrip based antenna arrays have been selected to radiate and receive the signal due to their established superior performance, ease of fabrication, and small planar geometry while offering high directivity and lower sidelobes.

#### **3.1.6 Signal processor selection**

The aspects of frequency generation, tuning and linearity become critical in FMCW radar due to the requirement of highly linear frequency sweeps. In FMCW radar the signal generation and sweep modulation can be accomplished using analog or digital modulation. Analog PLLs or Phase Locked Loops containing a VCO were used in early CW systems, however were overtaken by digital systems with better frequency response, excellent linearity, easier design and improved performance in noise [45].

In digital implementation of a radar transmitter, the control and modulation algorithm can be based on a Digital Signal Processor (DSP) or a Field Programmable Gate Array (FPGA). Due to their highly parallel nature, ability to run several tasks simultaneously without stalling other tasks, and on-chip resources (such as RAM blocks, LUTs, fast DSP multipliers) FPGAs are the preferred solution for digital signal processing for a radar sensor with a lower cycle time.

Even with a low clock frequency of 200 MHz the FPGA has comparable speed performance compared to the other processors at higher clock rates. Power consumption of a digital circuit is proportional to the total gate-level switching required to compute a

particular result: the higher the clock frequency and required clock cycles, the greater the amount of switching, and thus the higher the power consumption. Given the automotive scenario, FPGAs offer a desirable combination of speed and power efficiency.

Furthermore, to deal with possible VCO non-linearity FPGAs can be used to implement a DDS or Direct Digital Synthesis algorithm. DDS is a method of creating arbitrary yet repetitive waveforms using a RAM or LUT, a counter, and a DAC, components that are readily available on FPGA platforms. DDS promises optimal linearity in frequency sweeps, precise frequency tuning, and excellent phase error recovery [45].

### 3.1.7 New Radar Sensor Architecture

Based on these decisions, the architecture of a new radar sensor has been developed and is shown in the figure 3.1 below. The operating principle of the new radar sensor is as follows:

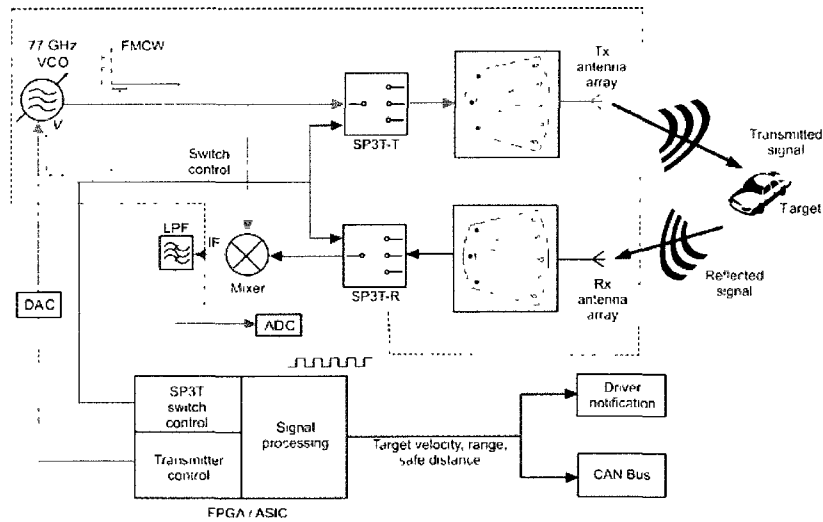


Figure 3.1 Block diagram of the new MEMS based radar sensor.

1. An FPGA implemented control circuit generates a triangular signal ( $V_{tune}$ ) to modulate a voltage controlled oscillator (VCO) to generate a FMCW signal having a frequency sweep range of 0-800 MHz centered at 77 GHz.
2. The signal is fed to a MEMS SP3T switch.

3. An FPGA implemented control algorithm controls the SP3T switch to sequentially switch the FMCW signal among the three beam ports of a MEMS implemented Rotman lens.
4. As the FMCW signal arrives at the array ports of the Rotman lens after traveling through the Rotman lens cavity, the time-delayed in-phase signals are fed to a microstrip antenna array that radiates the signal in a specific direction.
5. The sequential switching of the input signal among the beam ports of the Rotman lens enables the beam to be steered across the target area in steps by a pre-specific angle.
6. On the receiving side, a receiver antenna array receives the signal reflected off a vehicle or an obstacle and feeds the signal to another SP3T switch through another Rotman lens.
7. An FPGA based control circuit controls the operation of the receiver SP3T switch in tandem with the transmit SP3T switch so that the signal output at a specific beam port of the receiver Rotman lens can be mixed with the corresponding transmit signal.
8. The output of the receiver SP3T switch is passed through a mixer to generate an IF signal in the range of 0-200 KHz.
9. An analog-to-digital converter (ADC) samples the received IF signal and converts it to a digital signal.
10. Finally, an FPGA implemented algorithm processes the digital signal from the ADC to determine the range and velocity of the detected target. In mass volume production, the FPGA will be substituted by an ASIC.

### **3.2 Rotman Lens Design Principles**

A schematic diagram of a typical Rotman lens is shown in figure 3.2. The inner contour is determined by the design equations and locates the positions of the array ports. The outer contour is a straight line and defines the positions of the radiating elements.

The array ports on the inner contour are connected to the radiating elements on the outer contour via transmission lines of length  $W$ . Inner contour is defined by two coordinates  $(x, y)$  that are specified relative to a point  $O_1$  on the central axis of the lens. Radiating elements on the outer contour are determined by a single coordinate  $N$ . Point  $P$  on the inner contour is connected to point  $Q$  on the outer contour by a transmission line of length  $W$ . To obtain the path length equations, two off axis focal points  $F_1, F_2$  are defined at the two perfect focal points and an on axis focal point  $F_0$  at the center having coordinates of  $(-F \cos \alpha, F \sin \alpha)$ ,  $(-F \cos \alpha, -F \sin \alpha)$  and  $(-G, 0)$  respectively.

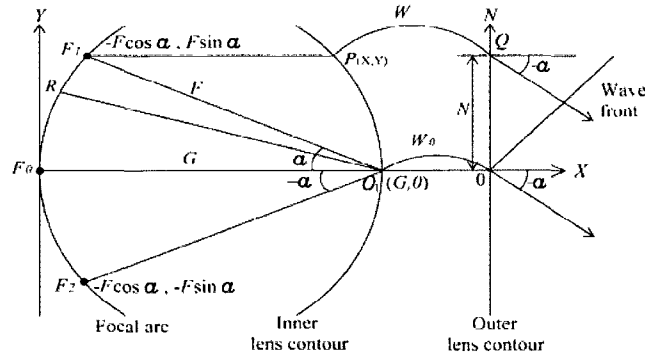


Figure 3.2 Rotman lens schematic diagram.

In figure 3.2:

$G$  is the on-axis focal length.

$F$  is the off-axis focal length.

$W$  is off-axis length of the transmission path.

$W_0$  is the on-axis length of the transmission path.

$\alpha$  is the scanning angle.

$\eta$  is the lens numerical aperture.

For any point  $P$  on the inner contour, the path lengths:  $F_1P$ ,  $F_2P$ , and  $F_0P$  as travelled by a signal fed at the beam ports can be determined from the geometry [46] as:

$$F_1P + W + N \sin \alpha = F + W_0 \quad (3.1)$$

$$F_2P + W - N \sin \alpha = F + W_0 \quad (3.2)$$

$$F_0P + W = G + W_0 \quad (3.3)$$

By normalizing all the parameters in (3.1)-(3.3) by the off-axis focal length  $F$ , one obtains

$$\eta = N/F, x = X/F, y = Y/F, w = \frac{W - W_0}{F}, g = G/F \quad (3.4)$$

By defining the following constants as:

$$a_0 = \cos \alpha, \quad b_0 = \sin \alpha \quad (3.5)$$

$$a = \left[ 1 - \eta^2 - \left( \frac{g-1}{g-a_0} \right)^2 \right] \quad (3.6)$$

$$b = \left[ 2g \left( \frac{g-1}{g-a_0} \right) - \frac{(g-1)}{(g-a_0)^2} b_0^2 \eta^2 + 2\eta^2 \right] - 2g \quad (3.7)$$

$$c = \left[ \frac{g b_0^2 \eta^2}{g-a_0} - \frac{b_0^4 \eta^4}{4(g-a_0)^2} - \eta^2 \right] \quad (3.8)$$

The Rotman lens dimensions (width, length, transmission line length, and height) can be found as follows

$$x = \left[ \frac{1-g}{g-a_0} w - \frac{b_0^2 \eta^2}{2(g-a_0)} \right] \quad (3.9)$$

$$y = \eta(1-w) \quad (3.10)$$

$$w = \frac{-b + \sqrt{b^2 - 4ac}}{2a} \quad (3.11)$$

In [46], it has been mentioned that to ensure propagation of the TEM mode only, the thickness of the lens cavity needed to be less than half of the modified wavelength  $\lambda_m$  [46-47] defined as

$$\lambda_m = \lambda_0 / \sqrt{\epsilon_r} = c / (f \sqrt{\epsilon_r}) \quad (3.12)$$

In (3.12),  $\lambda_0$  is the wavelength of the operating frequency  $f$ ,  $c$  is the velocity of light, and  $\epsilon_r$  is the dielectric constant of the material filling the lens cavity.

Following [48], if only TEM mode propagates inside the lens region and if there is no variation with lens height, the lens can be treated as a two-dimensional transmitting and receiving antenna system without considering multiple reflections inside lens cavity. This

enables to use a two-dimensional equivalent of the Friis transmission formula derived in [48] as given in (3.13) to calculate the power  $P_r$  received by each array port for a transmit power of  $P_t$  at any of the beam ports.

$$\frac{P_r}{P_t} = \frac{l_a l_b}{\lambda} \cos^2 \theta_a \cos^2 \theta_b \left[ \frac{\sin\left(\frac{\pi l_a \sin \theta_a}{\lambda}\right)}{\pi l_a \sin \theta_a / \lambda} \right]^2 \times \left[ \frac{\sin\left(\frac{\pi l_b \sin \theta_b}{\lambda}\right)}{\pi l_b \sin \theta_b / \lambda} \right]^2 e^{-2\alpha_c r} \quad (3.13)$$

where  $l_a, l_b$  are the array and the beam ports lengths respectively,  $\theta_a, \theta_b$  are the array port and beam ports angles with respect to the positive  $x$  axis (lens axis), respectively, and  $\alpha_c$  is the attenuation factor that count for material losses in the lens cavity.

To minimize grating lobes, port spacing  $d$  can be determined following [47]:

$$\frac{d}{\lambda} = \frac{1}{2 + \sin \alpha} \quad (3.14)$$

Reflections from the sidewalls are the biggest limiting factor affecting lens performance. Dummy ports are essential in any Rotman lens design to minimize or eliminate the reflections from the sidewalls.

### 3.3 Rotman Lens Design for Automotive Radar

For automotive applications, the radar needs to provide the angular position as well as the distance of the vehicle or obstacle ahead. It is determined that at least three directional beams are needed to cover the left, right and the main sights respectively [2-9]. It has been determined that a Rotman lens with 3 beam ports, 5 array ports and a beam steering capability of  $\pm 4^\circ$  is sufficient for an automotive long range radar. In the design process of the Rotman lens, there are four basic design parameters that determine the lens performance:

- Off-axis focal length  $F$
- Focal angle  $\alpha$
- normalized lens aperture  $\eta$  and
- On-axis to off-axis focal length ratio  $g$ .

Shape of the lens depends on the design parameters  $\alpha, \eta, g$  and  $F$ . The lens shape determines the mutual coupling between ports and multiple scattering between ports. As

$\eta$  increases, the height of the array contour increases up to a certain range. The value of  $\eta$  should be chosen to equalize the height of both contours. Equal heights of both contours are required to couple the maximum power from the feed contour to array elements.

For the design, three beam ports of the Rotman lens have been chosen at the three perfect focal points on the focal arc to avoid path length error (phase error) [46]. To detect a vehicle in the same lane at a distance of 150 meters, the scan angle  $\alpha$  between two steered beams at the extremities needs to be 2 degrees as shown in figure (3.3), whereas to detect vehicles ahead in two side lanes also,  $\alpha$  needs to be at least 4 degrees.

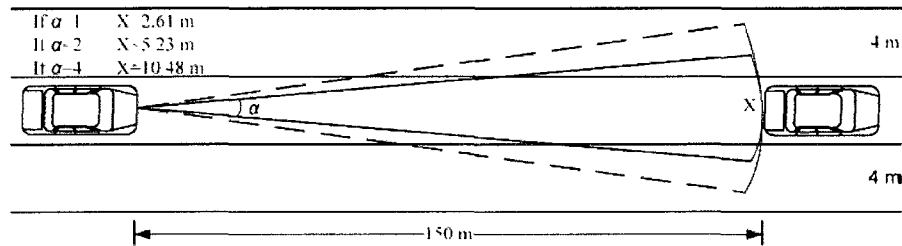


Figure 3.3 Target scanning angle

### 3.3.1 Rotman Lens Design Methodology

The specific tasks associated with the design of the Rotman lens are listed as follows:

1. Scanning angle resolution
2. Lens contour determination
3. Lens thickness
4. Port dimensions
5. Port spacing
6. Minimizing lens internal reflection
7. Radiation pattern
8. Transmission path length determination

Figure 3.4 shows the flowchart that summarizes the design methodology of the Rotman lens. The scanning angle  $\alpha$  should be specified in the range that the designed lens needs to cover. The aperture length and the I/O ports will be optimized so as to avoid any interference between the adjacent ports which will reduce the lens gain and affect the

return loss, insertion loss and isolation between the ports. The focal ratio is chosen so as to eliminate any path length error, i.e. the beam ports locations are chosen on the perfect off-axis foci and the middle one right on the horizontal axis  $\propto$  focal point. Lens contours will then be determined and the lens shape will be finalized.

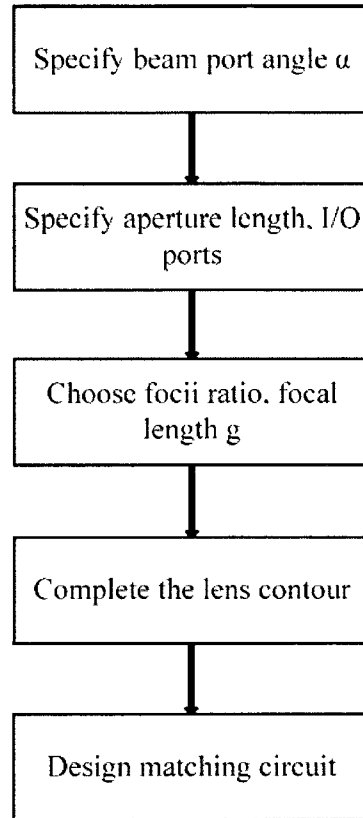


Figure 3.4 design methodology of the Rotman lens.

### 3.3.2 New Approach of Rotman Lens Design

Following (3.12), it is evident that using a high dielectric constant material will result in a lower thickness for the Rotman lens. However, to ensure batch microfabrication, the selected dielectric material must be deposited using some standard thin film deposition techniques. Investigation shows that Barium Strontium Titanate (BSTO) and Tantalum Pentaoxide ( $\text{Ta}_2\text{O}_5$ ) exhibit very high dielectric constants; however, the state-of-the-art deposition techniques available for these materials don't allow to deposit more than tens of nanometers. In [49, 50], it has been reported that Lead-Zirconium Titanate (PZT) can be deposited at a high thickness using the sol-gel deposition technique. Using  $\epsilon_r=1200$  for PZT and an operating frequency of 77 GHz,



(3.12) yields a modified wavelength  $\lambda_m$  of 112.5  $\mu\text{m}$  that translates into a cavity thickness of 56  $\mu\text{m}$ . One technique to realize a 56 thick PZT layer is successive deposition of 10-12  $\mu\text{m}$  thick PZT layers using the sol-gel deposition technique until the desired thickness is achieved. However, this technique is marred by the fact that at every deposition stage, the residual stress must be totally released to avoid layer detachment due to the residual stress. This makes the realization of a 56  $\mu\text{m}$  thick PZT layer as a very challenging task. Additionally, the high value of the dielectric constant of PZT (1200) will results in a higher level of attenuation (400 to 2100 dB/cm) [8]. This makes the PZT filled approach as not a suitable one and warrants to explore other possibilities to realize a microfabricated Rotman lens. The fabrication technique must satisfy the requirement of small thickness in the order of 10s of micrometers while the dielectric material filling the lens cavity needs to offer very low attenuation.

Investigation shows that if the target Rotman lens can be designed using the principle of a rectangular waveguide that supports the  $TE_{10}$  mode only, both the requirements of lower thickness and minimal attenuation can be satisfied.

The  $TE_{10}$  mode, frequently referred to as the dominant mode, is one of the simplest of all modes which may exist and has the following characteristics:

1. Cut-off frequency is independent of one of the dimensions of the cross section. Consequently for a given frequency this dimension may be made small enough so that the  $TE_{10}$  wave is the only wave which will propagate.
2. The polarization of the field is definitely fixed, electric field passing from top to bottom of the I/O ports.
3. For a given frequency the attenuation due to metal losses is not excessive compared with other wave types in guides of comparable size.

The expressions for the  $TE_{10}$  wave characteristic impedance  $Z_{TE}$ , phase velocity  $V_p$  and group velocity  $V_g$  are as follows:

$$Z_{TE} = \frac{\eta}{\sqrt{1 - \left(\frac{\lambda}{2a}\right)^2}} \quad (3.15)$$

$$V_p = \frac{1}{\sqrt{\mu\epsilon} \sqrt{1 - \left(\frac{\lambda}{2a}\right)^2}} \quad (3.16)$$

$$V_g = \frac{1}{\sqrt{\mu\epsilon}} \sqrt{1 - \left(\frac{\lambda}{2a}\right)^2} \quad (3.17)$$

where  $V_p$ ,  $V_g$  are the phase velocity, group velocity, respectively,  $\mu$ ,  $\epsilon$ , and  $\eta$  are permeability, permittivity and intrinsic impedance, respectively, for the dielectric filling the guide.

The propagation of the magnetic field can be reduced to two dimension wave equation.

$$\left( \frac{\partial^2}{\partial x^2} + \frac{\partial^2}{\partial y^2} + k_c^2 \right) H_z = 0 \quad (3.18)$$

Where  $k_c$  is the propagation constant and  $H_z$  is the magnetic field in the  $z$  direction. The TE wave impedance  $Z_{TE}$  can be found as

$$Z_{TE} = \frac{E_x}{H_y} = \frac{-E_y}{H_x} \quad (3.19)$$

The field distribution equations of the  $TE_{10}$  mode are as follows

$$E_y = E_0 \sin\left(\frac{\pi x}{a}\right) \quad (3.20)$$

$$H_x = -\left(\frac{E_0}{Z_{TE}}\right) \sin\left(\frac{\pi x}{a}\right) \quad (3.21)$$

$$H_z = \frac{jE_0}{\eta} \left(\frac{\lambda}{2a}\right) \cos\left(\frac{\pi x}{a}\right) \quad (3.22)$$

$$H_y = E_x = 0 \quad (3.23)$$

From the field distribution equations (3.20-3.23) [51] associated with the  $TE_{10}$  propagation mode in a rectangular waveguide, the  $TE_{10}$  propagation is shown in Figure 3.5

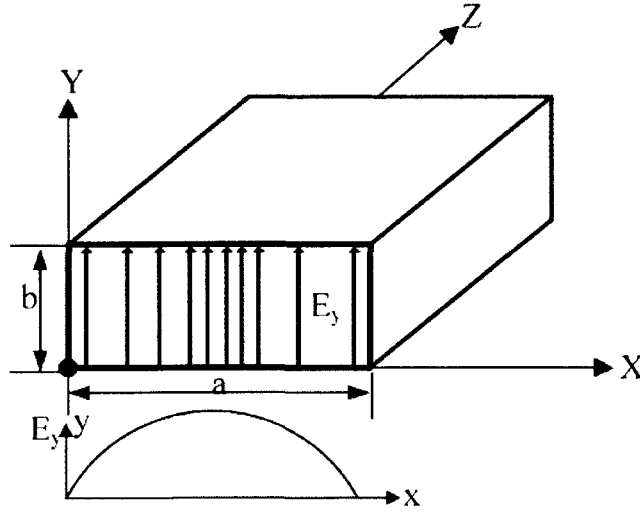


Figure 3.5 TE<sub>10</sub> propagation mode in a rectangular waveguide.

It is evident that both the Electric and magnetic field components are independent of the vertical dimension  $y$ . The only electric field component  $E_y$  is passing between the top and bottom, and it's maximum at the center and zero at the conducting walls ( $x = 0, x = a$ ) varying as a half sine wave as shown in figure 3.5.

From the expression of the cut-off frequency (the frequency for which the width of the guide is a half wavelength (cut-off wavelength)) of a TE<sub>10</sub> mode rectangular waveguide as shown in (3.24) and (3.25), it is also evident that the cut-off frequency  $f_c$  also is independent of the vertical dimension  $b$  of the rectangular waveguide.

$$\lambda_c = 2a \quad (3.24)$$

$$f_c = \frac{1}{2a\sqrt{\mu\epsilon}} \quad (3.25)$$

where  $\lambda_c$  represents the cut-off wavelength. As the cut-off frequency is independent of the vertical dimension  $b$ , the thickness of the lens can be lowered below  $\lambda/2$  if the lens is designed to have the characteristics of a rectangular waveguide. Consequently, there is no need to fill up the lens cavity with a high dielectric material as air can be used to fill up the lens cavity. This resolves the fabrication and attenuation issues associated with the use of a high dielectric material to fill up the lens cavity. However, though the thickness of a TE<sub>10</sub> mode rectangular waveguide is independent of the vertical dimension, there is a

lower limit on the height of the vertical dimension set by the attenuation  $\alpha_c$  due to the conduction loss associated with the imperfect conductivity of the waveguide walls expressed as:

$$\alpha_c = \frac{R_s}{b\eta\sqrt{1-\left(\frac{f_c}{f}\right)^2}} \left[ 1 + \frac{2b}{a} \left( \frac{f_c}{f} \right)^2 \right] \quad (3.26)$$

where

$R_s$  is the skin effect surface resistivity of the conducting walls

The precise value of the vertical dimension  $b$  considering the attenuation constant  $\alpha_c$  can be determined from simulation using HFSS.

Following this approach, beam port and the array port widths have been determined to be 2 mm. To minimize the reflections from the cavity sidewalls (path loss), two sets of dummy ports having the same dimensions as the beam ports and the array ports are incorporated in the design. Absorber material with impedance 50 Ohms are to be used to terminate the dummy ports.

Following this, the lens contours are initially determined by solving the equations (3.1)-(3.11) for different values of  $\alpha$  and  $g$  as shown in figures (3.6)-(3.9) which are optimized later on using HFSS. In the figures,  $g = G/F$  is the normalized on-axis focal length with respect to the off-axis focal length,  $\alpha$  is the scanning angle and  $\eta$  is the normalized numerical aperture.

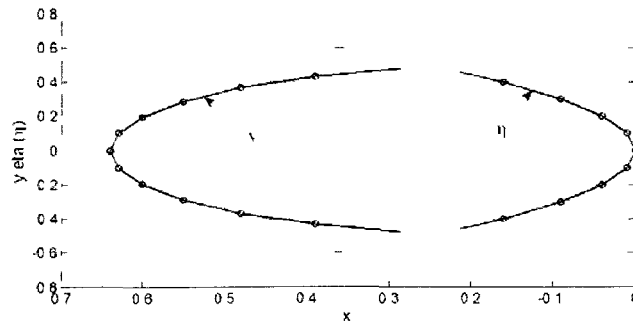


Figure 3.6 Lens contour for  $\alpha=1, g=1$

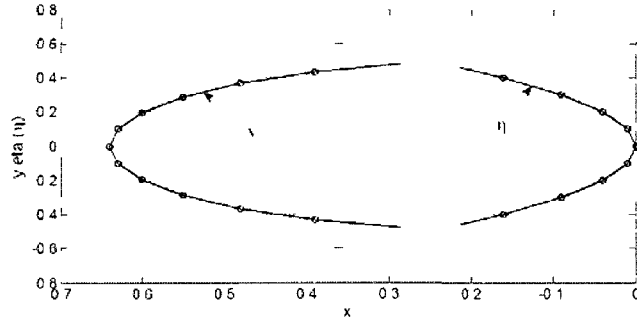


Figure 3.7 Lens contour for  $\alpha=2, g=1$

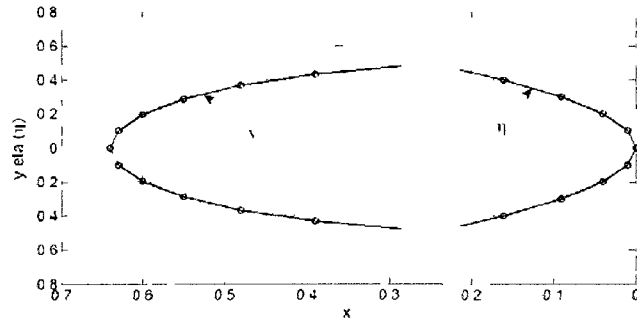


Figure 3.8 Lens contour for  $\alpha=3, g=1$

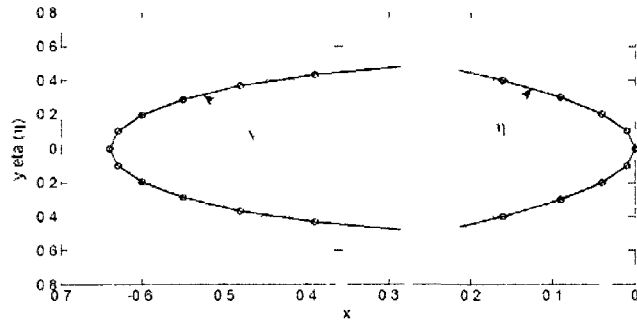


Figure 3.9 Lens contour for  $\alpha=4, g=1$

To determine the optimum thickness of the lens cavity, simulations using HFSS software has been carried out for different lens thicknesses. Program codes for designing the Rotman lens in visual basic code (VB code) is shown in appendix A. Figures 3.10 and 3.11 show the E field characteristics for 2.5  $\mu\text{m}$  and 10  $\mu\text{m}$  thick lenses, respectively. In the figures, the signal is fed through beam port 1 and the other two beam ports are terminated with a matching resistance of 50  $\Omega$ . For the 2.5  $\mu\text{m}$  thick lens (figure 3.10), the signal cannot propagate through the lens cavity due to the high attenuation constant associated with the wall conduction loss. Also the lens exhibits a very high characteristic

impedance and insertion loss. Little improved but far from desired response is observed for the 10  $\mu\text{m}$  thick lens (figure 3.11). Using an iterative process, it has been determined that at a thickness of 50  $\mu\text{m}$ , the signal propagation through the lens is optimal. Figures 3.12a, 3.12b and 3.12c shows the E field characteristics when the beam ports 1, 2, and 3 are excited, respectively. Figure 3.13 shows that at the 50  $\mu\text{m}$  thickness, the lens exhibits a characteristics impedance of 50 ohms at 77 GHz. The associated return loss and insertion losses are shown in the figures 3.14-3.19. From the figures, the lens exhibits a return loss of better than -20 dB and insertion losses better than -2 dB between beam port 1 and array ports 2,3,4,5 and 6 at the operating frequency of 77 GHz.

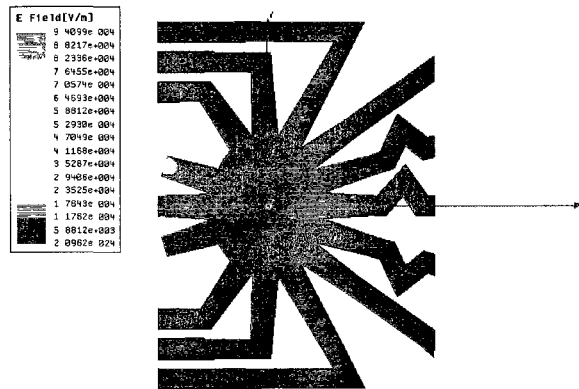


Figure 3.10 Rotman lens of 2.5  $\mu\text{m}$  thickness.

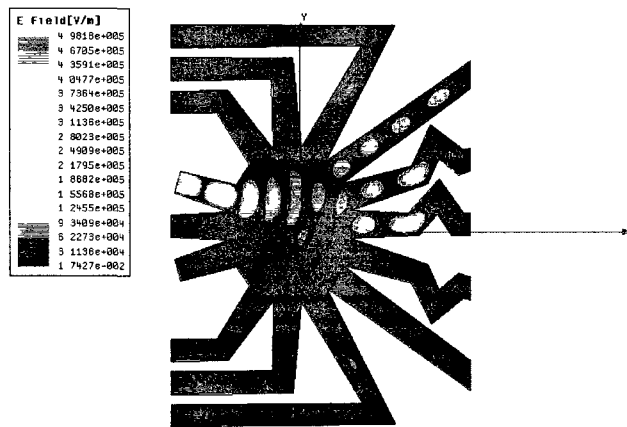


Figure 3.11 Rotman lens of 10  $\mu\text{m}$  thickness.

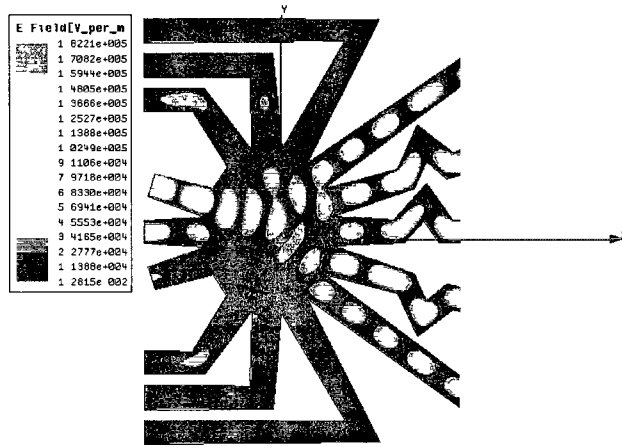


Figure 3.12 (a) Rotman lens of 50  $\mu\text{m}$  thickness excited from beam port 1.

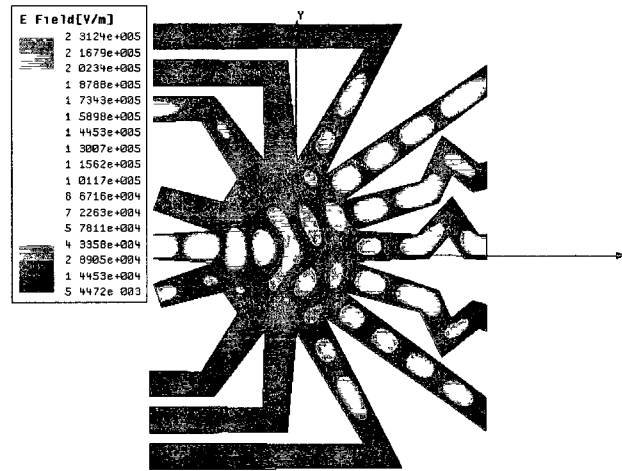


Figure 3.12 (b) Rotman lens of 50  $\mu\text{m}$  thickness excited from beam port 2.

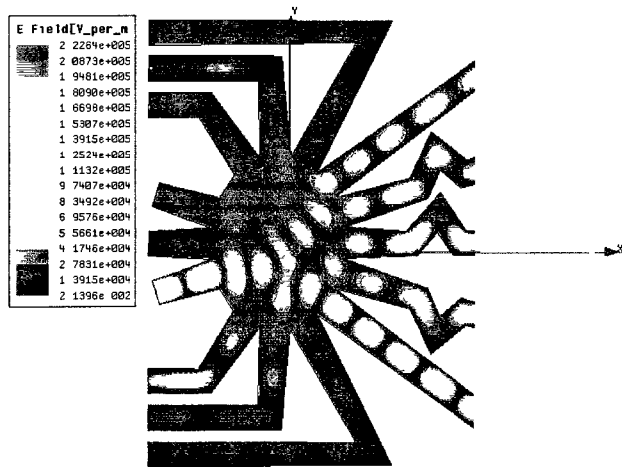


Figure 3.12 (c) Rotman lens of 50  $\mu\text{m}$  thickness excited from beam port 3.

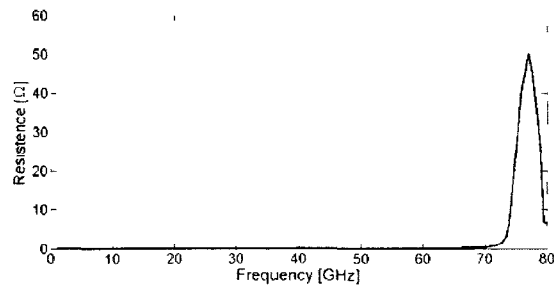


Figure 3.13 characteristic impedance of the Rotman lens.

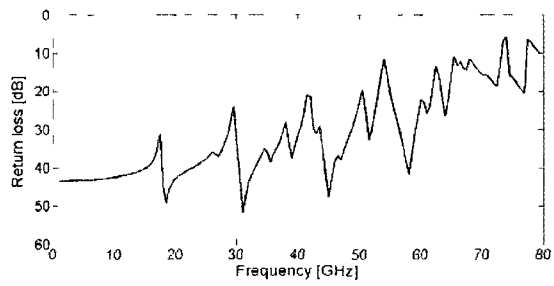


Figure 3.14 Return loss of the Rotman lens.

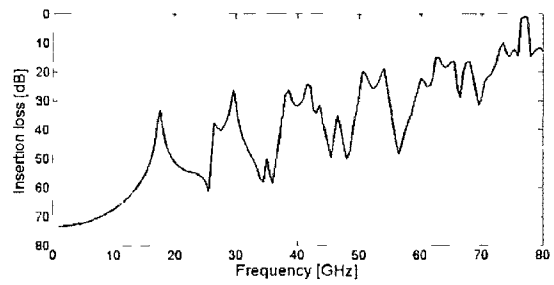


Figure 3.15 Insertion loss between beam port 1 and array port 2.

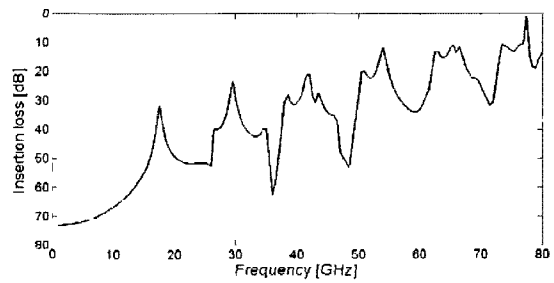


Figure 3.16 Insertion loss between beam port 1 and array port 3.



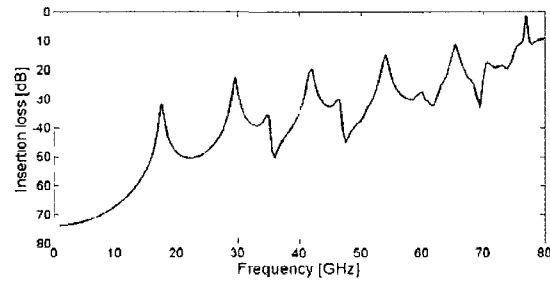


Figure 3.17 Insertion loss between beam port 1 and array port 4.

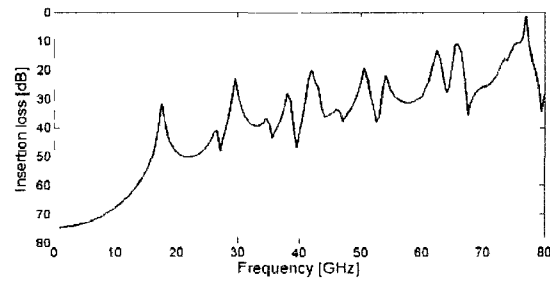


Figure 3.18 Insertion loss between beam port 1 and array port 5.

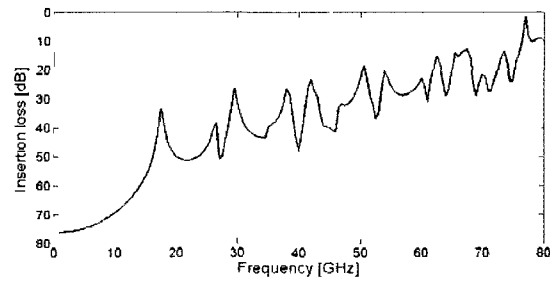


Figure 3.19 Insertion loss between beam port 1 and array port 6.

Similar insertion and return losses are observed for beam ports 2 and 3. This concludes the design process and the final device specifications are listed in Table 3.1

Table 3.1 Rotman Lens Final Design Specifications

Parameter	Value
Substrate thickness	500 $\mu\text{m}$
Lens cavity depth	50 $\mu\text{m}$
Lens width (including transmission line)	27 mm
Lens length (including transmission line)	36.2 mm
Number of beam ports	3
Number of array ports	5
Beam scanning angle $\alpha$	4°
Transmission line length	4.5 $\lambda$
Cavity foot print area	14x11 mm <sup>2</sup>
Frequency	77 GHz
Wavelength	3.89 mm
Characteristic impedance	50 $\Omega$
Return loss	-20 dB
Insertion loss	-2 dB

### 3.4 Fabrication

The Rotman lens is fabricated in the Center for RF Engineering (CIRFE) in the University of Waterloo, University of Western Ontario in London and Advotec company in Arizona using DRIE, E-beam and wafer thermo-coupling techniques in four steps as listed below

#### Step 1: Wafer Preparation

The wafer undergoes RCA cleaning to remove all organic contamination, oxide film or heavy metal contamination from the wafer.

Process Flow:

- 130 ml of Hydrogen Peroxide (Acid) is added into a beaker carrying 600 ml of DI water followed by 130 ml of Ammonium Hydroxide (Base).
- Heat the beaker till temperature rise to  $70 \pm 5$  C°. Place the sample inside the solution using Teflon holder for 15 minutes.
- When finished, turn on DI water tap and allow water to flush out the RCA-1 solution for 5 minutes.
- Dry the wafer using Nitrogen gas.

Figure 3.20 shows the Silicon wafers immersed in the RCA solution.



Figure 3.20 Silicon wafers immersed in the RCA solution.  
The Rotman lens mask to be etched on the silicon wafer is shown in figure 3.21.

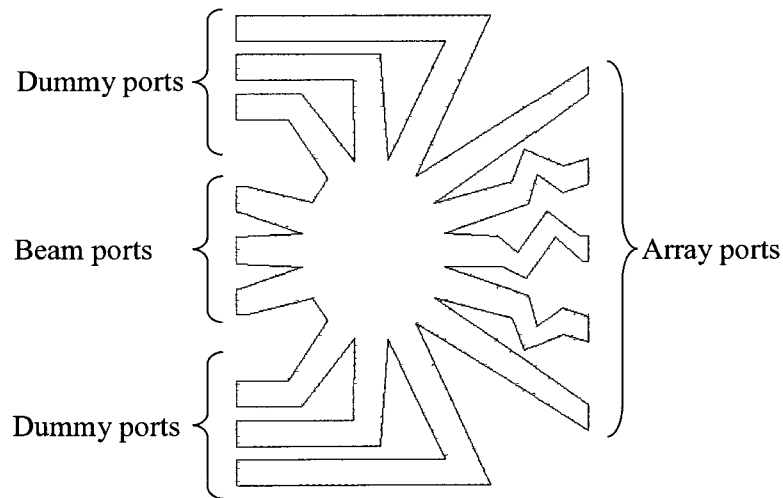


Figure 3.21 Rotman lens mask.

### **Step 2: DRIE (Deep Reactive Ion Etching)**

The wafer is etched to a depth of 50  $\mu\text{m}$  using DRIE (Deep Reactive Ion Etching) using Alcatel 601E Deep Silicon Etch machine in University of Western Ontario  
Process Flow:

- The patterns are defined by a thin layer of silicon oxide which is patterned lithographically prior to etching.
- Silicon is etched selectively relative to the oxide mask.
- The system is optimized for high etch rate and high aspect ratio etching of silicon.
- Vertical anisotropic deep plasma etching of silicon is used by depositing an ultra-thin layer of silicon-dioxide which is used for sidewall protection to control the (Bosch process).

Figure 3.22 shows the machine used for the process.

Figure 3.23 shows the SEM profiles of the silicon wafers after etching, captured at the University of Western Ontario

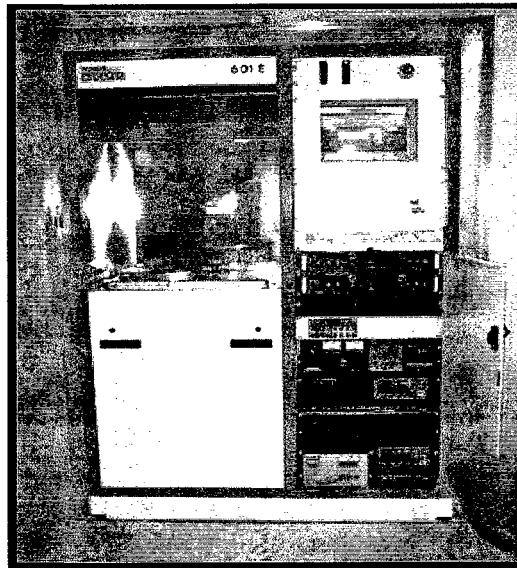


Figure 3.22 Alcatel 601E Deep Silicon Etch.

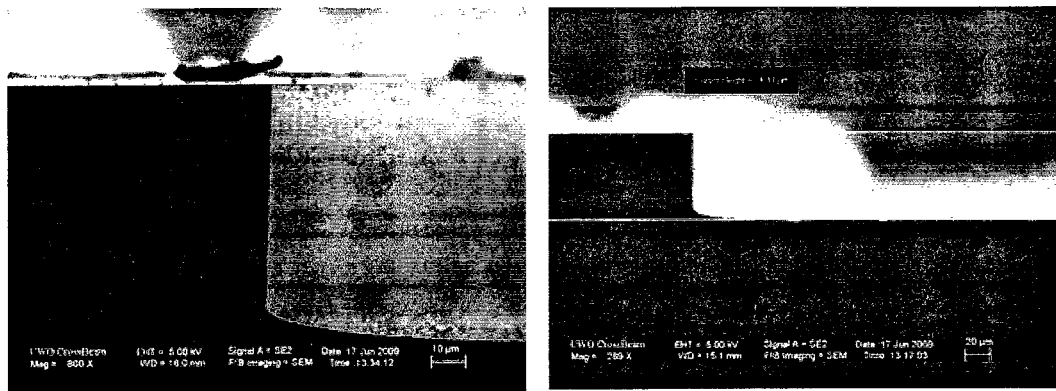


Figure 3.23 SEM profiles of the silicon wafers.

### **Step 3: Chromium (Cr) and Gold (Au) Deposition**

- Gold layer is used as a conductive layer.
- Chromium is used as an adhesion layer since Gold can't be deposited directly on Silicon.
- Electron Beam Evaporation method has been used to deposit both layers using Intlvac Nanochrome™ Deposition System

**Process Flow:**

- Chromium Deposition: 40 nm seed layer was deposited at 20% power which gives a rate of 3.0 Å/sec.
- Gold Deposition: 100 nm gold layer was deposited at 30% power which gives a rate of 9.2 Å/sec.

**Step 4: Au Electroplating and Bonding**

- Gold layer of 3 μm is electroplated by immersing the wafers in the solution for a specified period of time to get the required thickness.
- Lens cap and etched wafer are bonded together using a thermo-compression bonding and sidewall conductive epoxy technique to complete the fabrication
- Dummy ports are filled with RF absorbing materials with matched resistances of 50 Ω.

Figure 3.24 show the fabrication process diagram for the Rotman lens.

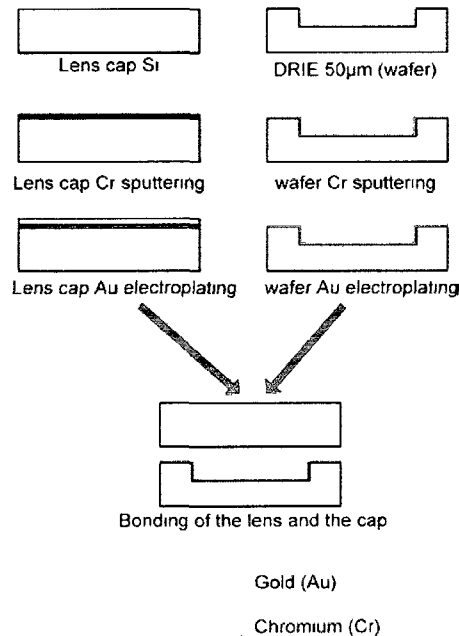


Figure 3.24 Rotman lens Fabrication process diagram.

Figure 3.25 shows the fabricated Rotman lens and the cap.

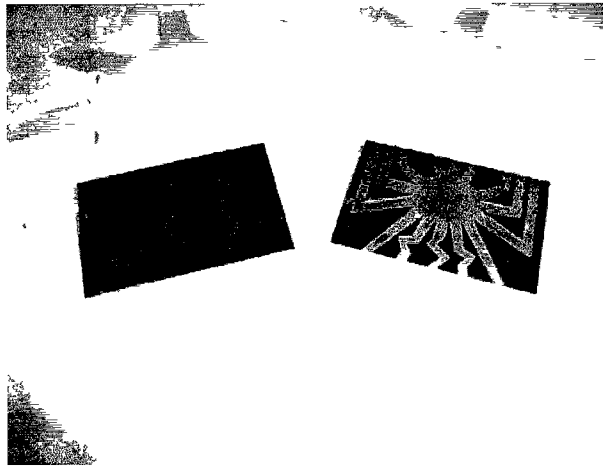


Figure 3.25 Fabricated Rotman lens and the cap.

Figure 3.26 shows the fabricated Rotman lens and the cap bonded together to complete the fabrication process

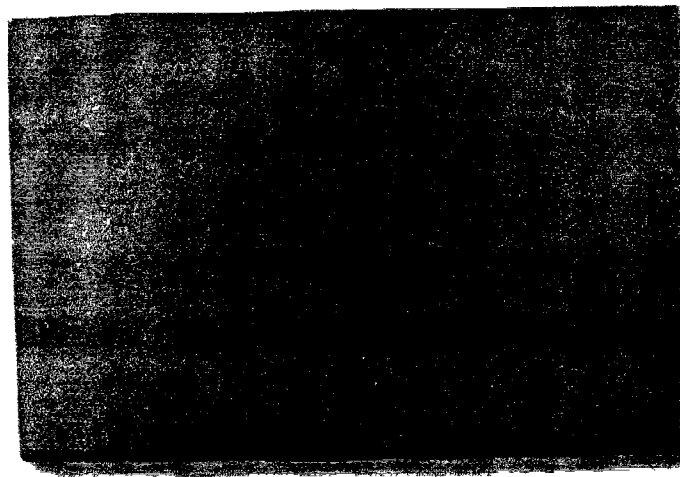


Figure 3.26 Fabricated Rotman lens after bonding process.

### 3.5 Conclusions

A new FMCW automotive radar architecture has been presented that can provide the best performance while addressing the design constraints, following the review of the state-of-the-art in automotive radars and requirements set by the auto industry for long range radar. The radar is to operate at the 77 GHz, a Rotman lens has been adopted to perform the operation of beamforming and beamsteering to eliminate the need for microelectronic based analog or digital beamforming engine. MEMS based RF switches have been selected to feed the FMCW signal to the beam ports of the Rotman lens. Microstrip based antenna arrays have been selected to radiate and receive the signal due to their established superior performance, ease of fabrication, and small planar geometry while offering high directivity and lower sidelobes.

The design of a MEMS based Rotman lens has been presented. The lens has a footprint area of  $27 \times 36.2 \text{ mm}^2$ , incorporates 3 beam ports, 5 array ports, and operates at 77 GHz. A novel  $\text{TE}_{10}$  mode rectangular waveguide type Rotman lens has been designed and fabricated. The new design enabled to reduce the lens size such that it can be batch fabricated using conventional micromachining techniques like conventional VLSI chips. The lens has been designed using full wave 3-D FEA simulation using industry standard HFSS software. The performance parameters of the Rotman lens are optimized to get excellent values for the insertion losses, return losses and characteristic impedance. A fabrication technique has been developed to fabricate the Rotman lens. The lens has been fabricated in the University of Waterloo, University of Western Ontario microfabrication facilities and assembled in Advotec company in Arizona. The device can provide a cost effective highly reliable and less complex solution compared to currently available radar based proximity detection systems for automobiles.

## **Chapter 4**

### **MEMS SP3T RF Switch**

The design and fabrication of a MEMS Single-Pole-Triple-Throw (SP3T) RF switch to sequentially feed the FMCW signal among the beam ports of a microfabricated Rotman lens that forms an integral part of a MEMS based 77 GHz automotive radar sensor has been presented. The series type MEMS RF switch relies on electrostatic actuation of a microfabricated cantilever beam and incorporates 1 input port and 3 output ports. Two different versions of the MEMS RF switch have been designed: a ground connecting bridge (GCB) conventional geometry where microfabricated bridges have been used to provide the ground connectivity and a new continuous ground (CG) without any bridge. Both the switches have been optimized for operation in the 77 GHz; however, the CG version provides improved performance as it eliminates the effects of coupling capacitance between the ports and the ground. The HFSS simulation results show that at 77 GHz, the CG configuration has 4 dB improvement for the return loss compared to the GCB version of the switch. The CG version of the switch also exhibits 0.5 dB improvement for insertion loss and 3 dB improvement for isolation as compared to the GCB version of the switch. The actuation voltage of the switch is 16.3 volts. The GCB type SP3T RF switch has been fabricated using the UWMEMS process and the fabrication of the CG version is in progress.

#### **4.1 MEMS RF Switch Overview**

RF switches are typically used in high frequency communication systems for signal routing, phase shifting, impedance matching and for changing the gain of amplifiers [52]. Spectrum allocation for different high frequency communication bands such as L-band (1-2 GHz), K- band (18–27 GHz), or W-band (75-110 GHz) sets different S-parameters requirements for the design of RF switches intended for use in those frequency bands. Consequently, different switching technology, such as electromechanical, Silicon FET, GaAs MOSFET, PIN diodes, and MEMS etc. are adopted to meet the design requirements specific to the target frequency range. A comparative overview of different RF switching systems is available in [53, 54]. Following [53, 54], at frequencies greater than a few GHz, the solid-state switches exhibit



large insertion loss and poor isolation whereas electromechanical switches exhibit slow switching speed, high isolation consequently, they are not suitable for the target 77 GHz MEMS radar. In contrast, MEMS based RF switches offer design factors not available in other RF switches, such as the setting of the gap height independently, change the dielectric that fills under the switching element from semiconductor to air and it change the effective area of switching.

In conclusion, MEMS based RF switches have excellent performance figures as they combine the low loss characteristic of the mechanical RF switches along with the small size characteristic of the semiconductor FET switches [55]. As the MEMS RF switches use air gaps for the OFF state, this result in excellent isolation and have very low insertion loss [55–58]. These switches also exhibit higher isolation among the ports in a multiport network to result in a lower leakage from an “ON” to an “OFF” port. Additionally, they have a very low actuation power consumption, faster switching time and speed, and extremely wide bandwidth characteristics [53, 54].

Actuation mechanisms used in MEMS RF switches include electrostatic, electromagnetic, magnetic, piezoelectric and thermal. However, the electrostatically actuated MEMS RF switches are the most efficient ones and electrostatic actuation has become the most common actuation mechanism for MEMS RF switches. They consume very low power and exhibits very large ON-OFF capacitance ratio.

Two common forms of MEMS RF switches are the series and the shunt types. In the series type, typically an electrostatically actuated cantilever beam is used to establish the connectivity between two RF ports whereas in the shunt type, an electrostatically actuated fixed-fixed beam is used to realize the switching operation.

#### **4.2 Cantilever MEMS RF Switches**

The cantilever structure consists of a thin strip of metal fixed at one end and is suspended over the metallic transmission line with a gap of a few micrometers. The cantilever can be connected in series with the transmission line as shown in Figure 4.1 in both OFF state (a) and ON state (b). When a bias voltage is applied between the cantilever and the lower actuation electrode, an electrostatic attraction force is developed between the cantilever beam and the lower actuation electrode. This force causes the cantilever to move down towards lower actuation electrode, independent of the charge

polarity. This creates an opposing tensile force on the cantilever as the structure starts bending. When the applied force reaches a threshold value, the tensile force is no longer balanced by the electrostatic force, so the cantilever abruptly falls to the bottom electrode and makes an electrical contact. The cantilever releases back when the applied voltage is reduced below the threshold value.

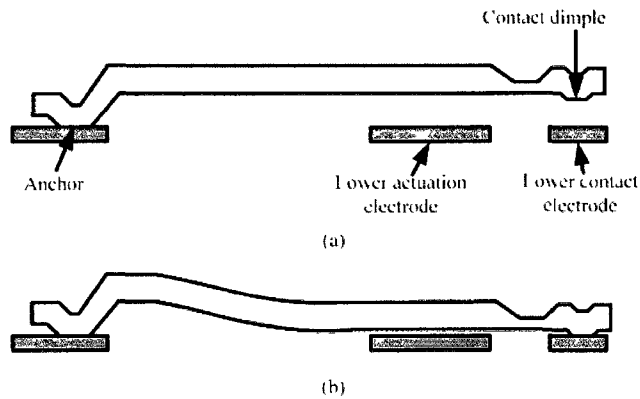


Figure 4.1 Cantilever MEMS RF switch.

### 4.3 Bridge MEMS RF Switches

The cross-sectional view of a bridge type MEMS RF switch is shown in Figure 4.2. The input RF signal traverses into a via interconnect to the top of the membrane. The output line, which is underneath the membrane, is connected using a thin metal strip.

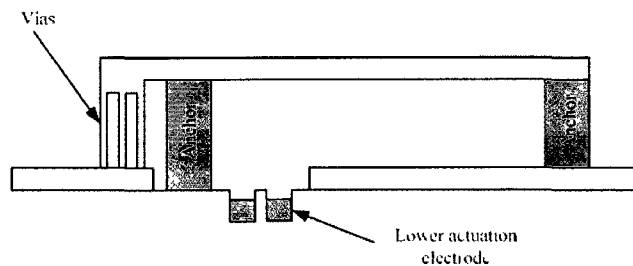


Figure 4.2 Bridge MEMS RF switch.

When an actuating voltage is applied to lower actuation electrode, the electrostatic force causes the bridge to pull downwards. With enough voltage, the bridge deforms and comes in contact with the bottom transmission line closing the two poles similar to the cantilever beam type MEMS RF switch.

Due to the establishment of a metal-metal contact during the switching operation, both types of switches exhibit good insertion loss and excellent linearity. Typically, a

bias tee circuit as shown in figure 4.3 is used to isolate the RF signal from the DC bias voltage [59], by bypassing the DC voltage to the ground via the inductor L and block it from the RF path by the capacitance C.

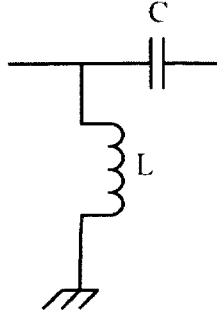


Figure 4.3 Bias tee.

#### 4.4 Design of SP3T MEMS RF Switch for 77 GHz Radar

As the Rotman lens has three beamports, an SP3T MEMS RF switch is necessary to sequentially feed the FMCW signal from the transceiver among the there beamports of the Rotman lens. A conceptual geometry of a typical SP3T switch is shown in figure 4.4. The switch has one input port (1) and three output ports (2, 3, 4). The grounds are connected via bridges. An input signal at port 1 can be directed to any of the three output ports by actuating the DC pad of the required port. The actuation of the DC pads is to be controlled by an FPGA or ASIC implemented control algorithm.

However, most of the reported designs of MEMS based SP3T RF switches use a discontinuous ground plane as shown in figure 4.4 [30, 31]. The grounds for individual ports are connected by using conductive bridges passing over the CPW lines as can be seen in the figure. These conducting bridges have a high resistance due to the limited size of the anchors and bridge widths. Additionally, the coupling capacitance between the bridge and the CPW underneath becomes significant at higher frequencies (77-81 GHz) as is visible in the HFSS simulation result as shown in figure 4.5. Both of these effects degrade the overall S-parameter figures associated with the switch performance resulting in a noisy and low efficiency operation at the target frequency range.

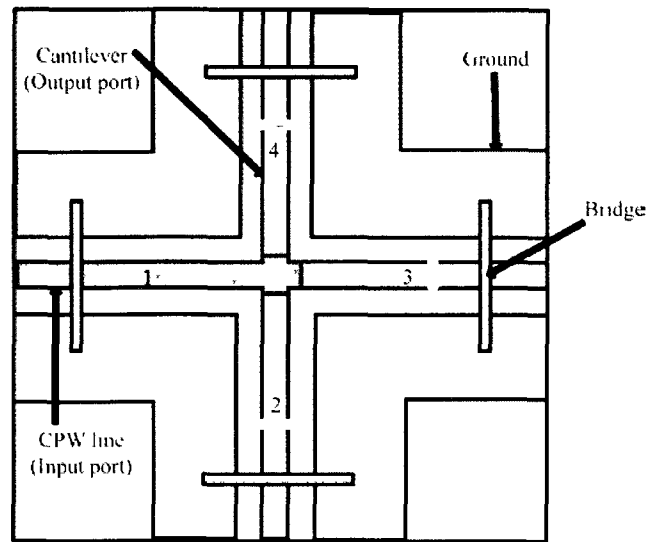


Figure 4.4 Conventional MEMS SP3T RF GCB switch.

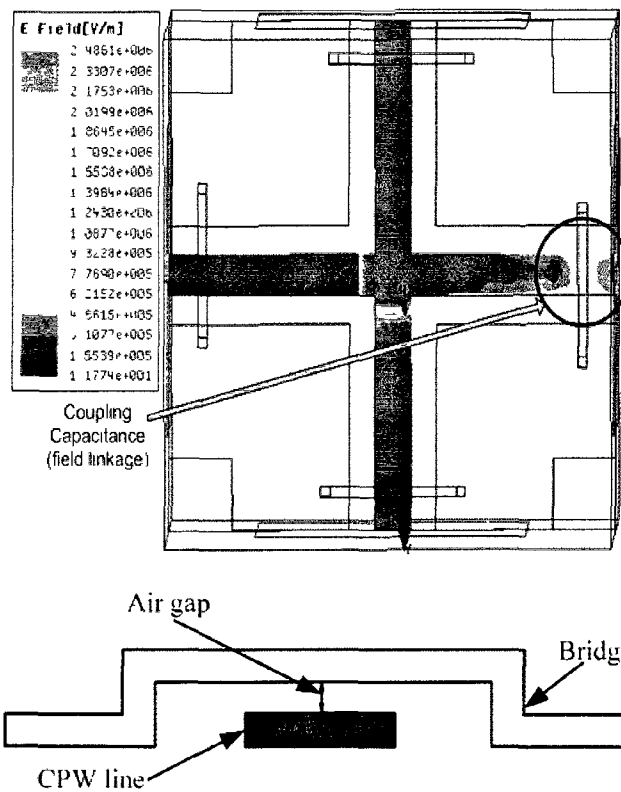


Figure 4.5 HFSS simulation shows the coupling capacitance between the GCB and a CPW line of a conventional MEMS SP3T RF operating at 77 GHz.

#### 4.5 CG MEMS SP3T RF Switch

To overcome this limitation of the conventional MEMS SP3T switches at the target frequency range of 77 GHz, a new SP3T RF switch has been designed that has a continuous ground plane as show in figure 4.6a. The RF switch consists of three actuating beams; each beam is connected to a 50  $\Omega$  CPW line at one end and is suspended on top of another CPW line of 50  $\Omega$  as shown in figure 4.6a. The beams and the coplanar lines are to be electrically connected with the drive and control circuitry using vias as shown in figure 4.6b.

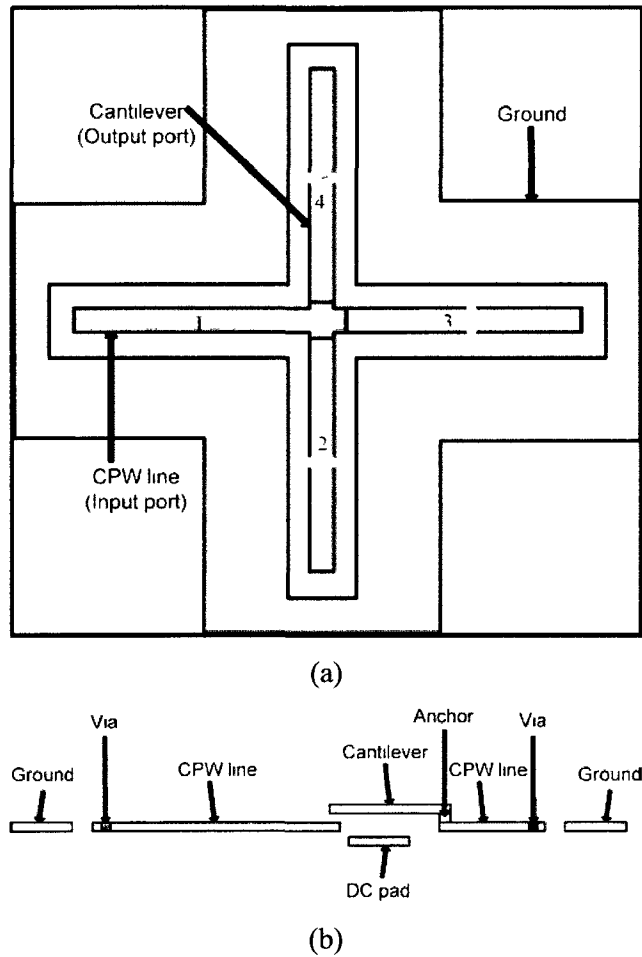


Figure 4.6 CG MEMS SP3T RF switch.

#### 4.6 Material Selection

As the target RF switch has been decided to be fabricated using the UWMEMS process available in the Centre for Integrated RF Engineering (CIRFE) of the University

of Waterloo due to lower fabrication cost, the material selection process and layer thicknesses are guided by the materials and design rules specific to the UWMEMS process. The materials and layer dimensions of the UWMMEMS process are shown in Table 4.1 [60].

Following Table 1, it appears that the G1 layer can be used to fabricate the CPW line and the ground and the G2 layer can be used to fabricate the cantilever beam. The 2.5  $\mu\text{m}$  thick sacrificial layer can be used to realize the anchor and the airgap. This dictates to choose the thickness of the CPW lines and the ground lines as 1  $\mu\text{m}$ . Similarly, the cantilever beam thickness needs to be 1.25  $\mu\text{m}$  (thickness of the G2 layer).

Table 4.1 Layer Names, Thickness and Mask Level.

Material	Thickness $\mu\text{m}$	Mask Level	Layer Description	Comments
Cr Chromium	0.04	Mask # 1	Resistive Voltage Biasing	Resistive layer
D1 Silicon Nitride	0.5	Mask # 2	Dielectric	Dielectric to cover Cr
G1 Gold 1	1	Mask # 3	Conductive Layer	0.5 $\mu\text{m}$ Cr + 1 $\mu\text{m}$ Au
D2 Silicon Nitride	0.7	Mask # 4	Dielectric	300 $\text{\AA}$ Cr + 0.7 $\mu\text{m}$ SiN
Sacrificial Layer	2.5	Mask # 5 & # 6	Sacrificial Layer	2.5 $\mu\text{m}$ Anchor and 1 $\mu\text{m}$ Dimple Openings
G2 Gold 2	1.25	Mask # 7	Top Conductive Layer	0.1 $\mu\text{m}$ Sputtered Au + 1.15 $\mu\text{m}$ Electroplated Au

#### 4.7 Mathematical Modeling

The cantilever beam stiffness  $k$  can be determined as follows [55]:

$$k = \frac{2Ew}{3} \left( \frac{t}{l} \right)^3 \quad (4.3)$$

Where  $E$  is the Young's modulus of the beam material,  $w$  is the beam width,  $t$  is beam thickness, and  $l$  represents the length of the beam

The pull-in voltage of the cantilever  $V_p$  can be calculated following the relation

$$V_p = \sqrt{\frac{8k}{27\epsilon_0 W} g_0^3} \quad (4.4)$$

Where  $g_0$  is the zero bias gap,  $\epsilon_0$  is the permittivity of free space, and  $W$  is the length of the DC pad.

The electrostatic force on the cantilever  $F$  can be determined as

$$F = \frac{\epsilon_0 A V^2}{2g^2} \quad (4.5)$$

Where  $A$  is the effective area of the capacitor and  $g$  is the physical separation between the contacts.

The deflection of the tip of the beam,  $\delta$  can be calculated from [61]

$$\delta = 6 \frac{F(1-\nu^2)L^3}{E} \frac{L^3}{Wt^3} \quad (4.6)$$

Where  $W$ ,  $L$  and  $t$  are the width, length and thickness of the beam respectively.  $E$  and  $\nu$  are the Young's modulus and poisson's ratio respectively and  $F$  is the electrostatic force.

Assuming the damping coefficient of the cantilever is relatively small, the switching time can be calculated as [62]

$$t_s = 0.584 \frac{V_p}{V_s f_0} \quad (4.7)$$

Where  $V_p$  is the pull-in voltage and  $V_s$  is the drive voltage. For fast switching,  $V_s$  is adopted to  $1.4V_p$ .

The up state capacitance  $C_u$  of the cantilever beam can be calculated as in [55]

$$C_u = C_s + C_p \quad (4.8)$$

Where  $C_s$  is the series capacitance between the beam and the transmission line and  $C_p$  is the parasitic capacitance between open ends of the transmission line

$C_s$  is represented by a parallel plate capacitance  $C_{pp} = \frac{\epsilon A}{g}$  and a fringing component of 30-60% of  $C_{pp}$ . The parasitic capacitance  $C_p$  of a CPW line of 40  $\mu\text{m}$  width is about 2fF.

The down state resistance  $R_s$  can be determined as in [55]

$$R_s = 2R_{s1} + R_l \quad (4.9)$$

Where  $2R_{s1}$  represent the transmission line resistance and  $R_l$  represent the DC contact resistance. The contact resistance depends on the size of the contact area, the mechanical force applied, and the quality of the metal-to-metal contact.

The CPW lines have been selected to design the target SP3T RF switch due to their smaller radiation loss and lower coupling to adjacent signal lines. The length of the cantilever has been chosen to be 150  $\mu\text{m}$  to realize a compact RF switch. In order to obtain a matching characteristic impedance of 50  $\Omega$ , the cantilever width of the three output ports (2, 3, and 4) and the input port 1 are chosen to be 40  $\mu\text{m}$ . The width of the ground line, the gap between the CPW line and the ground line have been optimized using HFSS™ as 100  $\mu\text{m}$  and 28  $\mu\text{m}$ , respectively.

The final design specifications for the SP3T RF switch are listed in Table 4.2.

Table 4.2 SP3T Design Specifications.

Parameter	Value	Unit
CPW line length	228	$\mu\text{m}$
CPW line width	100	$\mu\text{m}$
Characteristic impedance	50.5	$\Omega$
Input port length	300	$\mu\text{m}$
Port width	40	$\mu\text{m}$
Cantilever length	150	$\mu\text{m}$
Cantilever thickness	1.25	$\mu\text{m}$
Cantilever back length	80	$\mu\text{m}$
Bridge width	10	$\mu\text{m}$
Bridge height	2.5	$\mu\text{m}$
Bridge length	180	$\mu\text{m}$
Airgap thickness	2.5	$\mu\text{m}$
Frequency	77	GHz
Substrate height	635	$\mu\text{m}$

#### 4.8 HFSS and IntelliSuite Simulation Results for Both Types of RF Switches

The designed RF switches (both GCB type and the CG type) have been simulated using HFSS software to obtain the RF performance parameters and the IntelliSuite software has been used to obtain the static performance of the switch. A program code for



designing the RF switch in visual basic code (VB code) is shown in appendix B. Figure 4.7 shows that both the GCB type and the CG type switches exhibit a characteristic impedance of  $50.5 \Omega$  at the operating frequency of 77 GHz. Figures 4.8-4.12 shows the HFSS simulation results for S-parameters when a 77 GHz signal is fed at the input port (port 1 in figure 4.6) with one of the output ports (port 2 in figure 4.6) is actuated.

From the figures 4.8a and 4.8b, it is evident that while the GCB type switch exhibits a return loss better than -16 dB, the corresponding return loss for the CG type switch is better than -20 dB at 77 GHz. Thus, a return loss improvement of -4 dB can be achieved if the continuous ground version is used. The return loss figures compare better with the measured value of -15 dB for a MEMS cantilever type of the same width ( $40\mu\text{m}$ ) RF switch as reported in [63]. This validates the design of both types of switches. Figure 4.9(a) shows the HFSS simulation results for the insertion loss of the GCB switch (better than -1.1 dB) while figure 4.9 (b) shows the insertion loss of the CG switch (better than -0.65 dB) for the same simulation set up. Both the values compare better with the -3 dB measured insertion loss for the 77 GHz cantilever type switch published in [63]. Figures 4.10 (a) and 4.11 (a) show that isolations between the ports 1 and 3 , and the ports 1 and 4 with port 2 actuated are better than -13 dB for the GCB switch, while as the figures 4.10 (b) and 4.11 (b) show, isolations better than -16.5 dB can be achieved for the CG type switch. All of the isolation values are better than the -15 dB measured isolation value for the switch published in [63].

In summary, the CG configuration has improved the return loss by 4 dB compared with the GCB version of the switch. The insertion loss has improved by 0.5 dB and the isolation has been improved by 3 dB.

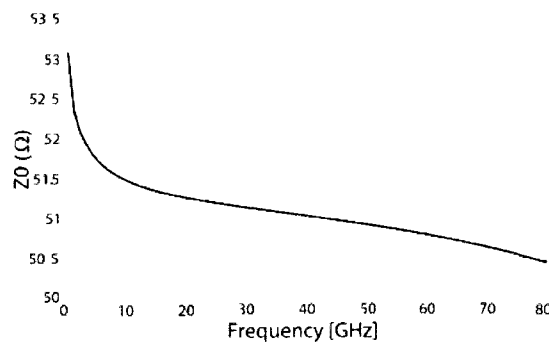
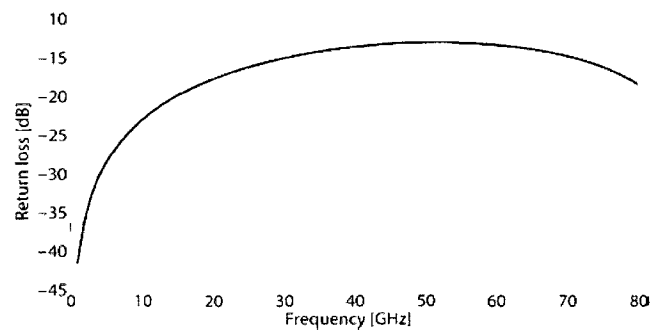
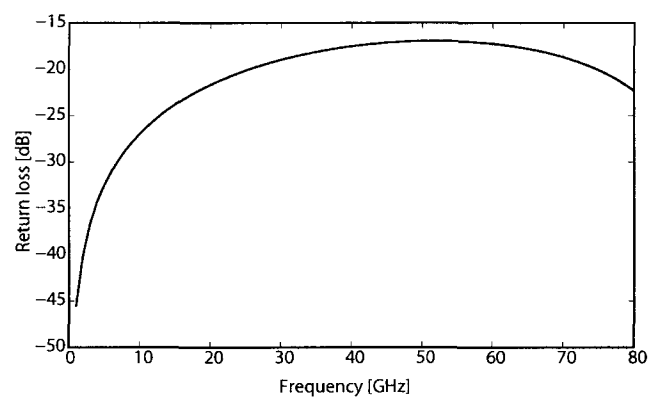


Figure 4.7 Characteristic impedance (Both GCB and CG type switches).

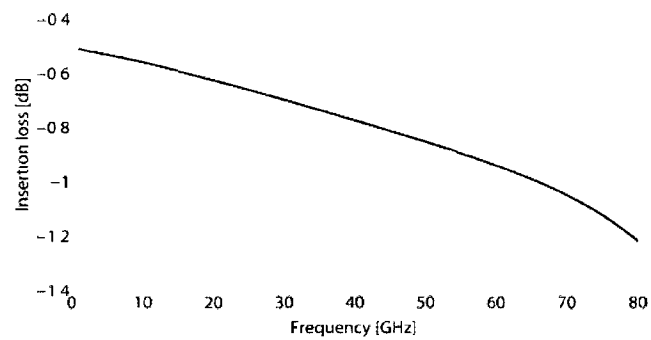


(a) GCB switch

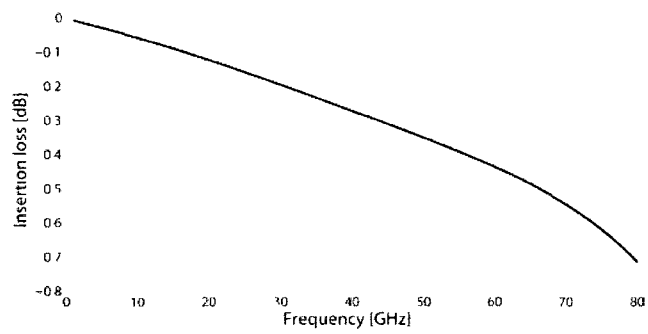


(b) CG switch

Figure 4.8 Return loss between ports 1 and 2.

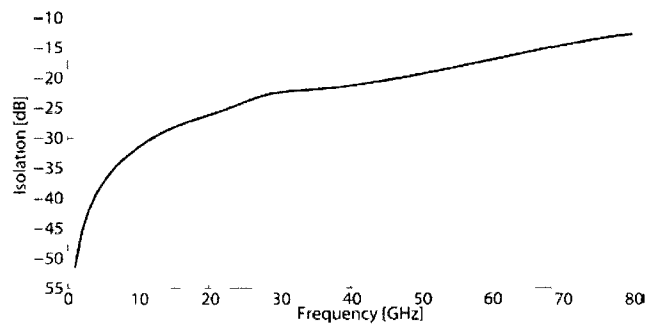


(a) GCB switch

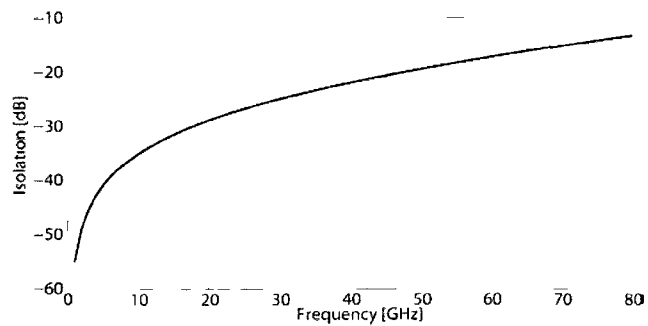


(b) CG switch

Figure 4.9 Insertion loss between ports 1 and 2.

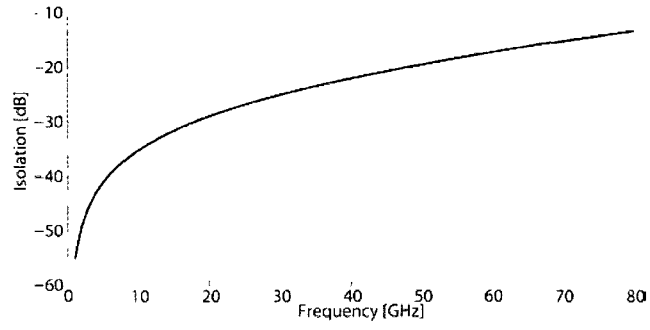


(a) GCB switch

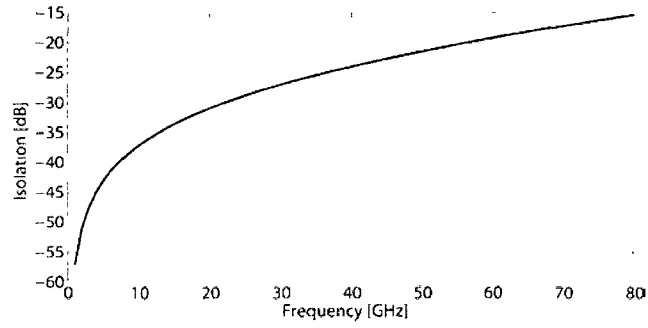


(b) CG switch

Figure 4.10 Isolation between ports 1 and 3.



(a) GCB switch



(b) CG switch

Figure 4.11 Isolation between ports 1 and 4.

Ports 1 to 2 actuation is identical to actuation of ports 1 to 4 and ports 1 to 3 and exhibit similar return loss, insertion loss and isolation values.

3-D electromechanical finite element analysis using industry standard software IntelliSuite has been carried out to determine the beam load-deflection simulation results. Figure 4.12 shows the cantilever collapsing state after carrying out the simulation. Figure 4.13 shows the cantilever displacement simulation, and figure 4.14 shows the pull-in voltage simulation of the beam. The cantilever stiffness  $k$  has been calculated using (4.3) to be of 1.203 N/m and the pull-in voltage  $V_p$  is calculated using (4.4) as  $16.3V$ .

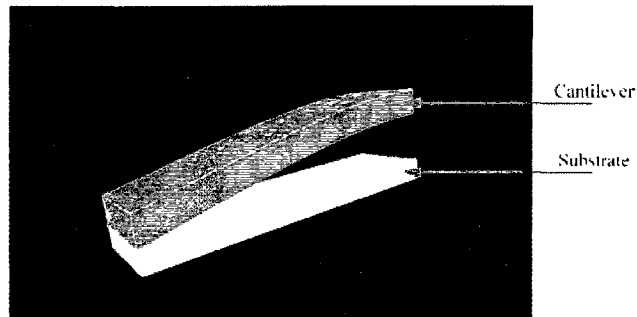


Figure 4.12 Cantilever collapsing simulation.

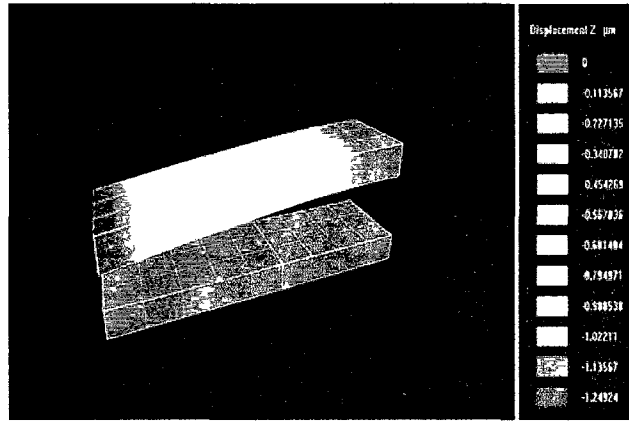


Figure 4.13 Cantilever displacement simulation.

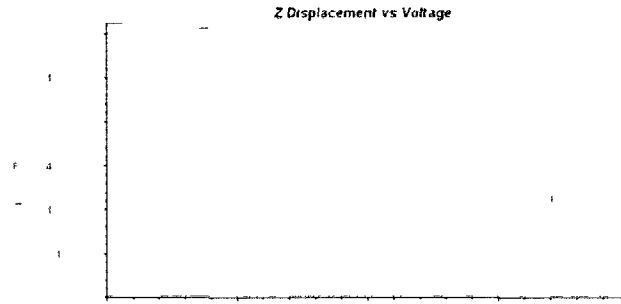


Figure 4.14 Cantilever pull-in voltage simulation.

In summary the RF characteristics of the designed SP3T are listed in table 4.3

Table 4.3 SP3T RF performance summary.

Parameter	Value	Unit
Return loss	-20	dB
Insertion loss	-0.65 dB	dB
Isolation	-16.5	dB
Pull in voltage	16.3	V
Beam stiffness	1.203	N/m
Switching time	$5.42 \times 10^{-12}$	sec
Up state capacitance	4	fF
Down state resistance	0.8	$\Omega$

#### 4.9 Fabrication

Surface micromachining has been the most important fabrication method for MEMS RF switches, but other processes such as bulk micromachining and fusion bonding are frequently used. Surface micromachining can be viewed as a three dimensional lithographic process and involves depositing various patterns of thin films on a substrate. Free-standing or suspended structures are created by applying patterns of sacrificial layers below non-sacrificial or release layers [64]. Selective etching of the sacrificial layers then leaves a suspended film which is capable of mechanical actuation.

The UWMEMS process is used to fabricate the SP3T RF switch on  $\text{Al}_2\text{O}_3$  substrate of a thickness of  $625\text{ }\mu\text{m}$ . All the cantilever beams and I/O ports are made of gold. The DC pads made of Chromium. A step by step fabrication process of the MEMS RF switch following the UWMEMS 7 masks process in the University of Waterloo is described below (both in GCB and CG versions). A low loss ceramic alumina wafer ( $\text{Al}_2\text{O}_3$ ) having a dielectric constant ( $\epsilon$ ) of 9.8 has been used as the substrate in surface micromachining process.

A  $0.5\text{ }\mu\text{m}$  thick layer of Chromium deposited on the wafer using an e-beam evaporation method as shown in figure 4.15. The layer is patterned using mask 1 and etched to create the CPW lines. The process of (Cr lift-off) is then used to pattern the DC biasing lines. The lift-off process is realized using thick insensitive resist (LOR) and negative photoresist on top.

An insulation layer is formed by depositing a  $0.7\text{ }\mu\text{m}$  of Silicon Nitride using PECVD process and patterned using mask 2 as shown in figure 4.16.

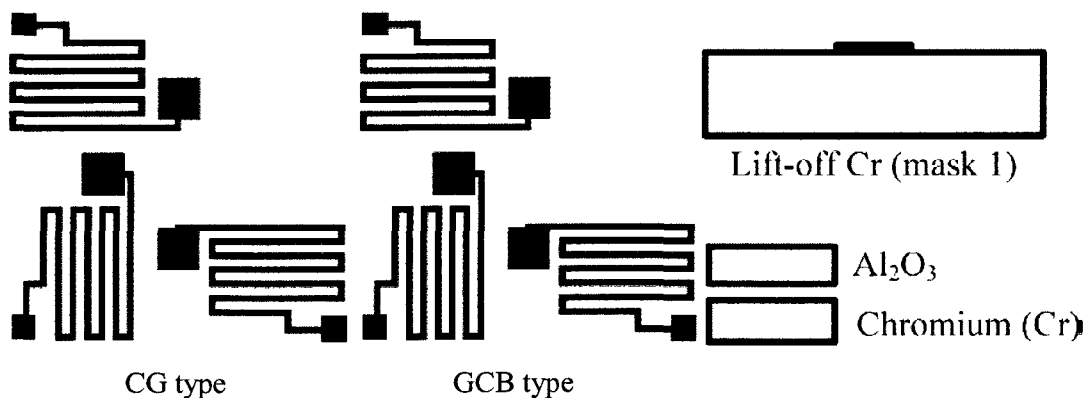


Figure 4.15 Chromium deposition and patterning.

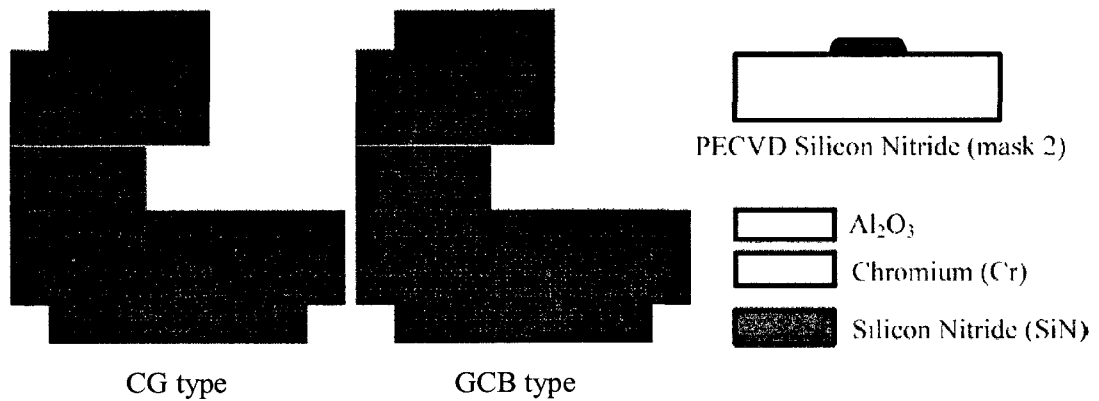


Figure 4.16 Silicon Nitride deposition and patterning.

Electron Beam Evaporation method has been used to deposit a  $0.5\ \mu\text{m}$  of Chromium and  $1\ \mu\text{m}$  of gold to form G1 layer as shown in figure 4.17.

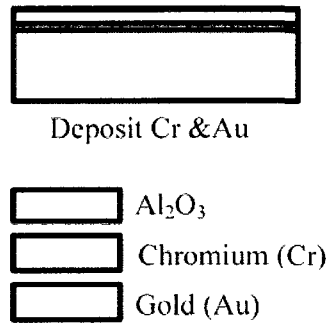


Figure 4.17 Chromium and Gold deposition.

Gold and chromium layers are patterned using mask 3 and etched to create the CPW lines as shown in figure 4.18

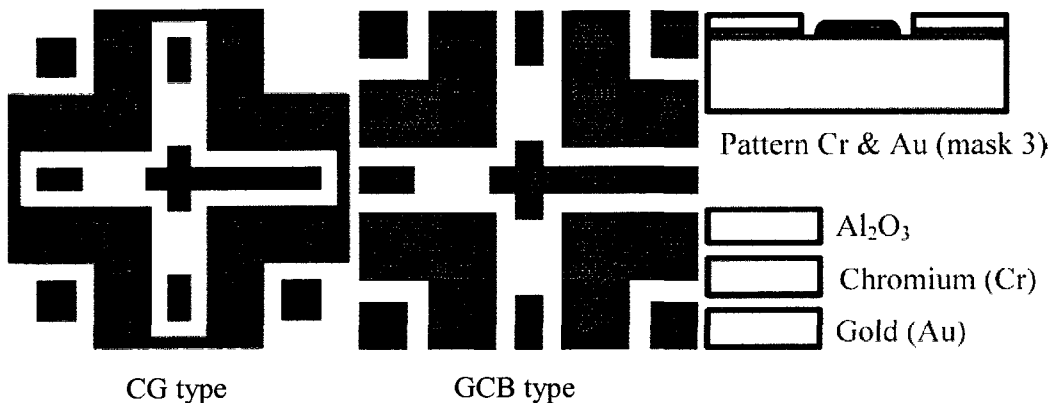


Figure 4.18 Gold and chromium patterning.

A  $2.5\ \mu\text{m}$  thick polyimide is added by spin deposition method to form a sacrificial layer to be patterned by mask 4 to form the anchors on the lower gold layer and patterned by

mask 5 to form a dimple on the top layer as shown in figure 4.19.



Figure 4.19 Anchor and dimple patterning.

A 1.25  $\mu\text{m}$  thick layer of gold is then deposited on the sacrificial layer to form the G2 layer as shown in figure 4.20.

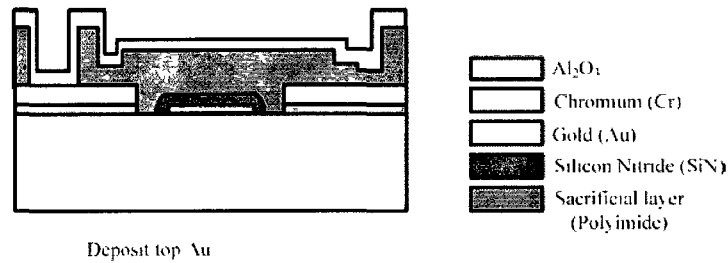


Figure 4.20 G2 deposition using Electron Beam Evaporation method.

The G2 gold layer is then patterned with mask 6 & 7 to form the cantilever beam and release holes in the cantilever beam as shown in figure 4.21.

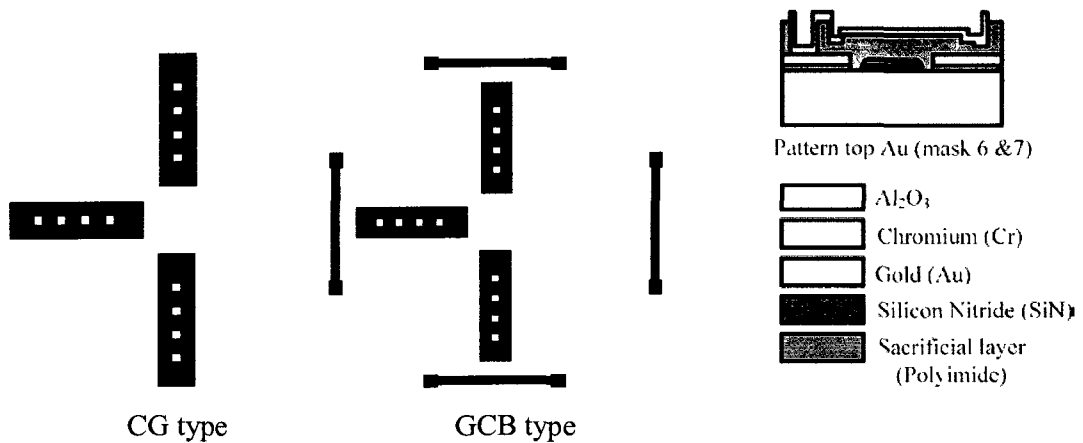


Figure 4.21 Pattern of the top gold G2.



The wafer is released by partial dry etching using oxygen plasma in RIE as shown in figure 4.22 and the release process is detailed in appendix C.

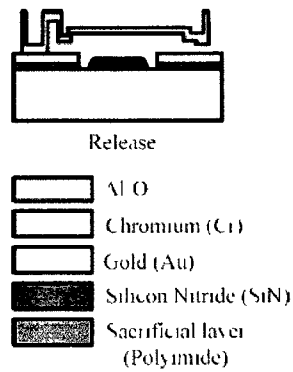


Figure 4.22 SP3T MEMS RF switch release.

The SEM pictures of the RF switch before and after release are shown in figure 4.23

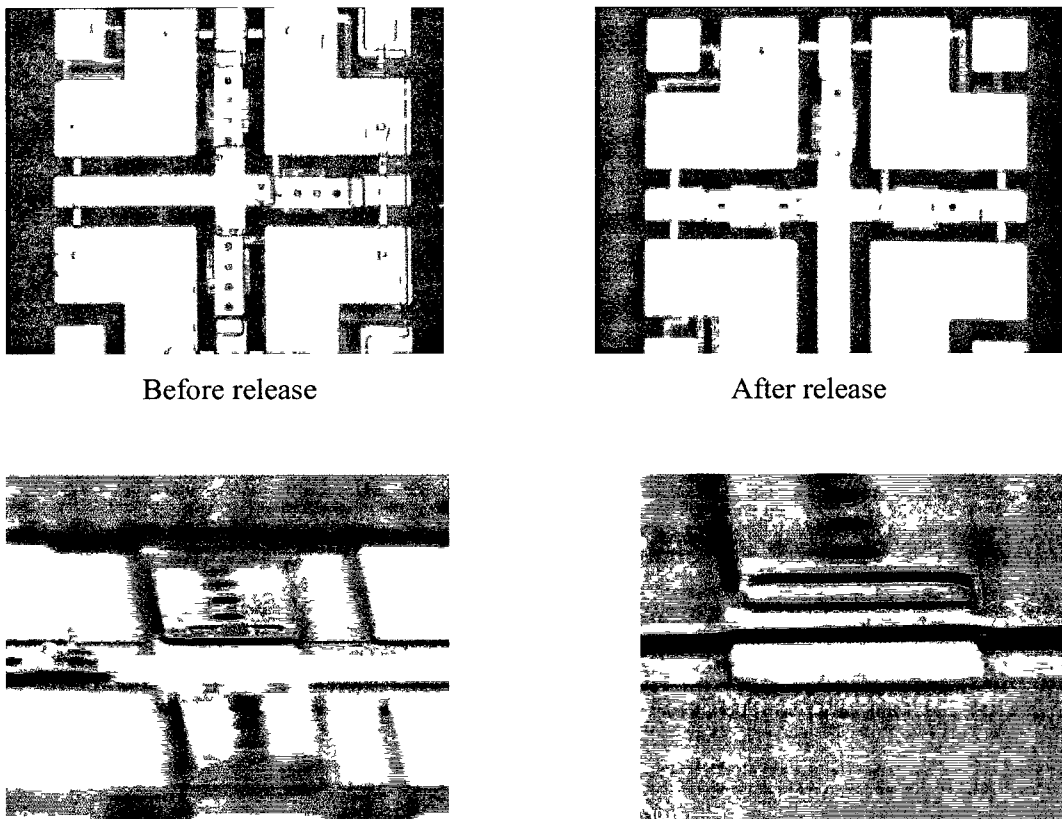


Figure 4.23 SEM pictures of the RF switch before and after release.

#### **4.10 Conclusions**

The Design, simulation and fabrication of a SP3T MEMS RF switch has been presented in the GCB and CG versions. The CG RF switch incorporates a continuous ground instead of typical bridge mechanism to connect the ground segments. This eliminates capacitive coupling between the bridge and the underneath beam to improve the RF switch performance. The RF switch has been modeled and simulated using HFSS and the simulation results show an insertion loss of better than -0.65 dB, -20 dB return loss, and isolation of -16.5 dB and an actuation voltage of 16.3 volts. A fabrication process sequence has been developed following University of Waterloo UWMEMS. The SP3T RF switch is to be used in conjunction with a MEMS based solid state Rotman lens to realize a compact MEMS radar for automotive collision avoidance application. The CG configuration has improved the return loss by 4 dB compared with the GCB version of the switch. The insertion loss has improved by 0.5 dB and the isolation has been improved by 3 dB.

# Chapter 5

## Microstrip Patch Antenna

The design, simulation and fabrication of a microstrip antenna array that forms an integral part of a MEMS based radar working in the 77 GHz range has been presented. The microstrip antenna array incorporates 5 sub-arrays and 12 patches in each sub-array. The design is based on a serial array inset fed method. The HFSS simulation results show that at 77 GHz, the microstrip antenna array exhibits a return loss of better than -15 dB, antenna array gain of 18.3 dB, half power beam width (HPBW) of 9° and an efficiency of 77% at the operating frequency of 77 GHz.

### 5.1 Microstrip Antenna Overview

Microstrip concepts were first proposed in the 1950's [35, 36] but their use did not gain momentum until the late 1960's and 1970's, mainly due to the lack of suitable low loss, dielectric substrates. Microstrip circuits consist of a single substrate with a ground plane on its bottom surface and a narrow strip of conducting transmission line on its top surface.

### 5.2 Microstrip Antenna

Microstrip antennas are planar resonant cavities that utilize the fringing fields along the edges of a microstrip patch to radiate electromagnetic energy. A typical microstrip patch antenna consists of a very thin metallic strip (patch) of thickness  $t$  placed on a dielectric substrate of thickness  $h$  and of dielectric constant of  $\epsilon_r$  above a ground plane as shown in figure 5.1

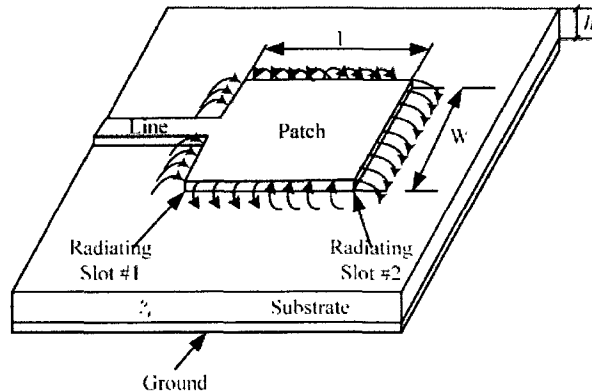


Figure 5.1 Microstrip patch antenna.

The maximum radiation pattern of a microstrip patch is normal to the patch. This is accomplished by properly choosing the field configuration of excitation of the patch. The fringing fields are cancelling each other along the microstrip patch length as shown in figure 5.1, so it can be represented by two radiating slots along the patch width. The radiation from these two relevant slots can be computed by considering them as a two-element array separated by a distance  $L$ . The amount of fringing is a function of the dimensions of the patch and the height of the substrate. The variation of the electric field along the patch length is represented in figure 5.2.

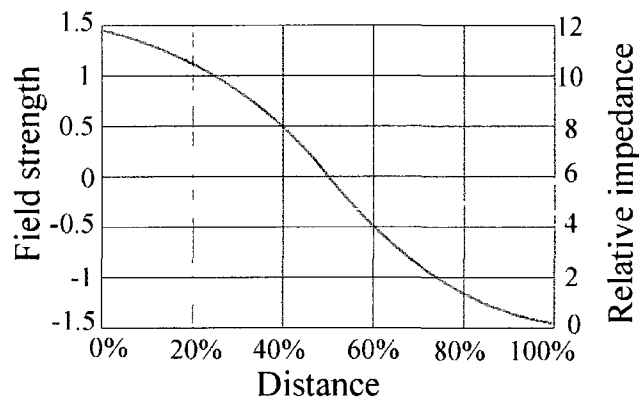


Figure 5.2 Electric field along the patch length.

There are numerous substrates that can be used for the design of microstrip antennas, and their dielectric constants are usually in the range of  $2.2 \leq \epsilon_r \leq 12$  [41]. The ones that are most desirable for good antenna performance are the substrates whose dielectric constant is in the lower end of the range because they provide better efficiency, larger bandwidth, loosely bound fields for radiation into space [37], also thin substrates are desirable for microwave circuitry because they require tightly bound fields to minimize undesired radiation and coupling, and lead to smaller element sizes.

Microstrip is basically printed circuits for microwaves and is usually fabricated like printed circuit boards, but requires higher-resolution photolithographic processes because of the dimensional accuracy required.

Microstrip limitations are few, the fundamental one being low power handling capability which may be overcome with the realization of good impedance matching circuitry. There are four separate mechanisms that can be identified for the power losses

and parasitic effects associated with microstrip lines [37], conductor losses, dissipation in the dielectric substrate, radiation losses, and surface wave propagation. Conductor and dielectric losses are lumped together and calculated as part of an attenuation coefficient for the line. Discontinuities such as abrupt open-circuit lines, steps, and bends will radiate to a certain extent and efforts must be made to reduce radiation and its undesirable side effects in circuits such as filters and amplifiers. Most of the propagating electromagnetic wave is confined to the region between the ground plane and the strip conductor but surface waves do account for some of the lost transmission power. Surface waves are waves trapped just beneath the surface of the dielectric substrate and propagate away from discontinuities in the form of higher order TM and TE radial modes.

The feed mechanism plays an important role in the design of microstrip patch antennas. There are many configurations that can be used to feed microstrip antennas. The four most popular are the microstrip line, coaxial probe, aperture coupling and proximity coupling [36-40]. A microstrip line inset feed was adopted in this research work, since the patch antenna typically yields a high input impedance and the current is low at the ends of a half-wave patch and increases in magnitude toward the center, the input impedance ( $Z=V/I$ ) could be reduced if the patch was fed closer to the center. One method of doing this is by using an inset feed. The inset fed microstrip line is suitable for developing high gain microstrip antenna arrays. The position or the inset feed length determines the input impedance [38].

There are many methods of analysis for microstrip antennas. The most popular models are the transmission-line, cavity, and full wave. The transmission-line model is the easiest of all, it gives good physical insight, but is less accurate and it is more difficult to model coupling. Compared to the transmission-line model, the cavity model is more accurate but at the same time more complex. However, it also gives good physical insight and is rather difficult to model coupling, although it has been used successfully. In general when applied properly, the full-wave models are very accurate, very versatile, and can treat single elements, finite and infinite arrays, stacked elements, arbitrary shaped elements, and coupling. It is the more popular and practical model.

Microstrip antennas are radiating structures derived from microstrip transmission lines (TL) as a means of integrating antennas with feed circuitry on the same substrate.

An obvious starting point for a simple analysis is thus the TL-model that uses a planar transmission line model to capture the transmission line properties, and uses an open end effect to capture the effects of radiation from the patch. A rectangular patch with length  $L$  and width  $W$  can be viewed as a very wide transmission line that is transversely resonating, with the electric field varying sinusoidally under the patch along its resonant length. The electric field is assumed to be invariant along the width  $W$  of the patch. Furthermore, it is assumed that the antenna's radiation comes from fields leaking out along the width, or radiating edges, of the antenna. The radiating edges of the patch can be thought of as radiating slots connected to each other by a microstrip transmission line.

The equivalent circuit for the microstrip patch is shown in figure 5.3. Each radiating slot is represented by a parallel equivalent admittance  $Y$  (with conductance  $G$  and susceptance  $B$ ). The slots are labeled as slot 1 and slot 2.

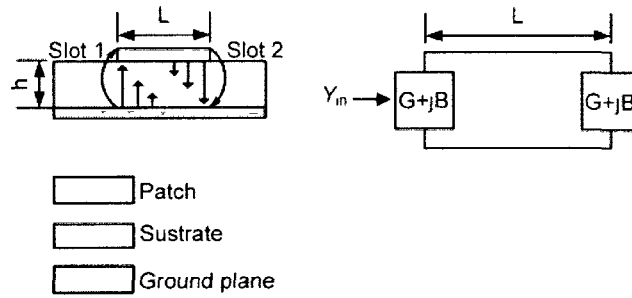


Figure 5.3 Microstrip patch equivalent circuit.

Based on the analysis presented so far, an inset fed microstrip antenna array has been selected for the target 77 GHz MEMS radar. A straightforward transmission-line model has been used to accurately model and analyze the designed microstrip inset fed antenna array. In the design, the substrate electrical parameters, feed line width, slot size and position are used to optimize the array performance. Impedance matching is performed by controlling the width of the feed line and the length of the slot.

The use of microstrip antennas in most practical applications usually requires multiple elements in an array configuration to achieve the required gain and beamwidth. The design of these arrays require feed structures that are impedance matched to the patch radiators and provide the proper amplitude and phase required at each radiator. Current Finite Element Analysis (FEA) software HFSS is available that represents microstrip network components by equivalent transmission lines.

### 5.3 Microstrip Single Patch Design

The rectangular patch that has been adopted in this research work is by far the most widely used configuration because it is very easy to analyze using the transmission-line model, which is the most accurate for thin substrates [39]. The substrate that has been used (RT 5880) is of thickness of 125  $\mu\text{m}$  which feature's the following:

- Lowest electrical loss for reinforced material.
- Low moisture absorption.
- Isotropic
- Uniform electrical properties over frequency.
- Excellent chemical resistance

RT 5880 specifications are listed in table 5.1.

Table 5.1 RT 5880 Specifications

Dielectric constant $\epsilon_r$	2.2
Dissipation factor, $\tan \delta$	0.0004
Moisture absorption	0.02 mg %
Thermal conductivity	0.20 w/m/k

To start the design process a predetermined values of dielectric constant, substrate height, resonant frequency, and patch length have to be specified. In this research work, the dielectric constant  $\epsilon_r$ , of 2.2, substrate height  $h$  of 125  $\mu\text{m}$  and resonance frequency  $f_r$  of 77 GHz has been predetermined. The patch length  $L$ , have to be  $\lambda/2$  to resonate at the operating frequency. The patch width  $W$  can be calculated as following [37].

$$W = \frac{1}{2f_r \sqrt{\mu_0 \epsilon_0}} \sqrt{\frac{2}{\epsilon_r + 1}} = \frac{c}{2f_r} \sqrt{\frac{2}{\epsilon_r + 1}} \quad (5.1)$$

Where

$\mu_0$  Permittivity of the air

$\epsilon_0$  Dielectric constant of the air

$c$  Velocity of the light

The next step in designing the patch is to calculate the effective dielectric constant  $\epsilon_{\text{reff}}$ . The effective dielectric constant is defined as the dielectric constant of the uniform dielectric material so that the microstrip line has identical electrical characteristics, particularly propagation constant, as the actual line that confine all the magnetic field lines in the propagated wave or that accounts for the fringing and wave propagation in the line [37]. The effective dielectric constant is also a function of frequency. As the frequency of operation increases, most of the electric field lines concentrate in the substrate. Therefore the microstrip line behaves more like a homogeneous line of one dielectric (only the substrate), and the effective dielectric constant approaches the value of the dielectric constant of the substrate. For a line with air above the substrate, the effective dielectric constant has values in the range of.

$$1 < \epsilon_{\text{reff}} < \epsilon_r \quad (5.2)$$

$$\epsilon_{\text{reff}} = \frac{\epsilon_r + 1}{2} + \frac{\epsilon_r - 1}{2} \left[ 1 + 12 \frac{h}{W} \right]^{-1/2} \quad (5.3)$$

Where

$\epsilon_{\text{reff}}$  Effective dielectric constant

$\epsilon_r$  Substrate dielectric constant

$h$  Substrate height

$W$  Microstrip patch width

Because of the fringing effects, electrically the patch of the microstrip antenna looks greater than its physical dimensions. For the principal  $E$ -plane ( $xy$ -plane), this is demonstrated in Figure 5.4 where the dimensions of the patch along its length have been extended on each end by a distance  $\Delta L$ , which is a function of the effective dielectric constant  $\epsilon_{\text{reff}}$  and the width-to-height ratio ( $W/h$ ).



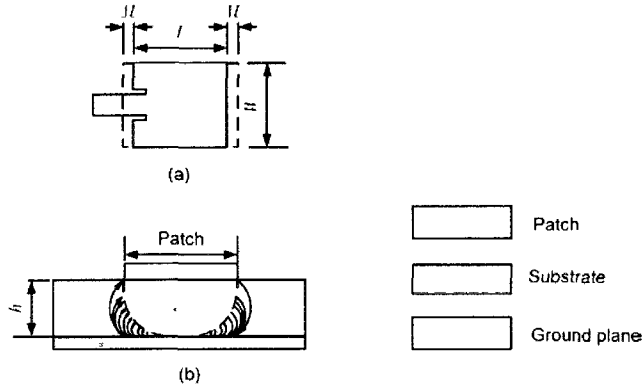


Figure 5.4 Physical and effective length of microstrip patch.

The normalized extension of the length is [37].

$$\frac{\Delta L}{h} = 0.412 \frac{(\epsilon_{reff} + 0.3) \left( \frac{W}{h} + 0.264 \right)}{(\epsilon_{reff} - 0.258) \left( \frac{W}{h} + 0.8 \right)} \quad (5.4)$$

Since the length of the patch has been extended by  $\Delta L$  on each side, the effective length of the patch is now

$$L_{eff} = L + 2\Delta L \quad (5.5)$$

The resonant frequency of the microstrip antenna  $f_r$  is a function of its length given by

$$f_r = \frac{c}{2L\sqrt{\epsilon_r}} \quad (5.6)$$

As the substrate height increases, fringing also increases and leads to larger separations between the radiating edges ( $L$ ) that in turn lowers the resonant frequency following (5.6).

Ideally the two slots should be separated by  $\lambda/2$ . However, because of fringing the length of the patch is electrically longer than the actual length. Therefore the actual separation of the two slots is slightly greater than  $\lambda/2$ . If the reduction of the length is properly chosen then (typically  $0.48\lambda < L < 0.49\lambda$ ) [38], the characteristic impedance  $Z_0$  is real, or

$$Z_0 = \frac{120\pi}{\sqrt{\epsilon_{reff}} \times \left[ \frac{w}{h} + 1.393 + \frac{2}{3} \ln \left( \frac{w}{h} + 1.444 \right) \right]} \quad (5.7)$$

To find the exact inset length  $y_0$  to achieve 50  $\Omega$  input impedance following [37] as following

$$y_0 = 10^{-4} \left\{ \frac{0.001699\varepsilon_r^7 + 0.13761\varepsilon_r^6 - 6.1783\varepsilon_r^5 + 93.187\varepsilon_r^4 - 682.69\varepsilon_r^3 + 2561.9\varepsilon_r^2 - 4043\varepsilon_r + 6697}{2} \right\} \frac{L}{2} \quad (5.8)$$

The radiation pattern of the patch is given by:

$$E_\theta = \frac{\sin\left(\frac{kW \sin \theta \sin \phi}{2}\right)}{\frac{kW \sin \theta \sin \phi}{2}} \cos\left(\frac{kL}{2} \sin \theta \cos \phi\right) \cos \phi \quad (5.9)$$

$$E_\phi = -\frac{\sin\left(\frac{kW \sin \theta \sin \phi}{2}\right)}{\frac{kW \sin \theta \sin \phi}{2}} \cos\left(\frac{kL}{2} \sin \theta \cos \phi\right) \cos \theta \sin \phi \quad (5.10)$$

Where  $k$  is the propagation constant given by  $k = 2\pi/\lambda$

The magnitude of the fields is given by

$$f(\theta, \phi) = \sqrt{E_\theta^2 + E_\phi^2} \quad (5.11)$$

The patch parameters that have been found above then optimized using FEA software HFSS to finalize the patch size and obtain it's RF performance. The microstrip patch feed line width is optimized using Advanced Design System (ADS) software and the inset fed is optimized using the HFSS software.

The standard procedure for antenna design starts with some pre-determined performance specifications the antenna is to meet. Based on these specifications, all the possible antenna configurations capable of meeting these requirement are evaluated, with their advantages and disadvantages detailed, and the most suitable configuration selected. When the antenna configuration is determined preliminary design work continues with selection of a substrate. This process is also performed by evaluating all potential substrate alternatives. A selection is made with equal emphasis on performance and manufacturability. Based on the results from these studies, microstrip antenna array design is to be pursued and be produced on Rogers RT5880 laminate material, because it provide better efficiency, larger bandwidth, loosely bound fields for radiation into space [39], also it's desirable for microwave circuitry because they require tightly bound fields

to minimize undesired radiation and coupling, and lead to smaller element sizes. This concludes the preliminary design work and provides the framework for the design of the radiating antenna element and the antenna array.

#### **5.4 Design Requirements for Target Automotive Radar Antenna**

The target application of this research work is to design an automotive radar antenna to be used at 77 GHz as an integral part of a MEMS based long range radar (LRR). The beamwidth required by for automotive radar is a crucial factor in the design process. A beamwidth of  $5^\circ$  was suggested by [29] to be sufficient for a LRR coverage, while a  $10^\circ$  beamwidth is considered as a reasonable value for automotive radars as stated in [40]. It's obvious from figure 3.6 that in order to cover two lanes at a distance of 100m, a  $4^\circ$  is required to cover a target at this range.

To realize a HPBW of 9-10 degrees it is necessary to use an array of microstrip patches. Based the industry requirements for a long range automotive radar [12, 13], a design requirement has been set to realize a high efficiency,  $9^\circ$  wide HPBW microstrip antenna array operating at 77 GHz.

#### **5.5 Microstrip Antenna Array Design Considerations**

Single element microstrip antennas typically have low gain, low radiation efficiency, and wide beam widths [38]. Most applications require higher antenna performance and must resort to an array of elements. Microstrip antenna array designs are based on element type, feed methods, and substrate configurations to be employed. In applications where antenna movement, multipath, or changing environments degrade antenna performance, adaptive microstrip beam steering arrays may be used. In large arrays, using a large number of array elements, feed losses may be excessive. There exists a practical limitation on array gain of approximately 20dB [39]. The goal of antenna array design is to find the easiest way to create multi-element units which meet or exceed design specifications with the minimum fabrication labour. In these large arrays, failure of a small portion of the array elements, or their feed circuitry, may cause a significant degradation in the antenna performance.

##### **5.5.1 Microstrip Antenna array Design**

Planar arrays are the most frequently designed form of microstrip array designed for automotive radar applications [12, 13]. The reasons for this are simply better

performance due to more control parameters that the designer can utilize to produce symmetrical patterns with lower side lobes [37]. The feed lines for a microstrip antenna array are characterized as in [34] as (1) series feed, (2) corporate feed, and (3) a combination of both series and corporate feed. The feed line lengths for a series fed array patches are inherently minimized compared to corporate fed, thus reducing line radiation and dissipation losses, which increase array efficiency. Further, in large arrays high-power feed lines are decoupled from elements radiating low-power levels. This permits tighter control of aperture distributions. Steered beams can be easily achieved, and the series configuration is particularly applicable when frequency scanning with single or dual polarization is desired.

Assuming that the designed array include  $N$  elements, and that all the elements have identical amplitudes but each succeeding element has a  $\beta$  progressive phase lead current excitation relative to the preceding one ( $\beta$  represents the phase by which the current in each element leads the current of the preceding element). The array factor  $AF$  can be obtained as follows

$$AF = \sum_{n=1}^N e^{j(n-1)\psi} \quad (5.9)$$

Where

$$\psi = kd \cos \theta + \beta$$

$N$  = Number of array patches

$k$  = Propagation constant ( $2\pi/\lambda$ )

$d$  = Space between elements

$\theta$  = Scanning angle

The directivity of the array  $D$  can be obtained as

$$D = 2N \left( \frac{d}{\lambda} \right) \quad (5.10)$$

The quality factor, bandwidth, and efficiency are antenna figures-of-merit. The quality factor is a figure-of-merit that is representative of the antenna losses. Typically there are radiation, conduction (ohmic), dielectric and surface wave losses. Therefore the total quality factor  $Q_t$  is influenced by all of these losses and is, in general, written as [53]

$$\frac{1}{Q_t} = \frac{1}{Q_{rad}} + \frac{1}{Q_c} + \frac{1}{Q_d} + \frac{1}{Q_{sw}} \quad (5.11)$$

where

$Q_t$  = total quality factor

$Q_{rad}$  = quality factor due to radiation (space wave) losses

$Q_c$  = quality factor due to conduction (ohmic) losses

$Q_d$  = quality factor due to dielectric losses

$Q_{sw}$  = quality factor due to surface waves

For very thin substrates, the losses due to surface waves are very small and can be neglected. However, for thicker substrates they need to be taken into account [53]. For very thin substrates ( $h \ll \lambda_0$ ), there are approximate formulas to represent the quality factors of the various losses [81]. These can be expressed as

$$Q_c = h \sqrt{\pi f \mu \sigma} \quad (5.12)$$

$$Q_d = \frac{1}{\tan \delta} \quad (5.13)$$

$$Q_{rad} = \frac{2 \omega \varepsilon_r}{h G_t / l} \quad (5.14)$$

Where

$h$  = Substrate thickness

$\delta$  = Loss tangent of the substrate material

$\sigma$  = Conductivity of the conductors associated with the patch and ground plane

$G_t / l$  = Total conductance per unit length of the radiating aperture

The bandwidth of the antenna is inversely proportional to the  $Q_t$  of the antenna and it is identified by

$$\frac{\Delta f}{f_0} = \frac{1}{Q_t} \quad (5.15)$$

The radiation efficiency of an antenna is defined as the power radiated over the input power. It can also be expressed in terms of the quality factors as [53]

$$Efficiency = \frac{Q_t}{Q_{rad}} \quad (5.16)$$

Array element spacing has to be in the range of  $\lambda_g$  to avoid grating lobes, where  $\lambda_g$  is guided wavelength defined as follows.

$$\lambda_g = \frac{\lambda}{\sqrt{\epsilon_r}} = \frac{c/f}{\sqrt{\epsilon_r}} \quad (5.17)$$

This spacing and amplitude distribution will be verified using simulations on the commercial full wave analysis software package HFSS. These simulations are performed separately on the linear arrays. These results should verify that the required spacing and amplitude distribution are being used. The simulated results will also be able to provide some information on the degree of mutual coupling between elements along these linear array planes. The final part of the array design is the creation of a computer model of the complete antenna array.

Through simulations it has been determined that 5 series fed linear arrays with 12 microstrip patches in each of the arrays as shown in figure 5.5 can realize a beam width of 9-10 degrees when they are fed simultaneously from the 5 array ports of the MEMS Rotman lens.

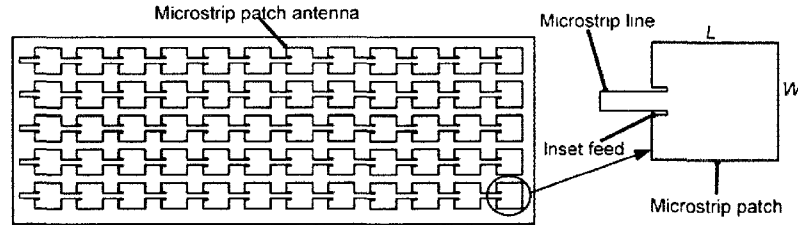


Figure 5.5 Microstrip antenna array.

Another parameter is the inset feed size required to obtain a well-matched, bandwidth and operating impedance while trying to optimize the microstrip antenna array performance. The antenna size must be adjusted whenever the substrate thickness is changed. The center frequency is controlled using the dimensions of the radiating patch, and also the spacing between these radiating elements. The inset feed length and a matching circuit will be used to match the antenna to a 50 ohm system impedance.

Based on the analysis parameter models presented in equations above and then employing the optimization technique using the industry standard full wave analysis

software HFSS, the final design specifications for the target microstrip antenna array are determined. Table 5.2 summarizes the specifications for the designed microstrip antenna array.

Table 5.2 Microstrip Antenna Array Specifications

Parameter	Value
Substrate thickness	125 $\mu$ m
Array length	32 mm
Array width	12 mm
Number of sub arrays	5
Number of patches in every sub array	12
Frequency	77 GHz
Wavelength	3.89 mm
Space between elements	$\lambda_g$
Patch dimensions	$\lambda_g/2$
Gain	18.3 dB
Efficiency	77%
Half power beam width (HPBW)	9°
Sidelobe power	3.5 dB

A layout of the designed array is shown in figure 5.5.

## 5.6 Microstrip Antenna Simulation Results

The radiation patterns obtained with a single element in general have relatively wide beamwidths and a low value of directivity. To obtain narrow beamwidths, high directivity, low side lobes or some other particularly desirable radiation characteristic, a group of antenna elements is used. This group of antenna elements is usually referred to as an antenna array or simply as an array. A program code for designing the microstrip antenna array in visual basic code (VB code) is shown in appendix D. Figure 5.6 shows the array return loss of -15 dB at the operating frequency compared to -7 dB in [40]. Which represent the microstrip antenna array transmission loss. Figure 5.7 shows the Microstrip antenna array gain of 18.3 dB compared to [40] of 17.5 dB and half power beam width (HPBW) of 9° compared to [40] of 12°. The high gain achieved and the sharp beam width will make this antenna array identical for automotive radar sensor applications that require narrow beam and high gain. Figure 5.8 shows the antenna array gain versus frequency which indicates a gain of 18.3 dB.

Figure 5.9 shows the antenna array efficiency at the operating frequency of 77% compared to 69% in [40]. Since The antenna efficiency is a factor used to account for all losses experienced. There are three mechanisms for loss in the antenna. The antenna will experience a mismatch loss if the antenna is not well matched to the feed circuit. The largest source of antenna losses are usually the conductor and dielectric losses, and for this high efficiency achieved through fine design and optimization processes made it well matched with the other components of the MEMS based automotive radar.

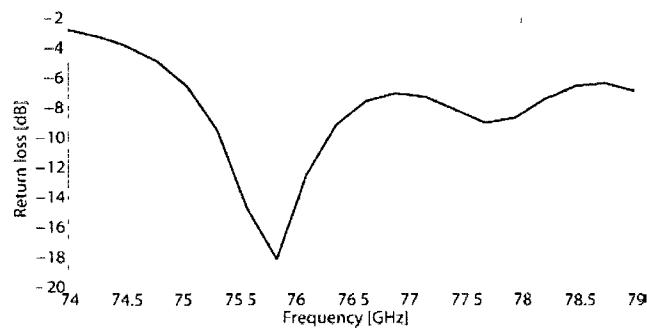


Figure 5.6 Microstrip antenna array return loss.

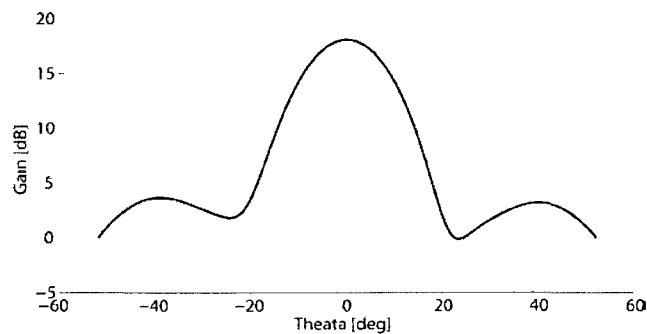


Figure 5.7 Microstrip antenna array gain and half power beam width (HPBW).



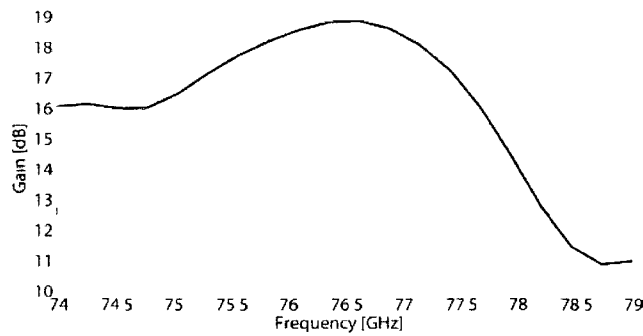


Figure 5.8 Antenna array gain versus frequency.



Figure 5.9 Antenna array efficiency.

## 5.7 Microstrip Antenna Fabrication

The microstrip antenna array has been fabricated using the facilities at the Clark MXR company in Dexter, Michigan using the PCB and ultra fast laser pulses technology [65]. The most fundamental feature of laser-matter interaction in the very fast pulse regime is that the heat deposited by the laser into the material does not have time to move away from the work spot during the time the laser pulse is illuminating the material. The duration of the laser pulse is shorter than the heat diffusion time. This is a very unusual and very desirable regime, which can be reached only with ultrafast lasers. This regime has numerous advantages as illustrated in Figure 5.10.

- 1) Because the energy does not have the time to diffuse away, the efficiency of the machining process is high. The laser energy has nowhere to go (or more precisely does not have the time to move away). It just piles up at the level of the working spot, whose temperature rises instantly past the melting point of the material and goes, very quickly, well beyond even the evaporation point. In fact, the temperature keeps on climbing into what is called the plasma regime.

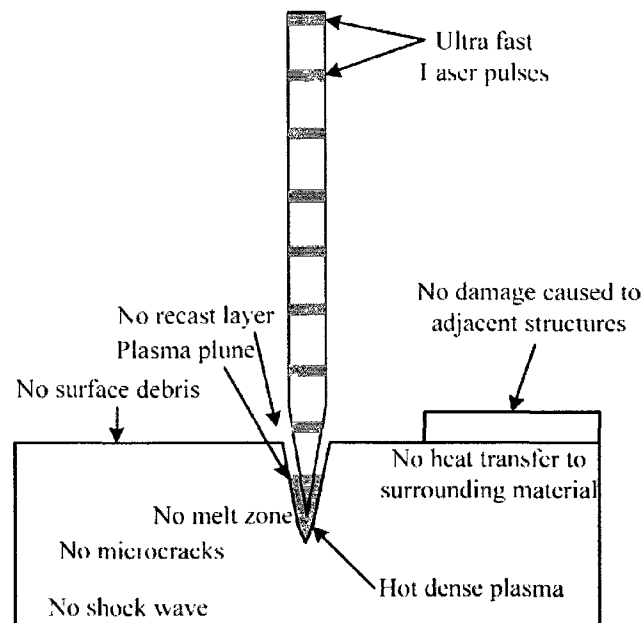


Figure 5.10 Ultrafast laser pulses [65].

- 2) Femtosecond lasers, deliver an incredible amount of peak power. These systems routinely deliver 5 to 10 Gigawatts of peak power (this is more than the average power delivered by a large nuclear plant). The laser intensity easily reaches the hundreds of Terawatts per square centimetre range at the work spot. Absolutely, positively nothing else that is man-made gets anywhere close to this power density.
- 3) No materials can withstand the forces at work at these power densities. This means that with ultrafast laser pulses we can machine very hard materials, as well as materials with extremely high melting points such as Molybdenum, Rhenium, etc.
- 4) After the ultrafast laser pulse creates the plasma in the surface of the material, the pressures created by the forces within it cause the material to expand outward from the surface in a highly energetic plume or gas. The internal forces that previously held the material together are vastly insufficient to contain this expansion of highly ionized atoms (ions) and electrons from the surface. Because the electrons are lighter and more energetic than the ions, they come off the material first, followed later by the ions. And because the ions all have some positive charge, they repel each other as they expand away from the material.

Consequently, there are no droplets that condense onto the surrounding material. Additionally, since there is no melt phase, there is no splattering of material onto the surrounding surface.

### 5.7.1 Microstrip Antenna Array Fabrication Steps

The complete antenna array is made in 5 steps depending on the fabrication zones as defined in figure 5.11 below.

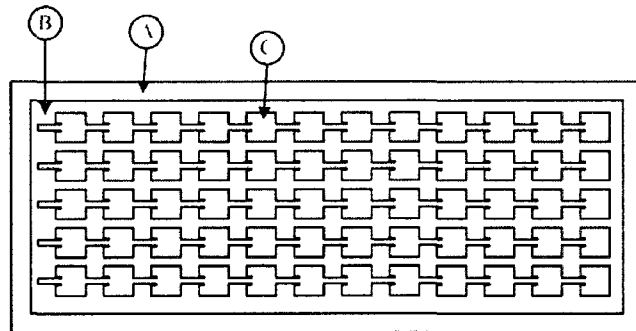


Figure 5.11 Microstrip antenna array fabrication zones.

Step 1: Region B is made using an ultrafast laser configured to have a cut width of approximately 0.05mm. The procedure to machine this area is to translate the part horizontally underneath the beam from one side to the other indexing vertically by 0.05 mm at the end of each pass. While translating the part the laser beam is turned on and off at the appropriate locations to leave a “rough out” of area C.

Step 2: The machining center is configured for more precise machining and the perimeter of area C is cut out to clean up rough edges left in step 1.

Step 3: The entire part is excised from the panel by machining along the outside perimeter of region A.

Step 4: The machining center is reconfigure again for more precise machining to allow the machining of inset feeds cuts into region C and 120 cuts are made.

Step 5: Areas B and C are masked off and Area A is etched using a PCB kit.

A fabricated antenna array is shown in figure 5.12.

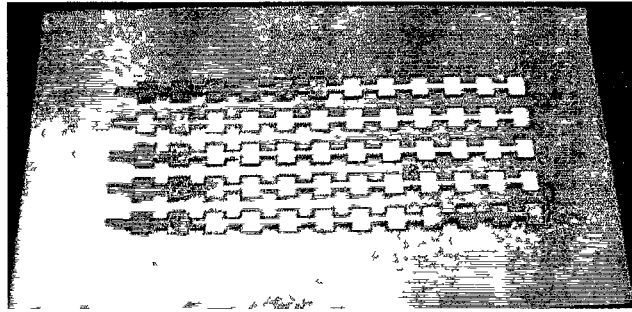
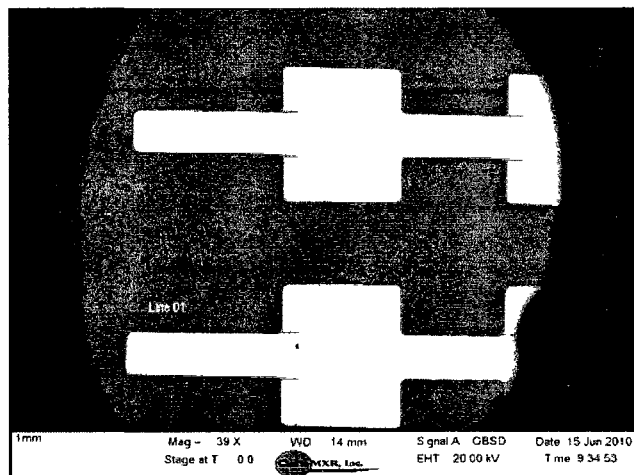
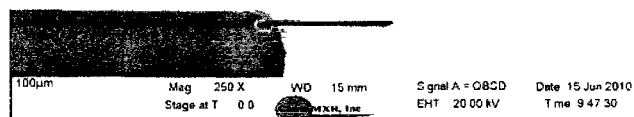


Figure 5 12 Fabricated microstrip antenna array

An SEM figures of the fabricated microstrip antenna array are shown in figure 5 13 (a,b)



(a)



(b)

Figure 5.13 SEM figures of the fabricated microstrip antenna array

## **5.8 Conclusions**

The Design, simulation and fabrication of a microstrip antenna array has been presented. The microstrip antenna incorporates an inset fed instead of typical feed mechanism to connect the array patches. This reduces the number of patches needed and improves the antenna performance. The microstrip antenna array has been modeled and simulated using HFSS software. The HFSS simulation results show that at 77 GHz, the microstrip antenna array exhibits a return loss of better than -15 dB, antenna array gain of 18.3 dB, half power beam width (HPBW) of 9° and efficiency at the operating frequency of 77%. A fabrication process sequence has been developed. The microstrip antenna is to be used in conjunction with a MEMS based solid state Rotman lens to realize compact MEMS radar for automotive collision avoidance application.

# Chapter 6

## Conclusions and Future Work

### 6.1 Conclusions

The thesis developed the architecture of a new MEMS based 77 GHz long range FMCW radar for an automotive collision avoidance applications. The detailed design, modeling and fabrication of the core components of the new radar: a microfabricated Rotman lens, a MEMS SP3T RF switch, and an inset feed microstrip antenna array are presented.

In the transmit segment, an FMCW signal is fed sequentially through the beam ports of the microfabricated Rotman lens that has an intrinsic beamforming and beamsteering capability. The output of the signal at the array ports of the Rotman lens are radiated through the inset feed microstrip antenna array. In the receiving segment, another set of antenna array, Rotman lens and SP3T switch and a mixer are used to generate an IF signal corresponding to the echo signal reflected back from the target. An FPGA based algorithm processes the digitized IF signal to extract the range and velocity of the target vehicles.

The novel microfabricated Rotman lens eliminates the need for microelectronics based analog or digital beamforming operations as necessary in conventional phased array based FMCW automotive radars. This reduces the system complexity significantly, enables to realize the complete radar sensor in a smaller form factor while offering superior performance.

An extensive literature search has been performed to review the state-of-the-art in automotive radars, radar technology, RF MEMS technology, and industry set requirements to set up the target design specifications. To minimize the system complexity and faster cycle time, a Rotman lens has been adopted for the beamforming operation. As the Rotman lens is a passive device, it doesn't consume any power and consequently, is free of all the issues related to microelectronic based analog or digital beamforming operations including hardware related thermal drift and integration issues.

A novel technique has been developed to realize the Rotman lens in silicon so that the lens can be batch fabricated using conventional microfabrication techniques to

minimize the manufacturing cost. The technique involves thermo-compression and externally applied conductive epoxy bonding of two silicon wafers, one with the gold-coated etched geometry and the other is a gold-coated planar geometry, to realize a TE<sub>10</sub> mode rectangular waveguide type Rotman lens with air as the dielectric material filling the lens cavity. The simple one mask fabrication of the Rotman lens has become possible due to TE<sub>10</sub> rectangular waveguide type design that enabled to shrink the lens cavity to 50  $\mu\text{m}$  that can be easily realized using a DRIE technique.

The 77 GHz Rotman lens has a footprint area of 27x36.2 mm<sup>2</sup> including the transmission lines and incorporates 3 beam ports, 5 array ports, and 6 dummy ports to prevent path loss due to sidewall reflections. The lens has been designed to steer the beam by  $\pm 4$  degrees. The lens has been designed using full wave 3-D FEA simulation using industry standard HFSS software and IntelliSuite™. The performance parameters of the Rotman lens are optimized to get excellent values for the insertion losses, return losses and characteristic impedance. The lens has been fabricated in the University of Waterloo and University of Western Ontario and was assembled in Advotec Inc. in Arizona.

The design, simulation and fabrication of a MEMS Single-Pole-Triple-Throw (SP3T) RF switch to sequentially feed the FMCW signal among the beam ports of the microfabricated Rotman lens has been presented. The series type MEMS RF switch relies on electrostatic actuation of a microfabricated cantilever beam and incorporates 1 input port and 3 output ports. Two different versions of the MEMS RF switch have been designed: a ground connecting bridge (GCB) conventional geometry where microfabricated bridges have been used to provide the ground connectivity and a new continuous ground (CG) without any bridge. Both the switches have been optimized for operation in the 77 GHz; however, the CG version provides improved performance as it eliminates the effects of coupling capacitance between the ports and the ground. The HFSS simulation results show that at 77 GHz, the CG configuration has 4 dB improvement for the return loss compared to the GCB version of the switch. The CG version of the switch also exhibits 0.5 dB improvement for insertion loss and 3 dB improvement for isolation as compared to the GCB version of the switch. The actuation

voltage of the switch is 16.3 volts. The GCB type SP3T RF switch has been fabricated using the UWMEMS process and the fabrication of the CG version is in progress.

Finally, the design, simulation and fabrication of a microstrip antenna array that forms an integral part of a MEMS based radar working in the 77 GHz range has been presented. The microstrip antenna array incorporates 5 sub-arrays and 12 patches in each sub-array. The design is based on a serial array inset fed method. The HFSS simulation results show that at 77 GHz, the microstrip antenna array exhibits a return loss of better than -15 dB, antenna array gain of 18.3 dB, half power beam width (HPBW) of 9° and an efficiency of 77% at the operating frequency of 77 GHz.

It is expected that the developed radar sensor will be able to provide a cost effective solution for long range radars to be used in an automotive collision avoidance application.

## 6.2 Future work

### MEMS Multimodal Radar

Investigation shows that the developed MEMS based radar technology can be further extended to realize a compact multimode (long range, mid range and short range) radar sensor as shown in the figure 6.1.

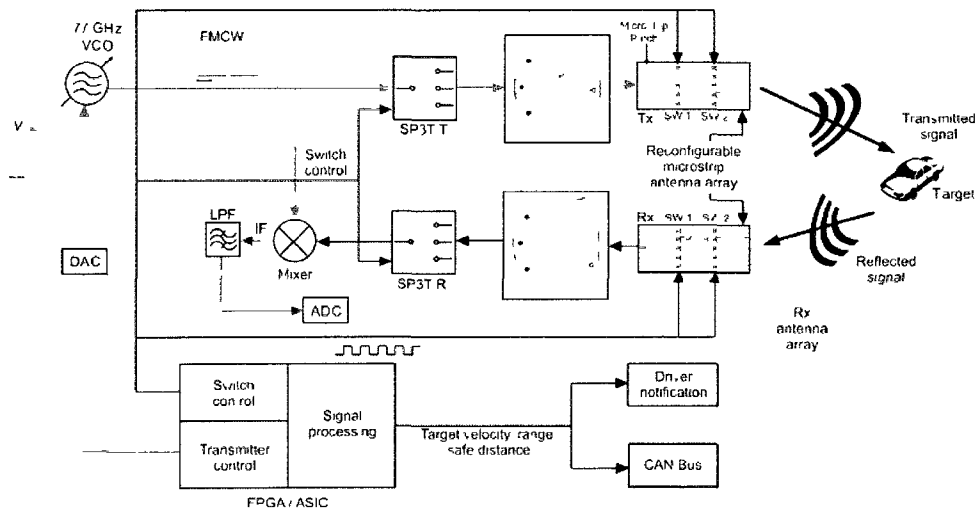


Figure 6.1 MEMS Multimodal radar block diagram

The conceived multimodal radar can operate in three basic modes: (1) long range (80-150 m), (2) mid-range (20-80 m), and (3) short range (0-20 m). While in operation, an FPGA implemented algorithm controls the MEMS based RF switches to reconfigure a



microstrip antenna array to switch the radar constantly from one mode to another with a pre-specified time constant to scan the near field and the far field regions. For the multimode radar, in addition to the components and functionality of the currently designed single mode radar, 2 additional sets of MEMS RF switches will be necessary as shown in figure 6.2.

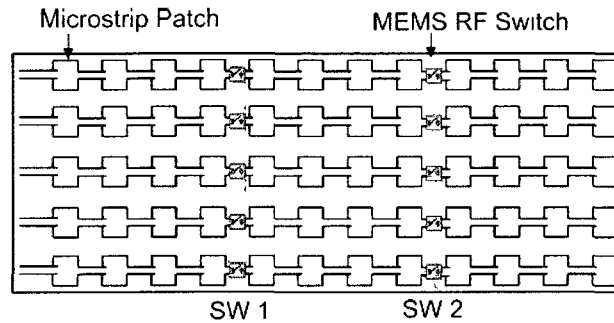


Figure 6.2 FPGA Reconfigurable microstrip antenna array

When both the switches are in the OFF position, 4 microstrip patches per linear array will provide short range coverage. When the switch SW 1 is turned ON and SW 2 is OFF, 8 microstrip patches per linear array will provide mid-range range coverage. Finally, when both the switches SW 1 and SW 2 are ON, 12 microstrip patches per linear array will provide long range coverage. An FPGA implemented control algorithm will control the operation of the switches. In this way a wider near-field area and a narrow far field area can be covered with a minimum hardware. The initial timing constant has been decided as 2 ms sweep time for each beam port (1 ms for up chirp, 1 ms for down chirp). The characteristics of all the three modes are listed in figure 6.3.

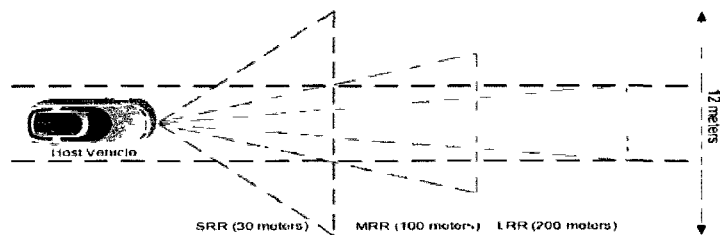


Figure 6.3 Operation modes of the MEMS based automotive radar

## References

- [1] M. Camiade, D. Domnesque, Z Ouarch, A. Sion, "Fully MMIC-based Front End for FMCW Automotive Radar at 77 GHz", *Proceeding of European Microwave Week 2000 (GAAS)*, 2000, pp. 280-283.
- [2] L. Hall, H. Hansen and D. Abbott, "Rotman lens for mm-wavelengths," *Proc. SPIE Smart Structures, Devices and Systems*, Melbourne, Australia, Vol. 4935, 16-18 December 2002, pp 215-221.
- [3] W. Rotman and R. Turner, "Wide-angle Microwave Lens for Line Source Applications," *IEEE Transactions on Antennas and Propagation*, vol. 11, pp. 623-632, 1963.
- [4] G. J. Monser, "Advances in Lens-Fed Multibeam Technology," *NTIS*, p. 22, Feb 1992.
- [5] D. H. Archer and M. J. Maybell, "Rotman lens development history at Raytheon Electronic Warfare Systems 1967-1995," 2005, pp. 31-34 vol. 2B.
- [6] D. H. Archer, "Lens-Fed Multiple-Beam Arrays," *Microwave J.*, vol. 18, p. 6, Oct 1975.
- [7] D. H. Archer, "Lens-Fed Multiple Beams Arrays," *Microwave J.*, vol. 27, p. 6, 1984.
- [8] World health organization WHO
- [9] History of Radar, en.wikipedia.org/wiki/History\_of\_radar
- [10] M. I. Skolnik, *Radar Handbook*, 2<sup>nd</sup> ed., New York: McGraw-Hill, 1970.
- [11] A. Anderson. (November 2005). *Mercedes-Benz Sudden Acceleration Incidents* [Online]. Available: [http://www.antony-anderson.com/Cruise/9.5 SA Links/Mercedes 20 Benz.html](http://www.antony-anderson.com/Cruise/9.5%20Benz.html)
- [12] J. Wenger, "Automotive Radar – Status and Perspectives," in *IEEE CSIC 2005 Dig.*, 2005, Sitges (Spain), 2005, pp. 21-24.
- [13] M. Schneider, "Automotive Radar – Status and Trends," in *German Microwave Conf. (GeMiC2005)*, Ulm (Germany), 2005, pp. 144-147.
- [14] J. Wenger, "Automotive Radar – Status and Perspectives," in *IEEE CSIC 2005 Dig.*, 2005, Sitges (Spain), 2005, pp. 21-24.
- [15] R. Schneider, J. Wenger, "Prototypic Realisation of Millimetre Wave Radar Imaging; Advanced Microsystems for Automotive Applications 2003 (eds. J. Valldorf, W. Gessner), *Springer-Verlag Berlin Heidelberg*, 2003, pp. 97-111.
- [16] M. Camiade, D. Domnesque, Z Ouarch,, A. Sion, "Fully MMIC-based front end for FMCW automotive radar at 77GHz, *European Microwave Week, GaAs 2000 Proceedings*, pp. 280-283, 2000.

- [17] V. Jain, B. Javid, P. Heydari, "A 24/77GHz Dual-Band BiCMOS Frequency Synthesizer," in *IEEE 2008 Conf. Custom Integrated Circuits Conference (CICC)*, San Jose, CA, 2008, pp. 487-490.
- [18] V. Jain, B. Javid, P. Heydari, "A BiCMOS Dual-Band Millimeter-Wave Frequency Synthesizer for Automotive Radars," *IEEE J. Solid-State Circuits*, Vol. 44, No. 8, pp. 2100-2113, Aug. 2009.
- [19] TRW Automotive (2009). *Adaptive Cruise Control (ACC)* [Online]. Available: [http://www.trw.com/sites/default/files/DAS\\_ACC\\_Eng09\\_0.pdf](http://www.trw.com/sites/default/files/DAS_ACC_Eng09_0.pdf)
- [20] H.-L. Bloecher, A. Sailer, G. Rollmann, J. Dickmann, "79 GHz UWB Automotive Short Range Radar – Spectrum Allocation and Technology Trends," *Adv. Radio Sc.*, Vol. 7, 2009, pp. 61-65.
- [21] R. A. Mucci, "A Comparison of Efficient Beamforming Algorithms," *IEEE Trans. Acoustics, Speech, and Signal Processing*, Vol. ASSP-32, No. 3, pp. 548-558, Jun. 1984.
- [22] C. Wolff. (2008). *Digital Beamforming* [Online]. Available: <http://www.radartutorial.eu/06.antennas/an51.en.html>
- [23] A.Sinjari, S. Chowdhury, "MEMS Automotive Collision Avoidance Radar Beamformer", in *Proc. of International Symposium on Circuits and Systems,ISCAS 2008*, 18-21 May 2008, pp. 2086 – 2089.
- [24] S. Weiss, S. Keller, and C. Ly, "Development of simple affordable beamformers for army platforms," *presented at 2007 GOMACTech Conf., Lake Buena Vista, Fl, March. 2007.*
- [25] Jaeheung Kim, *Senior Member, IEEE*, Chul Soon Park, *Senior Member, IEEE*, and Seungwook Min, "TM0 Mode Surface Wave Excited Dielectric Slab Rotman Lens," *IEEE ANTENNAS AND WIRELESS PROPAGATION LETTERS*, VOL. 6, 2007.
- [26] Weiss, S., Dahlstrom, R., "Rotman Lens Development at the Army Research Lab", *IEEE Aerospace Conference 2006*.pp. 1-7.
- [27] Schulwitz, L., Mortazawi, A., "A New Low Loss Rotman Lens Design for Multibeam Phased Arrays", *IEEE MTT-S International Microwave Symposium Digest 2006*. Pp 445-448.
- [28] Jaeheung Kim, *Senior Member, IEEE*, Chul Soon Park, *Senior Member, IEEE*, and Seungwook Min, "TM0 Mode Surface Wave Excited Dielectric Slab Rotman Lens," *IEEE ANTENNAS AND WIRELESS PROPAGATION LETTERS*, VOL. 6, 2007.

- [29] mipoh J. Schoebel, T. Buck, M. Reimann, M. Ulm, M. Schneider, A. Jourdain, G. Carchon, and H. A. C. Tilmans, "Design Considerations and Technology Assessment of Phased-Array Antenna Systems with RF MEMS for Automotive Radar Applications," *IEEE Trans. Antennas Propag.*, vol. AP-53, pp. 1968-1975, Jun. 2005.
- [30] M. Daneshmand and R. R. Mansour, "Monolithic RF MEMS Switch Matrix Integration", *IEEE MTT-S*, pp. 140 – 143, June 2006.
- [31] G. Wang; H. Ding; W. Woods, and E. Mina, "Wideband on-chip RF MEMS Switches in a BiCMOS Technology for 60 GHz Applications," *International Conference on Microwave and Millimeter Wave Technology ICMMT 2008*, April 2008, vol. 3, pp. 1389-1392.
- [32] L.E. Larson, R.H. Hachett, R.F. Lohr, "Microactuators for GaAs-Based Microwave Integrated Circuits", *Digest of technical papers; Solid State Sensors and Actuators*, P.743-746, June 1991.
- [33] I.J. Bahl and P. Bhartia, "Microstrip Antennas", Canton, Mass., Artech House, 1980
- [34] Constantine A. Balanis, "Antenna theory, analysis and design", Wiley interscience, 2005
- [35] K. R. Carver and J. W. Mink, "Microstrip Antenna Technology," *IEEE Trans. Antennas Propagat.*, Vol. AP-29, No. 1, pp. 2–24, January 1981.
- [36] J. R. James and P. S. Hall, *Handbook of Microstrip Antennas*, Vols. 1 and 2, Peter Peregrinus, London, UK, 1989.
- [37] D. M. Pozar, "Microstrip Antennas," *Proc. IEEE*, Vol. 80, No. 1, pp. 79–81, January 1992.
- [38] H. G. Oltman and D. A. Huebner, "Electromagnetically Coupled Microstrip Dipoles," *IEEE Trans. Antennas Propagat.*, Vol. AP-29, No. 1, pp. 151–157, January 1981.
- [39] G. Gronau and I. Wolff, "Aperture-Coupling of a Rectangular Microstrip Resonator," *Electronic Letters*, Vol. 22, pp. 554–556, May 1986.
- [40] F. D. L. Peters, B. Boukari, S. O. Tatu, and T. A. Denidni, "77GHz Millimeter wave antenna array with Wilkinson divider feeding network," *Progress In Electromagnetics Research Letters*, Vol. 9, pp. 193-199, 2009
- [41] Vinod Kumar Singh, Ashok Mittal, "design of wide-band microstrip antenna array at millimeter wave frequencies", DEAL, Government of India, 2000
- [42] Heui Cho, Cheol-Sik Pyo and Jae-Ick Choi, "A High-Gain Microstrip Patch Array Antenna Using a Superstrate Layer", *ETRI Journal*, vol. 25, no. 5, Oct 2003, pp. 407-411

- [43] A. Anderson. (November 2005). *Mercedes-Benz Sudden Acceleration Incidents* [Online]. Available: [http://www.antony-anderson.com/Cruise/9.5 SA Links/Mercedes 20 Benz.html](http://www.antony-anderson.com/Cruise/9.5%20Benz.html)
- [44] H. Rohling, *Some Radar Topics: Waveform Design, Range CFAR and Target Recognition, Advances in Sensing with Security Applications*. [NATO Security Through Science Book Series, Vol. 2]. Netherlands: Springer Netherlands, 2006. (ISBN: 978-1-4020-4284-3)
- [45] Y. K. Chan, S. Y. Lim, "Synthetic Aperture Radar (SAR) Signal Generation," *Progress in Electromagnetics Research B*, Vol. 1, pp. 269-290, 2008.
- [46] P. C. Sharma, R. D. Gupta and P. K. Singhal, "Recent Trades in Design and Analysis of Rotman Type Lens for Multiple Beamforming", *International Journal of RF and Microwave Computer aided Engineering CAE* 8, pp 321-338, 1998.
- [47] L. Musa and M. S. Smith; "Microstrip Port Design and Sidewall Absorption for Printed Rotman Lenses," *IEEE Proceedings on Microwaves, Antennas and propagation*, vol. 136, Issue 1, pp. 53-58, Feb. 1989.
- [48] Y. M. Tao, G. Y. Delisle, "Multiple Beam Antenna Arrays for Indoor Communications, *ANTEM 96*, Montreal (Quebec), 6-9 August 1996, pp. 725-728.
- [49] T. Tsurumi, S. Ozawa and S. Wada, "Preparation of PZT Thick Films by an Interfacial Polymerization Method", *Journal of Sol-Gel Science and Technology*, Vol 26, pp. 1037-1040, Jan. 2003.
- [50] L. Jang and K. Kuo, "Fabrication and Characterization of PZT Thick Films for Sensing and Actuation", *proc. of Sensors 2007*, 2007, vol. 7, pp 493-507.
- [51] David Pozar, *Microwave Engineering*, 3<sup>rd</sup> Edition, Wiley and sons (2003).
- [52] High isolation and low insertion loss switch IC using GaAs MESFETs', *IEEE Transactions Microwave Theory and Techniques* 43: 2175–2177.
- [53] V. K. Varadan, K J Vinoy, K. A. Jose, RF MEMS and their applications, John Wiley & Sons, 2003.
- [54] Grant, P.D., Denhoff, M.W., Mansour, R.R., "A comparison between RF MEMS Switches and Semiconductor Switches", *ICMENS International Conference on MEMS, NANO and Smart Systems*, pp 515-521, August 2004
- [55] G. M. Rebeiz, RF MEMS Theory, Design, and Technology: John Wiley & Sons, 2003.
- [56] J. Schobel, T. Buck, M. Reimann, M. Ulm, M. Schneider, "W-band RF-MEMS Subsystems for Smart Antennas in Automotive Radar Sensors," in *Proc. of 34th European Microwave Conference*, 11-15 Oct. 2004, vol. 3, pp. 1305 – 1308.

- [57] R. N. Simons, Coplanar Waveguide Circuits, Components and Systems. John Wiley & Sons, Inc, 2001.
- [58] J. Rizk and G. M. Rebeiz, "W-band CPW RF MEMS circuits on Quartz Substrates," *IEEE Transactions on Microwave Theory and Techniques*, vol. 51, no. 7, pp. 1857 - 1862, July 2003.
- [59] James R. Andrews, "Broadband Coaxial Bias Tees", Picosecond Pulse Labs, November 2000
- [60] UW-MEMS design handbook, University of Waterloo.
- [61] Hyman, D., Lam, J., Warneke, B., Schmitz, A., Hsu, T.Y., Brown, J., Schaffner, J., Waltson, A., Loo, R.Y., Mehregany, M., Lee, J., 1999a, 'Surface micromachined RF MEMS switches on GaAs Substrates', *International Journal of RF and Computer Aided Engineering* **9**: 348–361.
- [62] Rebeiz, G.M.; Muldavin, J.B. RF MEMS switches and switch circuits. *IEEE Microwave. Mag.* 2001, 2, 59-71.
- [63] Ghodsian, B.; Bogdanoff, P.; Hyman, D.; "Wideband DC-contact MEMS series switch", *Micro & Nano Letters*, September 2008 Page(s):66 - 69.
- [64] E. R. Brown, "RF-MEMs switches for reconfigurable integrated circuits," *IEEE Transactions on Microwave Theory and Techniques*, vol. 46, no. 11, pp. 1868-1880, November 1998.
- [65] Clark MXR corporation in Dexter, Michigan, USA.

## Patents and papers produced during Ph.d. study

### Patents

1. IP Protection Strategy For Radar Device published in United States Patents and Trademark Office. (US 61/282,595, March 5, 2010)
2. Three more patents in process

### Papers

1. A.Sinjari, S. Chowdhury, “MEMS Automotive Collision Avoidance Radar Beamformer”, in Proc. of *International Symposium on Circuits and Systems,ISCAS 2008*, 18-21 May 2008, pp. 2086 – 2089, Seattle, Washington.
2. A. Sinjari, S. Chowdhury, “Design of a PZT-based MEMS Rotman lens”, in *Proc. of Canadian Conference on Electrical and Computer Engineering (CCECE 2008)*, 4-7 May 2008, pp. 1121-1124, Niagara falls, Ontario.
3. A. Sinjari, S. Chowdhury, “A Single-Pole-Triple-Throw (SP3T) MEMS RF Switch for 24 GHz Short Range Radar”, in *IEEE INTERNATIONAL CONFERENCE on ELECTRO/INFORMATION TECHNOLOGY*, 7-9 June 2009, Windsor, Ontario.
4. A. Sinjari, S. Chowdhury, “High Performance 77 GHz Single Pole Triple Throw (SP3T) MEMS Switch”, in *Joint conference IEEE Toulouse France NEWCAS-TAISA '09*, June 28-July 01 2009, Toulouse, France.
5. A. Sinjari, S. Chowdhury, “MEMS sensors in automotive collision avoidende systems”, in *Ontario centre of excellence*, Special poster presentation, May 9 2008, Toronto, Ontario.
6. A. Sinjari, S. Chowdhury, “MEMS sensors for an integrated active vehicle safety systems (IAVSS)”, in *North American international auto show(NAIAS)*, Special poster presentation, Jan16-172008,Detroit,Michigan

## Appendix A

### Program code for Rotman lens design

```
$begin 'AnsoftProject'
  Product='HFSS'
  NextUniqueID=0
  MoveBackwards=false
  $begin 'Desktop'
    Version(11, 0)
    InfrastructureVersion(1, 0)
  $end 'Desktop'
  $begin 'HFSSEnvironment'
    Version(1, 0)
  $end 'HFSSEnvironment'
  $begin 'geometry3deditor'
    Version(1, 0)
  $end 'geometry3deditor'
  $begin 'ProjectDatasets'
    NextUniqueID=0
    MoveBackwards=false
    DatasetType='ProjectDatasetType'
    $begin 'DatasetDefinitions'
      $end 'DatasetDefinitions'
    $end 'ProjectDatasets'
  $begin 'Definitions'
    $begin 'Folders'
      Definitions(1104, 10000, 1, 1, 0, false, false)
      Materials(1104, 9500, 9, 2, 1, false, false)
    $end 'Folders'
    $begin 'Materials'
      $begin 'vacuum'
        CoordinateSystemType='Cartesian'
        $begin 'AttachedData'
          $end 'AttachedData'
        $begin 'ModifierData'
          $end 'ModifierData'
        permittivity='1'
        ModTime=1028307964
        Library='Materials'
        LibLocation='SysLibrary '
      $end 'vacuum'
      $begin 'gold'
        CoordinateSystemType='Cartesian'
        $begin 'AttachedData'
          $end 'AttachedData'
        $begin 'ModifierData'
          $end 'ModifierData'
        permeability='0.99996'
        conductivity='41000000'
        thermal_conductivity='315'
        mass_density='19300'
        specific_heat='129'
        youngs_modulus='80000000000'
        poissons_ratio='0.4'
        thermal_expansion_coefficient='1.4e-005'
        ModTime=1132068239
        Library='Materials'
        LibLocation='SysLibrary '
```



```

        $send 'gold'
    $send 'Materials'
    $begin 'Scripts'
    $send 'Scripts'
$send 'Definitions'
DesignIDServer=4
MoveBackwards=false
$begin 'HFSSModel'
    RepRewriteV2=true
    Name='HFSSDesign1'
    DesignID=0
    'Allow Material Override'=false
    SolutionType='DrivenModal'
    MaterialDensity=1
    MassOfTissue=1
    $begin 'OutputVariable'
        NextUniqueID=0
        MoveBackwards=false
    $send 'OutputVariable'
    $begin 'ModelSetup'
        $begin 'Editor3D Doc Preferences'
            'Plane Background'=true
            BackgroundColor1=16777215
            BackgroundColor2=0
            'Need Lights'=true
            'Ambient Light'=8355711
            'Num Lights'=2
            Light0[4: 8355711, 0.200000002980232,
0.4000000005960464, 1]
            Light1[4: 8355711, -0.200000002980232, -
0.4000000005960464, -1]
        $send 'Editor3D Doc Preferences'
        $begin 'DesignDatasets'
            NextUniqueID=0
            MoveBackwards=false
            DatasetType='DesignDatasetType'
            $begin 'DatasetDefinitions'
            $send 'DatasetDefinitions'
        $send 'DesignDatasets'
        SnapMode=2
        GroupByMaterial=true
        GroupSheetByMaterial=false
        $begin 'GeometryCore'
            BlockVersionID=3
            NativeKernel='ACIS'
            NativeKernelVersionID=1
            Units='mm'
            InstanceID=-1
            ExternalNativeGeometryAllowed=false
            $begin 'ValidationOptions'
                EntityCheckLevel='Strict'
            $send 'ValidationOptions'
            $begin 'GeometryOperations'
                BlockVersionID=2
                $begin 'AnsoftRangedIDServerManager'
                    $begin 'AnsoftRangedIDServer'
                        IDServerObjectTypeID=0
                        IDServerRangeMin=0

```

```

IDServerRangeMax=2146483647
NextUniqueID=4525
MoveBackwards=false
$send 'AnsoftRangedIDServer'
$begin 'AnsoftRangedIDServer'
IDServerObjectTypeID=1
IDServerRangeMin=2146483648
IDServerRangeMax=2146485547
NextUniqueID=2146483654
MoveBackwards=false
$send 'AnsoftRangedIDServer'
$send 'AnsoftRangedIDServerManager'
StartBackGroundFaceID=2146483648
$begin 'CoordinateSystems'
$send 'CoordinateSystems'
$begin 'ToplevelParts'
$begin 'GeometryPart'
$begin 'Attributes'
Name='Polyline57'
Flags=''
Color=(132 132 193)'

Transparency=0.400000005960464

PartCoordinateSystem=1
MaterialName='vacuum'
SolveInside=true
$send 'Attributes'
$begin 'Operations'
$begin 'Operation'

OperationType='Polyline'

ID=3599

ReferenceCoordSystemID=1

$begin
'PolylineParameters'

KernelVersion=1

CoordinateSystemID=-1

IsPolylineClosed=true

$begin
'PolylinePoints'

$begin
'PLPoint'

$begin 'rectangle'
rectangle(16, 17, 18, 19, 27)
$send 'rectangle'
$begin 'rectangle17_'
rectangle17_(1, 2, 3, 4)
$send 'rectangle17_'
$send 'CachedNames'
$send 'GeometryOperations'
$begin 'GeometryDependencies'
$begin 'DependencyInformation'
NumParents=1

```

```

                                $begin 'DependencyInformation'
                                    NumParents=2

DependencyObject('GeometryBodyOperation', 1877)

DependencyObject('GeometryBodyOperation', 1876)
                                DependencyObject('CoordinateSystem',
1)
                                    $send 'DependencyInformation'
                                    $begin 'DependencyInformation'
                                        NumParents=2

DependencyObject('GeometryBodyOperation', 1878)

DependencyObject('GeometryBodyOperation', 1877)
                                DependencyObject('CoordinateSystem',
1)
                                    $send 'DependencyInformation'
                                    $begin 'DependencyInformation'
                                        NumParents=2

DependencyObject('GeometryBodyOperation', 1879)

DependencyObject('GeometryBodyOperation', 1878)
                                DependencyObject('CoordinateSystem',
1)
                                    $send 'DependencyInformation'
                                    $begin 'DependencyInformation'
                                        NumParents=2

DependencyObject('GeometryBodyOperation', 1880)

DependencyObject('GeometryBodyOperation', 1879)
                                DependencyObject('CoordinateSystem',
1)
                                    $send 'DependencyInformation'
                                    $begin 'DependencyInformation'
                                        NumParents=2

DependencyObject('GeometryBodyOperation', 1936)
                                DependencyObject('CoordinateSystem',
1)

DependencyObject('GeometryBodyOperation', 1880)
                                $send 'DependencyInformation'
                                $begin 'DependencyInformation'
                                    NumParents=2

DependencyObject('GeometryBodyOperation', 1942)
                                DependencyObject('CoordinateSystem',
1)

DependencyObject('GeometryBodyOperation', 1936)
                                $send 'DependencyInformation'
                                $begin 'DependencyInformation'
                                    NumParents=2

DependencyObject('GeometryBodyOperation', 1945)

```

```

1) DependencyObject('CoordinateSystem',

DependencyObject('GeometryBodyOperation', 1942)
    $send 'DependencyInformation'
    $begin 'DependencyInformation'
        NumParents=2

DependencyObject('GeometryBodyOperation', 1951)
    DependencyObject('CoordinateSystem',
1)

DependencyObject('GeometryBodyOperation', 1945)
    $send 'DependencyInformation'
    $begin 'DependencyInformation'
        NumParents=2

DependencyObject('GeometryBodyOperation', 1954)
    DependencyObject('CoordinateSystem',
1)

DependencyObject('GeometryBodyOperation', 1951)
    $send 'DependencyInformation'
    $begin 'DependencyInformation'
        NumParents=2

DependencyObject('GeometryBodyOperation', 1980)
    DependencyObject('CoordinateSystem',
1)

DependencyObject('GeometryBodyOperation', 1954)
    $send 'DependencyInformation'
    $begin 'DependencyInformation'
        NumParents=2

DependencyObject('GeometryBodyOperation', 1982)
    DependencyObject('CoordinateSystem',
1)

DependencyObject('GeometryBodyOperation', 1980)
    $send 'DependencyInformation'
    $begin 'DependencyInformation'
        NumParents=2

DependencyObject('GeometryBodyOperation', 1983)
    DependencyObject('CoordinateSystem',
1)

DependencyObject('GeometryBodyOperation', 1982)
    $send 'DependencyInformation'
    $begin 'DependencyInformation'
        NumParents=1

DependencyObject('GeometryBodyOperation', 1958)
    DependencyObject('CoordinateSystem',
1)

    $send 'DependencyInformation'
    $begin 'DependencyInformation'

```

```

                                NumParents=1

DependencyObject('GeometryBodyOperation', 1968)

DependencyObject('GeometryBodyOperation', 1958)
                                $send 'DependencyInformation'
                                $begin 'DependencyInformation'
                                    NumParents=2

DependencyObject('GeometryBodyOperation', 1970)

DependencyObject('GeometryBodyOperation', 1968)
                                DependencyObject('CoordinateSystem',
1)
                                    $send 'DependencyInformation'
                                    $begin 'DependencyInformation'
                                        NumParents=2

DependencyObject('GeometryBodyOperation', 1971)

DependencyObject('GeometryBodyOperation', 1970)
                                DependencyObject('CoordinateSystem',
1)
                                    $send 'DependencyInformation'
                                    $begin 'DependencyInformation'
                                        NumParents=2

DependencyObject('GeometryBodyOperation', 1972)

DependencyObject('GeometryBodyOperation', 1971)
                                DependencyObject('CoordinateSystem',
1)
                                    $send 'DependencyInformation'
                                    $begin 'DependencyInformation'
                                        NumParents=2

DependencyObject('GeometryBodyOperation', 1973)

DependencyObject('GeometryBodyOperation', 1972)
                                DependencyObject('CoordinateSystem',
1)
                                    $send 'DependencyInformation'
                                    $begin 'DependencyInformation'
                                        NumParents=2

DependencyObject('GeometryBodyOperation', 1974)

DependencyObject('GeometryBodyOperation', 1973)
                                DependencyObject('CoordinateSystem',
1)
                                    $send 'DependencyInformation'
                                    $begin 'DependencyInformation'
                                        NumParents=2

DependencyObject('GeometryBodyOperation', 1975)

DependencyObject('GeometryBodyOperation', 1974)

```

```

DependencyObject('CoordinateSystem',
1)
    $send 'DependencyInformation'
    $begin 'DependencyInformation'
        NumParents=2

DependencyObject('GeometryBodyOperation', 1976)
DependencyObject('GeometryBodyOperation', 1975)
    DependencyObject('CoordinateSystem',
1)
        $send 'DependencyInformation'
        $begin 'DependencyInformation'
            NumParents=2

DependencyObject('GeometryBodyOperation', 1977)
DependencyObject('GeometryBodyOperation', 1976)
    DependencyObject('CoordinateSystem',
1)
        $send 'DependencyInformation'
        $begin 'DependencyInformation'
            NumParents=2

DependencyObject('GeometryBodyOperation', 1978)
DependencyObject('GeometryBodyOperation', 1977)
    DependencyObject('CoordinateSystem',
1)
        $send 'DependencyInformation'
        $begin 'DependencyInformation'
            NumParents=2

DependencyObject('GeometryBodyOperation', 1979)
DependencyObject('GeometryBodyOperation', 1978)
    DependencyObject('CoordinateSystem',
1)
        $send 'DependencyInformation'
        $begin 'DependencyInformation'
            NumParents=1

DependencyObject('GeometryBodyOperation', 1984)
    DependencyObject('CoordinateSystem',
1)
        $send 'DependencyInformation'
        $begin 'DependencyInformation'
            NumParents=1

DependencyObject('GeometryBodyOperation', 1994)
DependencyObject('GeometryBodyOperation', 1984)
    $send 'DependencyInformation'
    $begin 'DependencyInformation'
        NumParents=2

DependencyObject('GeometryBodyOperation', 1996)

```

```

DependencyObject('GeometryBodyOperation', 1994)
    DependencyObject('CoordinateSystem',
1)
        $Send 'DependencyInformation'
        $begin 'DependencyInformation'
            NumParents=2

DependencyObject('GeometryBodyOperation', 1997)
DependencyObject('GeometryBodyOperation', 1996)
    DependencyObject('CoordinateSystem',
1)
        $Send 'DependencyInformation'
        $begin 'DependencyInformation'
            NumParents=2

DependencyObject('GeometryBodyOperation', 1998)
DependencyObject('GeometryBodyOperation', 1997)
    DependencyObject('CoordinateSystem',
1)
        $Send 'DependencyInformation'
        $begin 'DependencyInformation'
            NumParents=2

DependencyObject('GeometryBodyOperation', 1999)
DependencyObject('GeometryBodyOperation', 1998)
    DependencyObject('CoordinateSystem',
1)
        $Send 'DependencyInformation'
        $begin 'DependencyInformation'
            NumParents=2

DependencyObject('GeometryBodyOperation', 2000)
DependencyObject('GeometryBodyOperation', 1999)
    DependencyObject('CoordinateSystem',
1)
        $Send 'DependencyInformation'
        $begin 'DependencyInformation'
            NumParents=2

DependencyObject('GeometryBodyOperation', 2001)
DependencyObject('GeometryBodyOperation', 2000)
    DependencyObject('CoordinateSystem',
1)
        $Send 'DependencyInformation'
        $begin 'DependencyInformation'
            NumParents=2

DependencyObject('GeometryBodyOperation', 2002)
DependencyObject('GeometryBodyOperation', 2001)
    DependencyObject('CoordinateSystem',
1)

```

```

                                $end 'DependencyInformation'
                                $begin 'DependencyInformation'
                                    NumParents=2

DependencyObject('GeometryBodyOperation', 2003)

DependencyObject('GeometryBodyOperation', 2002)
                                DependencyObject('CoordinateSystem',
1)
                                    $end 'DependencyInformation'
                                    $begin 'DependencyInformation'
                                        NumParents=2

DependencyObject('GeometryBodyOperation', 2004)

DependencyObject('GeometryBodyOperation', 2003)
                                DependencyObject('CoordinateSystem',
1)
                                    $end 'DependencyInformation'
                                    $begin 'DependencyInformation'
                                        NumParents=2

DependencyObject('GeometryBodyOperation', 2005)

DependencyObject('GeometryBodyOperation', 2004)
                                DependencyObject('CoordinateSystem',
1)
                                    $end 'DependencyInformation'
                                    $begin 'DependencyInformation'
                                        NumParents=2

DependencyObject('GeometryBodyOperation', 2006)

DependencyObject('GeometryBodyOperation', 2005)
                                DependencyObject('CoordinateSystem',
1)
                                    $end 'DependencyInformation'
                                    $begin 'DependencyInformation'
                                        NumParents=2

DependencyObject('GeometryBodyOperation', 2007)

DependencyObject('GeometryBodyOperation', 2006)
                                DependencyObject('CoordinateSystem',
1)
                                    $end 'DependencyInformation'
                                    $begin 'DependencyInformation'
                                        NumParents=1

DependencyObject('GeometryBodyOperation', 2049)
                                DependencyObject('CoordinateSystem',
1)
                                    $end 'DependencyInformation'
                                    $begin 'DependencyInformation'
                                        NumParents=1

DependencyObject('GeometryBodyOperation', 2061)

```



```

DependencyObject('GeometryBodyOperation', 2049)
    $send 'DependencyInformation'
    $begin 'DependencyInformation'
        NumParents=2

DependencyObject('GeometryBodyOperation', 2085)

DependencyObject('GeometryBodyOperation', 2061)

DependencyObject('GeometryBodyOperation', 2073)
    $send 'DependencyInformation'
    $begin 'DependencyInformation'
        NumParents=2

DependencyObject('GeometryBodyOperation', 2144)
    DependencyObject('CoordinateSystem',
1)

DependencyObject('GeometryBodyOperation', 2085)
    $send 'DependencyInformation'
    $begin 'DependencyInformation'
        NumParents=2

DependencyObject('GeometryBodyOperation', 2145)
    DependencyObject('CoordinateSystem',
1)

DependencyObject('GeometryBodyOperation', 2144)
    $send 'DependencyInformation'
    $begin 'DependencyInformation'
        NumParents=2

DependencyObject('GeometryBodyOperation', 2146)
    DependencyObject('CoordinateSystem',
1)

DependencyObject('GeometryBodyOperation', 2145)
    $send 'DependencyInformation'
    $begin 'DependencyInformation'
        NumParents=2

DependencyObject('GeometryBodyOperation', 2180)
    DependencyObject('CoordinateSystem',
1)

DependencyObject('GeometryBodyOperation', 2146)
    $send 'DependencyInformation'
    $begin 'DependencyInformation'
        NumParents=2

DependencyObject('GeometryBodyOperation', 2182)
    DependencyObject('CoordinateSystem',
1)

DependencyObject('GeometryBodyOperation', 2180)
    $send 'DependencyInformation'
    $begin 'DependencyInformation'

```

```

                                NumParents=2
DependencyObject('GeometryBodyOperation', 2218)
                                DependencyObject('CoordinateSystem',
1)
DependencyObject('GeometryBodyOperation', 2182)
                                $send 'DependencyInformation'
                                $begin 'DependencyInformation'
                                NumParents=2
DependencyObject('GeometryBodyOperation', 2219)
                                DependencyObject('CoordinateSystem',
1)
DependencyObject('GeometryBodyOperation', 2218)
                                $send 'DependencyInformation'
                                $begin 'DependencyInformation'
                                NumParents=2
DependencyObject('GeometryBodyOperation', 2257)
                                DependencyObject('CoordinateSystem',
1)
DependencyObject('GeometryBodyOperation', 2219)
                                $send 'DependencyInformation'
                                $begin 'DependencyInformation'
                                NumParents=2
DependencyObject('GeometryBodyOperation', 2258)
                                DependencyObject('CoordinateSystem',
1)
DependencyObject('GeometryBodyOperation', 2257)
                                $send 'DependencyInformation'
                                $begin 'DependencyInformation'
                                NumParents=2
DependencyObject('GeometryBodyOperation', 2375)
DependencyObject('GeometryBodyOperation', 2258)
DependencyObject('GeometryBodyOperation', 2111)
                                $send 'DependencyInformation'
                                $begin 'DependencyInformation'
                                NumParents=1
DependencyObject('GeometryBodyOperation', 2063)
                                DependencyObject('CoordinateSystem',
1)
                                $send 'DependencyInformation'
                                $begin 'DependencyInformation'
                                NumParents=1
DependencyObject('GeometryBodyOperation', 2073)
DependencyObject('GeometryBodyOperation', 2063)
                                $send 'DependencyInformation'

```

```

                                $begin 'DependencyInformation'
                                    NumParents=1

DependencyObject('GeometryBodyOperation', 2089)
                                DependencyObject('CoordinateSystem',
1)

                                $send 'DependencyInformation'
                                $begin 'DependencyInformation'
                                    NumParents=1

DependencyObject('GeometryBodyOperation', 2099)

DependencyObject('GeometryBodyOperation', 2089)
                                $send 'DependencyInformation'
                                $begin 'DependencyInformation'
                                    NumParents=2

DependencyObject('GeometryBodyOperation', 2113)
                                DependencyObject('CoordinateSystem',
1)

DependencyObject('GeometryBodyOperation', 2099)
                                $send 'DependencyInformation'
                                $begin 'DependencyInformation'
                                    NumParents=2

DependencyObject('GeometryBodyOperation', 2379)
                                DependencyObject('CoordinateSystem',
1)

DependencyObject('GeometryBodyOperation', 2113)
                                $send 'DependencyInformation'
                                $begin 'DependencyInformation'
                                    NumParents=2

DependencyObject('GeometryBodyOperation', 3344)
                                DependencyObject('CoordinateSystem',
1)

DependencyObject('GeometryBodyOperation', 2379)
                                $send 'DependencyInformation'
                                $begin 'DependencyInformation'
                                    NumParents=0
                                DependencyObject('GeometryOperation',
3367)

                                $send 'DependencyInformation'
                                $begin 'DependencyInformation'
                                    NumParents=0
                                DependencyObject('GeometryOperation',
3380)

                                $send 'DependencyInformation'
                                $begin 'DependencyInformation'
                                    NumParents=1

DependencyObject('GeometryBodyOperation', 2101)
                                DependencyObject('CoordinateSystem',
1)

                                $send 'DependencyInformation'

```

```

                                $begin 'DependencyInformation'
                                    NumParents=1

DependencyObject('GeometryBodyOperation', 2111)

DependencyObject('GeometryBodyOperation', 2101)
                                $send 'DependencyInformation'
                                $begin 'DependencyInformation'
                                    NumParents=0
                                    DependencyObject('GeometryOperation',
2327)
                                        $send 'DependencyInformation'
                                        $begin 'DependencyInformation'
                                            NumParents=0
                                            DependencyObject('GeometryOperation',
2343)
                                                $send 'DependencyInformation'
                                                $begin 'DependencyInformation'
                                                    NumParents=0
                                                    DependencyObject('GeometryOperation',
2359)
                                                        $send 'DependencyInformation'
                                                        $begin 'DependencyInformation'
                                                            NumParents=1

DependencyObject('GeometryBodyOperation', 2114)
                                DependencyObject('CoordinateSystem',
1)
                                    $send 'DependencyInformation'
                                    $begin 'DependencyInformation'
                                        NumParents=1

DependencyObject('GeometryBodyOperation', 2126)

DependencyObject('GeometryBodyOperation', 2114)
                                $send 'DependencyInformation'
                                $begin 'DependencyInformation'
                                    NumParents=2

DependencyObject('GeometryBodyOperation', 2128)

DependencyObject('GeometryBodyOperation', 2126)

DependencyObject('GeometryBodyOperation', 2142)
                                $send 'DependencyInformation'
                                $begin 'DependencyInformation'
                                    NumParents=1

DependencyObject('GeometryBodyOperation', 2132)
                                DependencyObject('CoordinateSystem',
1)
                                    $send 'DependencyInformation'
                                    $begin 'DependencyInformation'
                                        NumParents=1

DependencyObject('GeometryBodyOperation', 2142)

DependencyObject('GeometryBodyOperation', 2132)

```

```

                                $end 'DependencyInformation'
                                $begin 'DependencyInformation'
                                    NumParents=1

DependencyObject('GeometryBodyOperation', 2380)
                                DependencyObject('CoordinateSystem',
1)
                                    $end 'DependencyInformation'
                                    $begin 'DependencyInformation'
                                        NumParents=1

DependencyObject('GeometryBodyOperation', 2388)

DependencyObject('GeometryBodyOperation', 2380)
                                $end 'DependencyInformation'
                                $begin 'DependencyInformation'
                                    NumParents=2

DependencyObject('GeometryBodyOperation', 2390)

DependencyObject('GeometryBodyOperation', 2388)

DependencyObject('GeometryBodyOperation', 2375)
                                $end 'DependencyInformation'
                                $begin 'DependencyInformation'
                                    NumParents=1

DependencyObject('GeometryBodyOperation', 2846)
                                DependencyObject('CoordinateSystem',
1)
                                    $end 'DependencyInformation'
                                    $begin 'DependencyInformation'
                                        NumParents=1

DependencyObject('GeometryBodyOperation', 2868)

DependencyObject('GeometryBodyOperation', 2846)
                                $end 'DependencyInformation'
                                $begin 'DependencyInformation'
                                    NumParents=2

DependencyObject('GeometryBodyOperation', 2870)
                                DependencyObject('CoordinateSystem',
1)

DependencyObject('GeometryBodyOperation', 2868)
                                $end 'DependencyInformation'
                                $begin 'DependencyInformation'
                                    NumParents=2

DependencyObject('GeometryBodyOperation', 2878)
                                DependencyObject('CoordinateSystem',
1)

DependencyObject('GeometryBodyOperation', 2870)
                                $end 'DependencyInformation'
                                $begin 'DependencyInformation'
                                    NumParents=2

```

```

DependencyObject('GeometryBodyOperation', 2906)
1)      DependencyObject('CoordinateSystem',

DependencyObject('GeometryBodyOperation', 2878)
      $send 'DependencyInformation'
      $begin 'DependencyInformation'
      NumParents=2

DependencyObject('GeometryBodyOperation', 2907)
1)      DependencyObject('CoordinateSystem',

DependencyObject('GeometryBodyOperation', 2906)
      $send 'DependencyInformation'
      $begin 'DependencyInformation'
      NumParents=2

DependencyObject('GeometryBodyOperation', 2908)
1)      DependencyObject('CoordinateSystem',

DependencyObject('GeometryBodyOperation', 2907)
      $send 'DependencyInformation'
      $begin 'DependencyInformation'
      NumParents=1

DependencyObject('GeometryBodyOperation', 2910)
1)      DependencyObject('CoordinateSystem',

      $send 'DependencyInformation'
      $begin 'DependencyInformation'
      NumParents=1

DependencyObject('GeometryBodyOperation', 2932)

DependencyObject('GeometryBodyOperation', 2910)
      $send 'DependencyInformation'
      $begin 'DependencyInformation'
      NumParents=2

DependencyObject('GeometryBodyOperation', 2934)

DependencyObject('GeometryBodyOperation', 2932)
1)      DependencyObject('CoordinateSystem',

      $send 'DependencyInformation'
      $begin 'DependencyInformation'
      NumParents=2

DependencyObject('GeometryBodyOperation', 2935)

DependencyObject('GeometryBodyOperation', 2934)
1)      DependencyObject('CoordinateSystem',

      $send 'DependencyInformation'
      $begin 'DependencyInformation'

```

```

                                NumParents=1
DependencyObject('GeometryBodyOperation', 2995)
                                DependencyObject('CoordinateSystem',
1)
                                $Send 'DependencyInformation'
                                $begin 'DependencyInformation'
                                NumParents=1

DependencyObject('GeometryBodyOperation', 3005)
DependencyObject('GeometryBodyOperation', 2995)
                                $Send 'DependencyInformation'
                                $begin 'DependencyInformation'
                                NumParents=2

DependencyObject('GeometryBodyOperation', 3007)
DependencyObject('GeometryBodyOperation', 3005)
                                DependencyObject('CoordinateSystem',
1)
                                $Send 'DependencyInformation'
                                $begin 'DependencyInformation'
                                NumParents=2

DependencyObject('GeometryBodyOperation', 3008)
DependencyObject('GeometryBodyOperation', 3007)
                                DependencyObject('CoordinateSystem',
1)
                                $Send 'DependencyInformation'
                                $begin 'DependencyInformation'
                                NumParents=2

DependencyObject('GeometryBodyOperation', 3009)
DependencyObject('GeometryBodyOperation', 3008)
                                DependencyObject('CoordinateSystem',
1)
                                $Send 'DependencyInformation'
                                $begin 'DependencyInformation'
                                NumParents=2

DependencyObject('GeometryBodyOperation', 3010)
DependencyObject('GeometryBodyOperation', 3009)
                                DependencyObject('CoordinateSystem',
1)
                                $Send 'DependencyInformation'
                                $begin 'DependencyInformation'
                                NumParents=2

DependencyObject('GeometryBodyOperation', 3011)
DependencyObject('GeometryBodyOperation', 3010)
                                DependencyObject('CoordinateSystem',
1)
                                $Send 'DependencyInformation'

```

```

                                $begin 'DependencyInformation'
                                    NumParents=2

DependencyObject('GeometryBodyOperation', 3012)

DependencyObject('GeometryBodyOperation', 3011)
                                DependencyObject('CoordinateSystem',
1)
                                    $send 'DependencyInformation'
                                    $begin 'DependencyInformation'
                                        NumParents=2

DependencyObject('GeometryBodyOperation', 3013)

DependencyObject('GeometryBodyOperation', 3012)
                                DependencyObject('CoordinateSystem',
1)
                                    $send 'DependencyInformation'
                                    $begin 'DependencyInformation'
                                        NumParents=1

DependencyObject('GeometryBodyOperation', 3014)
                                DependencyObject('CoordinateSystem',
1)
                                    $send 'DependencyInformation'
                                    $begin 'DependencyInformation'
                                        NumParents=1

DependencyObject('GeometryBodyOperation', 3024)

DependencyObject('GeometryBodyOperation', 3014)
                                $send 'DependencyInformation'
                                $begin 'DependencyInformation'
                                    NumParents=2

DependencyObject('GeometryBodyOperation', 3026)

DependencyObject('GeometryBodyOperation', 3024)
                                DependencyObject('CoordinateSystem',
1)
                                    $send 'DependencyInformation'
                                    $begin 'DependencyInformation'
                                        NumParents=2

DependencyObject('GeometryBodyOperation', 3027)

DependencyObject('GeometryBodyOperation', 3026)
                                DependencyObject('CoordinateSystem',
1)
                                    $send 'DependencyInformation'
                                    $begin 'DependencyInformation'
                                        NumParents=2

DependencyObject('GeometryBodyOperation', 3028)

DependencyObject('GeometryBodyOperation', 3027)
                                DependencyObject('CoordinateSystem',
1)

```



```

                                $end 'DependencyInformation'
                                $begin 'DependencyInformation'
                                    NumParents=1

DependencyObject('GeometryBodyOperation', 3029)
                                DependencyObject('CoordinateSystem',
1)
                                    $end 'DependencyInformation'
                                    $begin 'DependencyInformation'
                                        NumParents=1

DependencyObject('GeometryBodyOperation', 3039)

DependencyObject('GeometryBodyOperation', 3029)
                                $end 'DependencyInformation'
                                $begin 'DependencyInformation'
                                    NumParents=2

DependencyObject('GeometryBodyOperation', 3041)

DependencyObject('GeometryBodyOperation', 3039)
                                DependencyObject('CoordinateSystem',
1)
                                    $end 'DependencyInformation'
                                    $begin 'DependencyInformation'
                                        NumParents=2

DependencyObject('GeometryBodyOperation', 3042)

DependencyObject('GeometryBodyOperation', 3041)
                                DependencyObject('CoordinateSystem',
1)
                                    $end 'DependencyInformation'
                                    $begin 'DependencyInformation'
                                        NumParents=2

DependencyObject('GeometryBodyOperation', 3043)

DependencyObject('GeometryBodyOperation', 3042)
                                DependencyObject('CoordinateSystem',
1)
                                    $end 'DependencyInformation'
                                    $begin 'DependencyInformation'
                                        NumParents=2

DependencyObject('GeometryBodyOperation', 3044)

DependencyObject('GeometryBodyOperation', 3043)
                                DependencyObject('CoordinateSystem',
1)
                                    $end 'DependencyInformation'
                                    $begin 'DependencyInformation'
                                        NumParents=2

DependencyObject('GeometryBodyOperation', 3045)

DependencyObject('GeometryBodyOperation', 3044)

```

```

DependencyObject('CoordinateSystem',
1)
    $send 'DependencyInformation'
    $begin 'DependencyInformation'
        NumParents=1
DependencyObject('GeometryBodyOperation', 3214)
    DependencyObject('CoordinateSystem',
1)
        $send 'DependencyInformation'
        $begin 'DependencyInformation'
            NumParents=1
DependencyObject('GeometryBodyOperation', 3228)
DependencyObject('GeometryBodyOperation', 3214)
    $send 'DependencyInformation'
    $begin 'DependencyInformation'
        NumParents=2
DependencyObject('GeometryBodyOperation', 3230)
    DependencyObject('CoordinateSystem',
1)
        DependencyObject('GeometryBodyOperation', 3228)
            $send 'DependencyInformation'
            $begin 'DependencyInformation'
                NumParents=2
DependencyObject('GeometryBodyOperation', 3231)
    DependencyObject('CoordinateSystem',
1)
        DependencyObject('GeometryBodyOperation', 3230)
            $send 'DependencyInformation'
            $begin 'DependencyInformation'
                NumParents=2
DependencyObject('GeometryBodyOperation', 3232)
    DependencyObject('CoordinateSystem',
1)
        DependencyObject('GeometryBodyOperation', 3231)
            $send 'DependencyInformation'
            $begin 'DependencyInformation'
                NumParents=2
DependencyObject('GeometryBodyOperation', 3379)
DependencyObject('GeometryBodyOperation', 3232)
DependencyObject('GeometryBodyOperation', 3368)
    $send 'DependencyInformation'
    $begin 'DependencyInformation'
        NumParents=2
DependencyObject('GeometryBodyOperation', 3503)

```

```

1) DependencyObject('CoordinateSystem',

DependencyObject('GeometryBodyOperation', 3379)
    $send 'DependencyInformation'
    $begin 'DependencyInformation'
        NumParents=2

DependencyObject('GeometryBodyOperation', 3506)
    DependencyObject('CoordinateSystem',
1)

DependencyObject('GeometryBodyOperation', 3503)
    $send 'DependencyInformation'
    $begin 'DependencyInformation'
        NumParents=2

DependencyObject('GeometryBodyOperation', 3509)
    DependencyObject('CoordinateSystem',
1)

DependencyObject('GeometryBodyOperation', 3506)
    $send 'DependencyInformation'
    $begin 'DependencyInformation'
        NumParents=2

DependencyObject('GeometryBodyOperation', 3515)
    DependencyObject('CoordinateSystem',
1)

DependencyObject('GeometryBodyOperation', 3509)
    $send 'DependencyInformation'
    $begin 'DependencyInformation'
        NumParents=2

DependencyObject('GeometryBodyOperation', 3518)
    DependencyObject('CoordinateSystem',
1)

DependencyObject('GeometryBodyOperation', 3515)
    $send 'DependencyInformation'
    $begin 'DependencyInformation'
        NumParents=2

DependencyObject('GeometryBodyOperation', 3527)
    DependencyObject('CoordinateSystem',
1)

DependencyObject('GeometryBodyOperation', 3518)
    $send 'DependencyInformation'
    $begin 'DependencyInformation'
        NumParents=2

DependencyObject('GeometryBodyOperation', 3532)
    DependencyObject('CoordinateSystem',
1)

DependencyObject('GeometryBodyOperation', 3527)

```

```

        $send 'DependencyInformation'
        $begin 'DependencyInformation'
            NumParents=2

DependencyObject('GeometryBodyOperation', 3535)
    DependencyObject('CoordinateSystem',
1)

DependencyObject('GeometryBodyOperation', 3532)
    $send 'DependencyInformation'
    $begin 'DependencyInformation'
        NumParents=2

DependencyObject('GeometryBodyOperation', 3538)
    DependencyObject('CoordinateSystem',
1)

DependencyObject('GeometryBodyOperation', 3535)
    $send 'DependencyInformation'
    $begin 'DependencyInformation'
        NumParents=2

DependencyObject('GeometryBodyOperation', 3541)
    DependencyObject('CoordinateSystem',
1)

DependencyObject('GeometryBodyOperation', 3538)
    $send 'DependencyInformation'
    $begin 'DependencyInformation'
        NumParents=2

DependencyObject('GeometryBodyOperation', 3544)
    DependencyObject('CoordinateSystem',
1)

DependencyObject('GeometryBodyOperation', 3541)
    $send 'DependencyInformation'
    $begin 'DependencyInformation'
        NumParents=2

DependencyObject('GeometryBodyOperation', 3547)
    DependencyObject('CoordinateSystem',
1)

DependencyObject('GeometryBodyOperation', 3544)
    $send 'DependencyInformation'
    $begin 'DependencyInformation'
        NumParents=2

DependencyObject('GeometryBodyOperation', 3553)
    DependencyObject('CoordinateSystem',
1)

DependencyObject('GeometryBodyOperation', 3547)
    $send 'DependencyInformation'
    $begin 'DependencyInformation'
        NumParents=1

```

```

DependencyObject('GeometryBodyOperation', 3258)
    DependencyObject('CoordinateSystem',
1)
        $send 'DependencyInformation'
        $begin 'DependencyInformation'
            NumParents=1

DependencyObject('GeometryBodyOperation', 3272)

DependencyObject('GeometryBodyOperation', 3258)
    $send 'DependencyInformation'
    $begin 'DependencyInformation'
        NumParents=2

DependencyObject('GeometryBodyOperation', 3274)
    DependencyObject('CoordinateSystem',
1)

DependencyObject('GeometryBodyOperation', 3272)
    $send 'DependencyInformation'
    $begin 'DependencyInformation'
        NumParents=2

DependencyObject('GeometryBodyOperation', 3275)
    DependencyObject('CoordinateSystem',
1)

DependencyObject('GeometryBodyOperation', 3274)
    $send 'DependencyInformation'
    $begin 'DependencyInformation'
        NumParents=2

DependencyObject('GeometryBodyOperation', 3392)

DependencyObject('GeometryBodyOperation', 3275)

DependencyObject('GeometryBodyOperation', 3381)
    $send 'DependencyInformation'
    $begin 'DependencyInformation'
        NumParents=2

DependencyObject('GeometryBodyOperation', 3504)
    DependencyObject('CoordinateSystem',
1)

DependencyObject('GeometryBodyOperation', 3392)
    $send 'DependencyInformation'
    $begin 'DependencyInformation'
        NumParents=2

DependencyObject('GeometryBodyOperation', 3507)
    DependencyObject('CoordinateSystem',
1)

DependencyObject('GeometryBodyOperation', 3504)
    $send 'DependencyInformation'
    $begin 'DependencyInformation'

```

```

                                NumParents=2
DependencyObject('GeometryBodyOperation', 3510)
                                DependencyObject('CoordinateSystem',
1)

DependencyObject('GeometryBodyOperation', 3507)
                                $send 'DependencyInformation'
                                $begin 'DependencyInformation'
                                NumParents=2

DependencyObject('GeometryBodyOperation', 3516)
                                DependencyObject('CoordinateSystem',
1)

DependencyObject('GeometryBodyOperation', 3510)
                                $send 'DependencyInformation'
                                $begin 'DependencyInformation'
                                NumParents=2

DependencyObject('GeometryBodyOperation', 3519)
                                DependencyObject('CoordinateSystem',
1)

DependencyObject('GeometryBodyOperation', 3516)
                                $send 'DependencyInformation'
                                $begin 'DependencyInformation'
                                NumParents=2

DependencyObject('GeometryBodyOperation', 3528)
                                DependencyObject('CoordinateSystem',
1)

DependencyObject('GeometryBodyOperation', 3519)
                                $send 'DependencyInformation'
                                $begin 'DependencyInformation'
                                NumParents=2

DependencyObject('GeometryBodyOperation', 3531)
                                DependencyObject('CoordinateSystem',
1)

DependencyObject('GeometryBodyOperation', 3528)
                                $send 'DependencyInformation'
                                $begin 'DependencyInformation'
                                NumParents=2

DependencyObject('GeometryBodyOperation', 3534)
                                DependencyObject('CoordinateSystem',
1)

DependencyObject('GeometryBodyOperation', 3531)
                                $send 'DependencyInformation'
                                $begin 'DependencyInformation'
                                NumParents=2

DependencyObject('GeometryBodyOperation', 3537)

```

```

DependencyObject('CoordinateSystem',
1)

DependencyObject('GeometryBodyOperation', 3534)
    $send 'DependencyInformation'
    $begin 'DependencyInformation'
        NumParents=2

DependencyObject('GeometryBodyOperation', 3540)
    DependencyObject('CoordinateSystem',
1)

DependencyObject('GeometryBodyOperation', 3537)
    $send 'DependencyInformation'
    $begin 'DependencyInformation'
        NumParents=2

DependencyObject('GeometryBodyOperation', 3543)
    DependencyObject('CoordinateSystem',
1)

DependencyObject('GeometryBodyOperation', 3540)
    $send 'DependencyInformation'
    $begin 'DependencyInformation'
        NumParents=2

DependencyObject('GeometryBodyOperation', 3546)
    DependencyObject('CoordinateSystem',
1)

DependencyObject('GeometryBodyOperation', 3543)
    $send 'DependencyInformation'
    $begin 'DependencyInformation'
        NumParents=2

DependencyObject('GeometryBodyOperation', 3552)
    DependencyObject('CoordinateSystem',
1)

DependencyObject('GeometryBodyOperation', 3546)
    $send 'DependencyInformation'
    $begin 'DependencyInformation'
        NumParents=1

DependencyObject('GeometryBodyOperation', 3326)
    DependencyObject('CoordinateSystem',
1)

    $send 'DependencyInformation'
    $begin 'DependencyInformation'
        NumParents=1

DependencyObject('GeometryBodyOperation', 3340)

DependencyObject('GeometryBodyOperation', 3326)
    $send 'DependencyInformation'
    $begin 'DependencyInformation'
        NumParents=2

```

```

DependencyObject('GeometryBodyOperation', 3342)
1) DependencyObject('CoordinateSystem',

DependencyObject('GeometryBodyOperation', 3340)
    $send 'DependencyInformation'
    $begin 'DependencyInformation'
        NumParents=2

DependencyObject('GeometryBodyOperation', 3343)
1) DependencyObject('CoordinateSystem',

DependencyObject('GeometryBodyOperation', 3342)
    $send 'DependencyInformation'
    $begin 'DependencyInformation'
        NumParents=2

DependencyObject('GeometryBodyOperation', 3396)

DependencyObject('GeometryBodyOperation', 3343)

DependencyObject('GeometryBodyOperation', 3344)
    $send 'DependencyInformation'
    $begin 'DependencyInformation'
        NumParents=2

DependencyObject('GeometryBodyOperation', 3505)
1) DependencyObject('CoordinateSystem',

DependencyObject('GeometryBodyOperation', 3396)
    $send 'DependencyInformation'
    $begin 'DependencyInformation'
        NumParents=2

DependencyObject('GeometryBodyOperation', 3508)
1) DependencyObject('CoordinateSystem',

DependencyObject('GeometryBodyOperation', 3505)
    $send 'DependencyInformation'
    $begin 'DependencyInformation'
        NumParents=2

DependencyObject('GeometryBodyOperation', 3511)
1) DependencyObject('CoordinateSystem',

DependencyObject('GeometryBodyOperation', 3508)
    $send 'DependencyInformation'
    $begin 'DependencyInformation'
        NumParents=2

DependencyObject('GeometryBodyOperation', 3517)
1) DependencyObject('CoordinateSystem',

```



```

DependencyObject('GeometryBodyOperation', 3511)
    $send 'DependencyInformation'
    $begin 'DependencyInformation'
        NumParents=2

DependencyObject('GeometryBodyOperation', 3520)
    DependencyObject('CoordinateSystem',
1)

DependencyObject('GeometryBodyOperation', 3517)
    $send 'DependencyInformation'
    $begin 'DependencyInformation'
        NumParents=2

DependencyObject('GeometryBodyOperation', 3529)
    DependencyObject('CoordinateSystem',
1)

DependencyObject('GeometryBodyOperation', 3520)
    $send 'DependencyInformation'
    $begin 'DependencyInformation'
        NumParents=2

DependencyObject('GeometryBodyOperation', 3530)
    DependencyObject('CoordinateSystem',
1)

DependencyObject('GeometryBodyOperation', 3529)
    $send 'DependencyInformation'
    $begin 'DependencyInformation'
        NumParents=2

DependencyObject('GeometryBodyOperation', 3533)
    DependencyObject('CoordinateSystem',
1)

DependencyObject('GeometryBodyOperation', 3530)
    $send 'DependencyInformation'
    $begin 'DependencyInformation'
        NumParents=2

DependencyObject('GeometryBodyOperation', 3536)
    DependencyObject('CoordinateSystem',
1)

DependencyObject('GeometryBodyOperation', 3533)
    $send 'DependencyInformation'
    $begin 'DependencyInformation'
        NumParents=2

DependencyObject('GeometryBodyOperation', 3539)
    DependencyObject('CoordinateSystem',
1)

DependencyObject('GeometryBodyOperation', 3536)
    $send 'DependencyInformation'
    $begin 'DependencyInformation'

```

```

                                NumParents=2
DependencyObject('GeometryBodyOperation', 3542)
                                DependencyObject('CoordinateSystem',
1)
DependencyObject('GeometryBodyOperation', 3539)
                                $send 'DependencyInformation'
                                $begin 'DependencyInformation'
                                NumParents=2
DependencyObject('GeometryBodyOperation', 3545)
                                DependencyObject('CoordinateSystem',
1)
DependencyObject('GeometryBodyOperation', 3542)
                                $send 'DependencyInformation'
                                $begin 'DependencyInformation'
                                NumParents=2
DependencyObject('GeometryBodyOperation', 3551)
                                DependencyObject('CoordinateSystem',
1)
DependencyObject('GeometryBodyOperation', 3545)
                                $send 'DependencyInformation'
                                $begin 'DependencyInformation'
                                NumParents=2
DependencyObject('GeometryBodyOperation', 3368)
DependencyObject('GeometryBodyOperation', 3344)
                                DependencyObject('GeometryOperation',
3367)
                                $send 'DependencyInformation'
                                $begin 'DependencyInformation'
                                NumParents=2
DependencyObject('GeometryBodyOperation', 3381)
DependencyObject('GeometryBodyOperation', 3344)
                                DependencyObject('GeometryOperation',
3380)
                                $send 'DependencyInformation'
                                $begin 'DependencyInformation'
                                NumParents=1
DependencyObject('GeometryBodyOperation', 3400)
                                DependencyObject('CoordinateSystem',
1)
                                $send 'DependencyInformation'
                                $begin 'DependencyInformation'
                                NumParents=1
DependencyObject('GeometryBodyOperation', 3414)
DependencyObject('GeometryBodyOperation', 3400)
                                $send 'DependencyInformation'

```

```

                                $begin 'DependencyInformation'
                                    NumParents=2

DependencyObject('GeometryBodyOperation', 3416)

DependencyObject('GeometryBodyOperation', 3414)
                                DependencyObject('CoordinateSystem',
1)
                                    $send 'DependencyInformation'
                                    $begin 'DependencyInformation'
                                        NumParents=2

DependencyObject('GeometryBodyOperation', 3417)

DependencyObject('GeometryBodyOperation', 3416)
                                DependencyObject('CoordinateSystem',
1)
                                    $send 'DependencyInformation'
                                    $begin 'DependencyInformation'
                                        NumParents=2

DependencyObject('GeometryBodyOperation', 3418)

DependencyObject('GeometryBodyOperation', 3417)
                                DependencyObject('CoordinateSystem',
1)
                                    $send 'DependencyInformation'
                                    $begin 'DependencyInformation'
                                        NumParents=2

DependencyObject('GeometryBodyOperation', 3419)

DependencyObject('GeometryBodyOperation', 3418)

DependencyObject('GeometryBodyOperation', 3481)
                                $send 'DependencyInformation'
                                $begin 'DependencyInformation'
                                    NumParents=1

DependencyObject('GeometryBodyOperation', 3420)
                                DependencyObject('CoordinateSystem',
1)
                                    $send 'DependencyInformation'
                                    $begin 'DependencyInformation'
                                        NumParents=1

DependencyObject('GeometryBodyOperation', 3434)

DependencyObject('GeometryBodyOperation', 3420)
                                $send 'DependencyInformation'
                                $begin 'DependencyInformation'
                                    NumParents=2

DependencyObject('GeometryBodyOperation', 3436)

DependencyObject('GeometryBodyOperation', 3434)
                                DependencyObject('CoordinateSystem',
1)

```

```

                                $send 'DependencyInformation'
                                $begin 'DependencyInformation'
                                    NumParents=2

DependencyObject('GeometryBodyOperation', 3437)

DependencyObject('GeometryBodyOperation', 3436)
                                DependencyObject('CoordinateSystem',
1)
                                    $send 'DependencyInformation'
                                    $begin 'DependencyInformation'
                                        NumParents=2

DependencyObject('GeometryBodyOperation', 3438)

DependencyObject('GeometryBodyOperation', 3437)

DependencyObject('GeometryBodyOperation', 3492)
                                $send 'DependencyInformation'
                                $begin 'DependencyInformation'
                                    NumParents=1

DependencyObject('GeometryBodyOperation', 3442)
                                DependencyObject('CoordinateSystem',
1)
                                    $send 'DependencyInformation'
                                    $begin 'DependencyInformation'
                                        NumParents=1

DependencyObject('GeometryBodyOperation', 3456)

DependencyObject('GeometryBodyOperation', 3442)
                                $send 'DependencyInformation'
                                $begin 'DependencyInformation'
                                    NumParents=2

DependencyObject('GeometryBodyOperation', 3458)

DependencyObject('GeometryBodyOperation', 3456)
                                DependencyObject('CoordinateSystem',
1)
                                    $send 'DependencyInformation'
                                    $begin 'DependencyInformation'
                                        NumParents=2

DependencyObject('GeometryBodyOperation', 3459)

DependencyObject('GeometryBodyOperation', 3458)
                                DependencyObject('CoordinateSystem',
1)
                                    $send 'DependencyInformation'
                                    $begin 'DependencyInformation'
                                        NumParents=2

DependencyObject('GeometryBodyOperation', 3460)

DependencyObject('GeometryBodyOperation', 3459)

```

```

DependencyObject('GeometryBodyOperation', 3478)
    $send 'DependencyInformation'
    $begin 'DependencyInformation'
        NumParents=1

DependencyObject('GeometryBodyOperation', 3464)
    DependencyObject('CoordinateSystem',
1)
        $send 'DependencyInformation'
        $begin 'DependencyInformation'
            NumParents=1

DependencyObject('GeometryBodyOperation', 3474)

DependencyObject('GeometryBodyOperation', 3464)
    $send 'DependencyInformation'
    $begin 'DependencyInformation'
        NumParents=2

DependencyObject('GeometryBodyOperation', 3476)

DependencyObject('GeometryBodyOperation', 3474)
    DependencyObject('CoordinateSystem',
1)
        $send 'DependencyInformation'
        $begin 'DependencyInformation'
            NumParents=2

DependencyObject('GeometryBodyOperation', 3477)

DependencyObject('GeometryBodyOperation', 3476)
    DependencyObject('CoordinateSystem',
1)
        $send 'DependencyInformation'
        $begin 'DependencyInformation'
            NumParents=2

DependencyObject('GeometryBodyOperation', 3478)

DependencyObject('GeometryBodyOperation', 3477)
    DependencyObject('CoordinateSystem',
1)
        $send 'DependencyInformation'
        $begin 'DependencyInformation'
            NumParents=0
        DependencyObject('GeometryOperation',
3479)
            $send 'DependencyInformation'
            $begin 'DependencyInformation'
                NumParents=0
            DependencyObject('GeometryOperation',
3480)
                $send 'DependencyInformation'
                $begin 'DependencyInformation'
                    NumParents=2

DependencyObject('GeometryBodyOperation', 3481)

```

```

DependencyObject('GeometryBodyOperation', 3478)
DependencyObject('GeometryOperation',
3479)
    Send 'DependencyInformation'
    $begin 'DependencyInformation'
        NumParents=2

DependencyObject('GeometryBodyOperation', 3492)

DependencyObject('GeometryBodyOperation', 3478)
DependencyObject('GeometryOperation',
3480)
    Send 'DependencyInformation'
    Send 'GeometryDependencies'
    Send 'GeometryCore'
    $begin 'LastUserInputs'
    Send 'LastUserInputs'
Send 'ModelSetup'
$begin 'BoundarySetup'
    $begin 'GlobalBoundData'
        PortImpedance='1'
        GlobalMaterialEnv='vacuum'
    Send 'GlobalBoundData'
    $begin 'Boundaries'
        NextUniqueID=45
        MoveBackwards=false
    Send 'Boundaries'
    $begin 'ProductSpecificData'
        $begin 'PMLData'
            $begin 'PMLGroups'
            Send 'PMLGroups'
        Send 'PMLData'
        $begin 'SortOrder'
            Port[1: -1]
            Terminal[1: -1]
        Send 'SortOrder'
    Send 'ProductSpecificData'
Send 'BoundarySetup'
$begin 'MeshSetup'
    $begin 'MeshOperations'
        NextUniqueID=0
        MoveBackwards=false
    Send 'MeshOperations'
Send 'MeshSetup'
$begin 'AnalysisSetup'
    $begin 'HfssGlobalData'
        NextUniqueID=0
        MoveBackwards=false
    Send 'HfssGlobalData'
    $begin 'SolveSetups'
        NextUniqueID=3
        MoveBackwards=false
    Send 'SolveSetups'
Send 'AnalysisSetup'
$begin 'Optimetrics'
    $begin 'OptimetricsSetups'
        NextUniqueID=0

```

```

        MoveBackwards=false
    $send 'OptimetricsSetups'
$send 'Optimetrics'
$begin 'Solutions'
    FieldType='NoIncidentWave'
$send 'Solutions'
$begin 'PortFieldDisplay'
    $begin 'PortFieldDisplay'
        ScaleFactor=5
        Frequency='1GHz'
    $send 'PortFieldDisplay'
$send 'PortFieldDisplay'
$begin 'FieldsReporter'
    $begin 'FieldsCalculator'
        Line_Discretization=1000
    $send 'FieldsCalculator'
    $begin 'PlotDefaults'
        Default_SolutionId=-1
        Default_PlotFolder='Automatic'
    $send 'PlotDefaults'
    $begin 'FieldsPlotManagerID'
        NextUniqueID=5
        MoveBackwards=false
        NumQuantityType=0
        NumPlots=0
    $send 'FieldsPlotManagerID'
$send 'FieldsReporter'
$begin 'RadField'
    $begin 'FarFieldSetups'
        NextUniqueID=0
        MoveBackwards=false
    $send 'FarFieldSetups'
    $begin 'ArraySetup'
        UseOption='NoArray'
        $begin 'RegularArray'
            NumUCells='10'
            NumVCells='10'
            CellUDist='10mm'
            CellVDist='10mm'
            UDirnX='1'
            UDirnY='0'
            UDirnZ='0'
            VDirnX='0'
            VDirnY='1'
            VDirnZ='0'
            FirstCellPosX='0mm'
            FirstCellPosY='0mm'
            FirstCellPosZ='0mm'
            UseScanAngle=true
            ScanAnglePhi='45deg'
            ScanAngleTheta='45deg'
            UDirnPhaseShift='0deg'
            VDirnPhaseShift='0deg'
        $send 'RegularArray'
        $begin 'CustomArray'
            NumCells=0
            $begin 'Cell'
            $send 'Cell'

```





```
        $begin 'Reports'
        $end 'Reports'
        $begin 'ReportsWindowPositions'
        $end 'ReportsWindowPositions'
    $end 'ReportSetup'
$end 'HfssDesignInstance'
    $end 'Instance'
$end 'DataInstances'
$end 'AnsoftProject'
```

## Appendix B

### Program code for Single pole triple through (SP3T) switch design

```
$begin 'AnsoftProject'
  Product='HFSS'
  NextUniqueID=0
  MoveBackwards=false
  $begin 'Desktop'
    Version(11, 0)
    InfrastructureVersion(1, 0)
  $end 'Desktop'
  $begin 'HFSSEnvironment'
    Version(1, 0)
  $end 'HFSSEnvironment'
  $begin 'geometry3deditor'
    Version(1, 0)
  $end 'geometry3deditor'
  $begin 'ProjectDatasets'
    NextUniqueID=0
    MoveBackwards=false
    DatasetType='ProjectDatasetType'
    $begin 'DatasetDefinitions'
      $end 'DatasetDefinitions'
    $end 'ProjectDatasets'
    $begin 'Definitions'
      $begin 'Folders'
        Definitions(1104, 10000, 1, 1, 0, false, false)
        Materials(1104, 9500, 9, 2, 1, false, false)
      $end 'Folders'
      $begin 'Materials'
        $begin 'vacuum'
          CoordinateSystemType='Cartesian'
          $begin 'AttachedData'
            $end 'AttachedData'
          $begin 'ModifierData'
            $end 'ModifierData'
          permittivity='1'
          ModTime=1028307964
          Library='Materials'
          LibLocation='SysLibrary '
        $end 'vacuum'
        $begin 'gold'
          CoordinateSystemType='Cartesian'
          $begin 'AttachedData'
            $end 'AttachedData'
          $begin 'ModifierData'
            $end 'ModifierData'
          permeability='0.99996'
          conductivity='41000000'
          thermal_conductivity='315'
          mass_density='19300'
          specific_heat='129'
          youngs_modulus='800000000000'
          poissons_ratio='0.4'
          thermal_expansion_coefficient='1.4e-005'
          ModTime=1132068239
          Library='Materials'
          LibLocation='SysLibrary '
```

```

$send 'gold'
$begin 'Al2_O3_ceramic'
    CoordinateSystemType='Cartesian'
    $begin 'AttachedData'
    $send 'AttachedData'
    $begin 'ModifierData'
    $send 'ModifierData'
    permittivity='9.8'
    thermal_conductivity='35'
    mass_density='3960'
    specific_heat='850'
    youngs_modulus='370000000000'
    poissons_ratio='0.22'
    thermal_expansion_coefficient='8.1e-006'
    ModTime=1132068239
    Library='Materials'
    LibLocation='SysLibrary '
$send 'Al2_O3_ceramic'
$send 'Materials'
$begin 'Scripts'
$send 'Scripts'
$send 'Definitions'
DesignIDServer=2
MoveBackwards=false
$begin 'HFSSModel'
    RepRewriteV2=true
    Name='HFSSDesign1'
    DesignID=0
    'Allow Material Override'=false
    SolutionType='DrivenModal'
    MaterialDensity=1
    MassOfTissue=1
    $begin 'OutputVariable'
        NextUniqueID=0
        MoveBackwards=false
    $send 'OutputVariable'
    $begin 'ModelSetup'
        $begin 'Editor3D Doc Preferences'
            'Plane Background'=true
            BackgroundColor1=16777215
            BackgroundColor2=0
            'Need Lights'=true
            'Ambient Light'=8355711
            'Num Lights'=2
            Light0[4: 8289918, 0.200000002980232,
0.400000005960464, 1]
            Light1[4: 8289918, -0.200000002980232, -
0.400000005960464, -1]
        $send 'Editor3D Doc Preferences'
        $begin 'DesignDatasets'
            NextUniqueID=0
            MoveBackwards=false
            DatasetType='DesignDatasetType'
            $begin 'DatasetDefinitions'
            $send 'DatasetDefinitions'
        $send 'DesignDatasets'
        $begin 'Properties'
            VariableProp('G1', 'UD', 'cpw length', '200um')

```

```

VariableProp('G2', 'UD', 'cpw width', '130um')
VariableProp('P1IN', 'UD', 'Input port length',
'296um')
VariableProp('P2IN', 'UD', 'Input port width',
'40um')
VariableProp('P25', 'UD', '', '40um')
VariableProp('CL', 'UD', 'Cantilever length',
'150um')
VariableProp('CW', 'UD', 'Cantilever width',
'40um')
VariableProp('CBL', 'UD', 'Cantilever back part
length', '80um')
VariableProp('CPAD', 'UD', 'Cantilever pad square
length', '60um')
VariableProp('sub_length', 'UD', '', '496um')
VariableProp('subs_length', 'UD', 'substrate
length', '496um')
VariableProp('subs_height', 'UD', 'substrate
height', '635um')
VariableProp('wpwidth', 'UD', 'wave port width',
'300um')
VariableProp('wpheight', 'UD', 'wave port height',
'900um')
VariableProp('airboxh', 'UD', 'air box height',
'1800um')

VariableProp('ANCHORL', 'UD', '', '20um')
VariableProp('ANCHORW', 'UD', '', '40um')
VariableProp('CTIP', 'UD', '', '20um')
$end 'Properties'
SnapMode=2
GroupByMaterial=true
GroupSheetByMaterial=false
$begin 'GeometryCore'
BlockVersionID=3
NativeKernel='ACIS'
NativeKernelVersionID=1
Units='um'
InstanceID=-1
ExternalNativeGeometryAllowed=false
$begin 'ValidationOptions'
EntityCheckLevel='Strict'
$end 'ValidationOptions'
$begin 'GeometryOperations'
BlockVersionID=2
$begin 'AnsoftRangedIDServerManager'
$begin 'AnsoftRangedIDServer'
IDServerObjectTypeID=0
IDServerRangeMin=0
IDServerRangeMax=2146483647
NextUniqueID=9344
MoveBackwards=false
$end 'AnsoftRangedIDServer'
$begin 'AnsoftRangedIDServer'
IDServerObjectTypeID=1
IDServerRangeMin=2146483648
IDServerRangeMax=2146485547
NextUniqueID=2146483654
MoveBackwards=false

```

```

        $send 'AnsoftRangedIDServer'
$send 'AnsoftRangedIDServerManager'
StartBackGroundFaceID=2146483648
$begin 'CoordinateSystems'
$send 'CoordinateSystems'
$begin 'ToplevelParts'
    $begin 'GeometryPart'
        $begin 'Attributes'
            Name='air_box'
            Flags=''
            Color='(132 132 193)'
            Transparency=1
            PartCoordinateSystem=1
            MaterialName='vacuum'
            SolveInside=true
        $send 'Attributes'
        $begin 'Operations'
            $begin 'Operation'
                OperationType='Box'
                ID=1826

ID=2
BoundType='Radiation'
Faces(1832, 1831, 1830, 1833, 1828)
ParentBndID=-1
IsIncidentField=false
IsEnforcedField=false
IsFssReference=false
IsForPML=false
UseAdaptiveIE=false
$send 'Radl_sides_top_air_box'
$begin 'Finite_cond_bottom_air_box'
    ID=8
    BoundType='Finite Conductivity'
    Faces(1829)
    ParentBndID=-1
    UseMaterial=false
    Material='vacuum'
    Conductivity='58000000'
    Permeability='1'
    Roughness='0um'
    UseThickness=false
    Thickness='0mm'
    InfGroundPlane=false
$send 'Finite_cond_bottom_air_box'
$begin '1'
    ID=19
    BoundType='Wave Port'
    Objects(9280)
    NumModes=1
    ParentBndID=-1
    PolarizeEField=false
    DoDeembed=false
    DeembedDist='0um'
    $begin 'Modes'
        $begin 'Model'
            ModeNum=1

```

```

UseIntLine=true
$begin 'IntLine'
    $begin 'GeometryPosition'

IsAttachedToEntity=true

    EntityID=8672
    PositionType='OnEdge'
    UParam=0
    VParam=0
    XPosition='0'
    YPosition='0'
    ZPosition='0'
    $send 'GeometryPosition'
    $begin 'GeometryPosition'

IsAttachedToEntity=true

    EntityID=7705
    PositionType='OnEdge'

UParam=0.45967741935484

    VParam=0
    XPosition='0'
    YPosition='0'
    ZPosition='0'
    $send 'GeometryPosition'
    $send 'IntLine'
    CharImp='Zp1'
    RenormImp='50ohm'
    $send 'Model'
    $send 'Modes'
    $send '1'
    $begin '2'
        ID=21
        BoundType='Wave Port'
        Objects(9306)
        NumModes=1
        ParentBndID=-1
        PolarizeEField=false
        DoDeembed=false
        DeembedDist='0um'
        $begin 'Modes'
            $begin 'Model'
                ModeNum=1
                UseIntLine=true
                $begin 'IntLine'
                    $begin 'GeometryPosition'

IsAttachedToEntity=true

    EntityID=8368
    PositionType='OnEdge'
    UParam=0
    VParam=0
    XPosition='0'
    YPosition='0'
    ZPosition='0'
    $send 'GeometryPosition'
    $begin 'GeometryPosition'

```

IsAttachedToEntity=true

EntityID=7706  
PositionType='OnEdge'

UParam=0.459677419354837

VParam=0  
XPosition='0'  
YPosition='0'  
ZPosition='0'  
\$send 'GeometryPosition'  
\$send 'IntLine'  
CharImp='Zp1'  
RenormImp='50ohm'  
\$send 'Model'  
\$send 'Modes'  
\$send '2'  
\$begin '3'  
ID=22  
BoundType='Wave Port'  
Objects(9319)  
NumModes=1  
ParentBndID=-1  
PolarizeEField=false  
DoDeembed=false  
DeembedDist='0um'  
\$begin 'Modes'  
\$begin 'Model'  
ModeNum=1  
UseIntLine=true  
\$begin 'IntLine'  
\$begin 'GeometryPosition'

IsAttachedToEntity=true

EntityID=8333  
PositionType='OnEdge'  
UParam=0  
VParam=0  
XPosition='0'  
YPosition='0'  
ZPosition='0'  
\$send 'GeometryPosition'  
\$begin 'GeometryPosition'

IsAttachedToEntity=true

EntityID=7703  
PositionType='OnEdge'

UParam=0.459677419354838

VParam=0  
XPosition='0'  
YPosition='0'  
ZPosition='0'  
\$send 'GeometryPosition'  
\$send 'IntLine'  
CharImp='Zp1'  
RenormImp='50ohm'  
\$send 'Model'

```

        $send 'Modes'
$send '3'
$begin '4'
    ID=23
    BoundType='Wave Port'
    Objects(9332)
    NumModes=1
    ParentBndID=-1
    PolarizeEField=false
    DoDeembed=false
    DeembedDist='0um'
    $begin 'Modes'
        $begin 'Model'
            ModeNum=1
            UseIntLine=true
            $begin 'IntLine'
                $begin 'GeometryPosition'

IsAttachedToEntity=true

EntityID=8603
PositionType='OnEdge'
UParam=0
VParam=0
XPosition='0'
YPosition='0'
ZPosition='0'
$send 'GeometryPosition'
$begin 'GeometryPosition'

IsAttachedToEntity=true

EntityID=6311
PositionType='OnEdge'
UParam=0
VParam=0
XPosition='0'
YPosition='0'
ZPosition='0'
$send 'GeometryPosition'
$send 'IntLine'
CharImp='Zpi'
RenormImp='50ohm'
$send 'Model'
$send 'Modes'
$send '4'
$send 'Boundaries'
$begin 'ProductSpecificData'
    $begin 'PMLData'
        $begin 'PMLGroups'
            $send 'PMLGroups'
        $send 'PMLData'
    $begin 'SortOrder'
        Port[1: -1]
        Terminal[1: -1]
    $send 'SortOrder'
$send 'ProductSpecificData'
$send 'BoundarySetup'
$begin 'MeshSetup'
    $begin 'MeshOperations'

```



```

        NextUniqueID=0
        MoveBackwards=false
    $end 'MeshOperations'
$end 'MeshSetup'
$begin 'AnalysisSetup'
    $begin 'HfssGlobalData'
        NextUniqueID=0
        MoveBackwards=false
    $end 'HfssGlobalData'
    $begin 'SolveSetups'
        NextUniqueID=5
        MoveBackwards=false
        $begin 'Setup1'
            ID=4
            SetupType='HfssDriven'
            Frequency='77GHz'
            PortsOnly=false
            MaxDeltaS=0.02
            UseMatrixConv=false
            MaximumPasses=9
            MinimumPasses=1
            MinimumConvergedPasses=1
            PercentRefinement=30
            BasisOrder=1
            UseIterativeSolver=false
            DoLambdaRefine=true
            DoMaterialLambda=true
            SetLambdaTarget=false
            Target=0.3333
            UseConvOutputVariable=false
            IsEnabled=true
            ExternalMesh=false
            UseMaxTetIncrease=false
            MaxTetIncrease=100000
            PortAccuracy=2
            UseABConPort=false
            SetPortMinMaxTri=false
            PortMinTri=100
            PortMaxTri=500
            $begin 'Sweeps'
                NextUniqueID=1
                MoveBackwards=false
                $begin 'Sweep1'
                    ID=0
                    IsEnabled=true
                    SetupType='LinearStep'
                    StartValue='1GHz'
                    StopValue='80GHz'
                    StepSize='1GHz'
                    Type='Discrete'
                    SaveFields=false
                    ExtrapolateToDC=false
                $end 'Sweep1'
            $end 'Sweeps'
        $end 'Setup1'
    $end 'SolveSetups'
$end 'AnalysisSetup'
$begin 'Optimetrics'

```

```

$begin 'OptimetricsSetups'
    NextUniqueID=0
    MoveBackwards=false
$end 'OptimetricsSetups'
$send 'Optimetrics'
$begin 'Solutions'
    FieldType='NoIncidentWave'
    SourceEntry(ID=19, Index=0, Terminal=false,
Terminated=false, Magnitude='1W', Phase='0deg')
    SourceEntry(ID=21, Index=0, Terminal=false,
Terminated=false, Magnitude='0W', Phase='0deg')
    SourceEntry(ID=22, Index=0, Terminal=false,
Terminated=false, Magnitude='0W', Phase='0deg')
    SourceEntry(ID=23, Index=0, Terminal=false,
Terminated=false, Magnitude='0W', Phase='0deg')
$end 'Solutions'
$begin 'PortFieldDisplay'
    $begin 'PortFieldDisplay'
        ScaleFactor=5
        Solution='Setup1 : LastAdaptive'
        Frequency='77GHz'
    $end 'PortFieldDisplay'
$send 'PortFieldDisplay'
$begin 'FieldsReporter'
    $begin 'FieldsCalculator'
        Line_Discretization=1000
    $end 'FieldsCalculator'
    $begin 'PlotDefaults'
        Default_SolutionId=1644
        Default_PlotFolder='Automatic'
    $end 'PlotDefaults'
    $begin 'FieldsPlotManagerID'
        NextUniqueID=24
        MoveBackwards=false
        NumQuantityType=1
        $begin 'QuantityFolder_1'
            PlotFolder='E Field'
            'Real time mode'=true
            $begin 'ColorMapSettings'
                ColorMapType='Spectrum'
                SpectrumType='Rainbow'
                UniformColor(127, 255, 255)
                RampColor(255, 127, 127)
            $end 'ColorMapSettings'
            $begin 'Scale3DSettings'
                m_nLevels=15
                m_autoScale=true
                minvalue=11.7735624313354
                maxvalue=2486059.75
                log=false
                IntrinsicMin=11.7735624313354
                IntrinsicMax=2486059.75
                LimitFieldValuePrecision=false
                FieldValuePrecisionDigits=4
            $end 'Scale3DSettings'
            $begin 'Marker3DSettings'
                MarkerType=9
                MarkerMapSize=true

```

```

        MarkerMapColor=false
        MarkerSize=0.25
    $end 'Marker3DSettings'
    $begin 'Arrow3DSettings'
        ArrowType=1
        ArrowMapSize=true
        ArrowMapColor=true
        ShowArrowTail=true
        ArrowSize=0.25
    $end 'Arrow3DSettings'
$end 'QuantityFolder_1'
NumPlots=1
$begin 'PlotDefinition_1'
    PlotName='Mag_E1'
    PlotDefinitionId=23
    VersionID=0
    SolutionId=1644
    QuantityId=2
    PlotFolder='E Field'
    UserSpecifyName=0
    UserSpecifyFolder=0
    IntrinsicVar='Freq=\'77GHz\' Phase=\'0deg\''
    $begin 'PlotOnSurfaceSettings'
        Filled=false
        IsoValType='Fringe'
        SmoothShade=true
        AddGrid=false
        MapTransparency=true
        Refinement=0
        Transparency=0
        $begin 'Arrow3DSpacingSettings'
            ArrowUniform=true
            ArrowSpacing=28.9777030944824
            MinArrowSpacing=19.3184680938721
            MaxArrowSpacing=38.6369361877441
        $end 'Arrow3DSpacingSettings'
        GridColor(255, 255, 255)
    $end 'PlotOnSurfaceSettings'
    $end 'PlotDefinition_1'
    $end 'FieldsPlotManagerID'
$end 'FieldsReporter'
$begin 'RadField'
    $begin 'FarFieldSetups'
        NextUniqueID=0
        MoveBackwards=false
    $end 'FarFieldSetups'
    $begin 'ArraySetup'
        UseOption='NoArray'
        $begin 'RegularArray'
            NumUCells='10'
            NumVCells='10'
            CellUDist='10mm'
            CellVDist='10mm'
            UDirnX='1'
            UDirnY='0'
            UDirnZ='0'
            VDirnX='0'
            VDirnY='1'

```

```

        VDirnZ='0'
        FirstCellPosX='0mm'
        FirstCellPosY='0mm'
        FirstCellPosZ='0mm'
        UseScanAngle=true
        ScanAnglePhi='45deg'
        ScanAngleTheta='45deg'
        UDirnPhaseShift='0deg'
        VDirnPhaseShift='0deg'
    $end 'RegularArray'
    $begin 'CustomArray'
        NumCells=0
        $begin 'Cell'
        $end 'Cell'
    $end 'CustomArray'
$end 'ArraySetup'
$begin 'NearFieldSetups'
    NextUniqueID=0
    MoveBackwards=false
$end 'NearFieldSetups'
RadFieldComputationVersion=1.4
RadfieldHeaderFile='RAD4998327212247095220.tmp'
$end 'RadField'
$begin 'SolutionManager'
    $begin 'SimSetup'
        TypeName='BaseSetup'
        ID=1642
        Name='Setup1'
        $begin 'Solution'
            ID=1643
            Name='AdaptivePass'
            $begin 'SimDataExtractor'
                $begin 'Sweeps'
                    $begin 'Sweep'
                        Variable='Pass'
                        Column='1;2;3;4;5;6;7;8;9'
                        Units=''
                    $end 'Sweep'
                    $begin 'Sweep'
                        Variable='Freq'
                        Column='77GHz'
                        Units='GHz'
                    $end 'Sweep'
                $begin 'PostprocessSweep'

Variable='NormalizedDistance'

RegularSweep=1
Units=''
Minimum=0
Maximum=1
Increment=0.01

CreateIndexedSubsweepFlag=false

$end 'PostprocessSweep'
$begin 'PostprocessSweep'
    Variable='Phi'
    RegularSweep=1
    Units='deg'

```

```

Minimum=0
Maximum=6.28318530717959

Increment=0.0872664625997165

CreateIndexedSubsweepFlag=false
$send 'PostprocessSweep'
$begin 'PostprocessSweep'
    Variable='Theta'
    RegularSweep=1
    Units='deg'
    Minimum=0
    Maximum=6.28318530717959

Increment=0.0872664625997165

CreateIndexedSubsweepFlag=false
$send 'PostprocessSweep'
$begin 'PostprocessSweep'
    Variable='Phase'
    RegularSweep=1
    Units='deg'
    Minimum=0
    Maximum=6.28318530717959

Increment=0.0872664625997165

CreateIndexedSubsweepFlag=false
$send 'PostprocessSweep'
$send 'Sweeps'
    IsPortOnly=false
$send 'SimDataExtractor'
$begin 'Solution'
    ID=1644
    Name='LastAdaptive'
$begin 'SimDataExtractor'
    $begin 'Sweeps'
        $begin 'Sweep'
            Variable='Freq'
            Column='77GHz'
            Units='GHz'
        $end 'Sweep'
    $begin 'PostprocessSweep'

Variable='NormalizedDistance'
    RegularSweep=1
    Units=''
    Minimum=0
    Maximum=1
    Increment=0.01

CreateIndexedSubsweepFlag=false
$send 'PostprocessSweep'
$begin 'PostprocessSweep'
    Variable='Phi'
    RegularSweep=1
    Units='deg'

```

```

Minimum=0
Maximum=6.28318530717959

Increment=0.0872664625997165

CreateIndexedSubsweepFlag=false
$send 'PostprocessSweep'
$begin 'PostprocessSweep'
    Variable='Theta'
    RegularSweep=1
    Units='deg'
    Minimum=0
    Maximum=6.28318530717959

Increment=0.0872664625997165

CreateIndexedSubsweepFlag=false
$send 'PostprocessSweep'
$begin 'PostprocessSweep'
    Variable='Phase'
    RegularSweep=1
    Units='deg'
    Minimum=0
    Maximum=6.28318530717959

Increment=0.0872664625997165

CreateIndexedSubsweepFlag=false
$send 'PostprocessSweep'
$send 'Sweeps'
    IsPortOnly=false
$send 'SimDataExtractor'
$begin 'Solution'
    ID=1645
    Name='Sweep1'
$begin 'SimDataExtractor'
    SimValue('S(1,1)', 2, 90, false,
SimValueID=4325, 3, 0, 2, 0, false, false, -1, 1, 0, 1, 1, '', 0, 0)
    SimValue('S(1,2)', 2, 90, false,
SimValueID=4326, 3, 0, 2, 0, false, false, -1, 1, 0, 1, 1, '', 0, 0)
    SimValue('S(1,3)', 2, 90, false,
SimValueID=4327, 3, 0, 2, 0, false, false, -1, 1, 0, 1, 1, '', 0, 0)
    SimValue('S(1,4)', 2, 90, false,
SimValueID=4328, 3, 0, 2, 0, false, false, -1, 1, 0, 1, 1, '', 0, 0)
$begin 'Sweeps'
    $begin 'Sweep'
        Variable='Freq'

        Column='1GHz;2GHz;3GHz;4GHz;5GHz;6GHz;7GHz;8GHz;9GHz;10GHz;11GHz;12
GHz;13GHz;14GHz;15GHz;16GHz;17GHz;18GHz;19GHz;20GHz;21GHz;22GHz;23GHz;24G
Hz;25GHz;26GHz;27GHz;28GHz;29GHz;30GHz;31GHz;32GHz;33GHz;35GHz;36GH
z;37GHz;38GHz;39GHz;40GHz;41GHz;42GHz;43GHz;44GHz;45GHz;46GHz;47GHz;48GHz
;49GHz;50GHz;51GHz;52GHz;53GHz;54GHz;55GHz;56GHz;57GHz;58GHz;59GHz;60GHz;
61GHz;62GHz;63GHz;64GHz;65GHz;66GHz;67GHz;68GHz;69GHz;70GHz;71GHz;72GHz;7
3GHz;74GHz;75GHz;76GHz;77GHz;78GHz;79GHz;80GHz'

        Units='GHz'
    $end 'Sweep'

```

```

                                $begin 'PostprocessSweep'

Variable='NormalizedDistance'
                                RegularSweep=1
                                Units=''
                                Minimum=0
                                Maximum=1
                                Increment=0.01

CreateIndexedSubsweepFlag=false
                                $end 'PostprocessSweep'
                                $begin 'PostprocessSweep'
                                    Variable='Phi'
                                    RegularSweep=1
                                    Units='deg'
                                    Minimum=0
                                    Maximum=6.28318530717959

Increment=0.0872664625997165

CreateIndexedSubsweepFlag=false
                                $end 'PostprocessSweep'
                                $begin 'PostprocessSweep'
                                    Variable='Theta'
                                    RegularSweep=1
                                    Units='deg'
                                    Minimum=0
                                    Maximum=6.28318530717959

Increment=0.0872664625997165

CreateIndexedSubsweepFlag=false
                                $end 'PostprocessSweep'
                                $begin 'PostprocessSweep'
                                    Variable='Phase'
                                    RegularSweep=1
                                    Units='deg'
                                    Minimum=0
                                    Maximum=6.28318530717959

                                '3D
Modeler'(Editor3d(View(WindowPos(3, -1, -1, -8, -28, 0, 0, 695, 301),
OrientationMatrix(-0.0034198306966573, -1.28466917885817e-005, -
1.6184962078114e-005, 0, 1.3118437891535e-005, -0.00341943977400661, -
5.41112276550848e-005, 0, -1.59492446982767e-005, -5.42143643542659e-005,
0.00341942603699863, 0, 0.0470452755689621, -0.00393755361437798, -
8.80115509033203, 1, 0, -1.9488753080368, 1.9488753080368, -1, 1, -
8.62185668945313, 24.4116916656494), Drawings[12: 'air_box',
'Shorting_piece', 'Port_3', 'Port_1', 'Port_2', '1_1', 'Substrate_1',
'GND', 'wp1', 'wp2', 'wp3', 'wp4'], 'View Data'('Render Mode'=1)))
                                $end 'EditorWindow'
                                $end 'WindowPosition'
                                $begin 'ReportSetup'
                                    $begin 'ReportManager'
                                        $begin 'Reports'
                                            $begin 'XY Plot 1'
                                                ReportID=327
                                                ReportName='XY Plot 1'

```

```

TraceDefinitionType='TraceDefinition'

ID=323
VersionID=671
Name='dB(S(1,1))'
TieNameToExpr=true
$begin 'Components'
    $begin
'TraceComponentDefinition'
    Expr='Freq'
    $send
'TraceComponentDefinition'
    $begin
'TraceComponentDefinition'
    Expr='dB(S(1,1))'
    $send
'TraceComponentDefinition'
    $send 'Components'
    $begin
'ExtendedTraceInfo'
    NumPoints=0
    TraceType=0
    Offset=0
    XLabel=''

    SamplingPeriod='0'
    SamplingPeriodOffset='0'
    YAxis=1
    $send
'ExtendedTraceInfo'
    $begin
'DesignSolnDefn'
    $begin
'DESIGN_SOLUTION_SIM_VALUE_CONTEXT'
    DesignID=0
    SolutionID=1645
    $begin
'REPORT_TYPE_SIM_VALUE_CONTEXT'
    ReportType=0
    SimValueContext(3, 0, 2, 0, false, false, -1, 1, 0, 1, 1, '', 0, 0)
    $send
'REPORT_TYPE_SIM_VALUE_CONTEXT'
    $send
'DESIGN_SOLUTION_SIM_VALUE_CONTEXT'
    $send 'DesignSolnDefn'

name='XY Plot 2'
ReportID=329
ReportType=0

```



```

DisplayType=1
Title=''
Domain=''
$begin 'Graph2DsV2'
    $begin 'Graph2D'
        TraceDefID=328

Type='Continuous'

Axis='Y1'
$end 'Graph2D'
$end 'Graph2DsV2'
$begin

'PlotDisplayDataManager'

NextUniqueID=33
MoveBackwards=false
$begin

'PlotHeaderDataSource'

CompanyName='Ansoft Corporation'

ShowDesignName=true

ProjectFileName=''

$end

'PlotHeaderDataSource'

StockNameIDMap(AxisX=4, AxisY1=5, AxisY2=6, AxisY3=7, AxisY4=8,
Grid=9, Header=0, Legend=2)

$begin 'SourceList'
$end 'SourceList'
$begin

'PlotAttributeStoreMap'

$begin

'MainMapItem'

$begin

'SubMapItem'

DataSourceID=9

$begin 'CartesianGridDescAttribute'

ShowXMinor=true

ShowYMinor=true

ShowXMajor=true

ShowYMajor=true

$end

'CartesianGridDescAttribute'

$end

'SubMapItem'

$end

'MainMapItem'

$begin

'MainMapItem'

$begin

'SubMapItem'

```

```

DataSourceID=19

$begin 'CurveCartesianAttribute'

YAxis='Y1'
$end
'CurveCartesianAttribute'
$end
'SubMapItem'
$end
'MainMapItem'
$begin
'MainMapItem'
$begin
'SubMapItem'

DataSourceID=19

$begin 'CurveRenderAttribute'

$begin 'LineRenderAttribute'

LineStyle='Solid'

LineWidth=2

LineColor(R=255, G=0, B=0)

$end 'LineRenderAttribute'

TraceType='Continuous'

SymbolType='HorizontalLeftTriangle'

SymbolColor(R=0, G=25, B=185)

ShowSymbols=false

SymbolFrequency=15

ShowArrows=false
$end
'CurveRenderAttribute'
$end
'SubMapItem'
$end
'MainMapItem'
$begin
$begin 'XY Plot 4'
ReportID=333
$begin 'Report2D'
name='XY Plot 4'
ReportID=333
ReportType=0
DisplayType=1
Title=''
Domain=''

```

```

Type='Continuous'

$begin 'Graph2DsV2'
    $begin 'Graph2D'
        TraceDefID=332
        Axis='Y1'
    $end 'Graph2D'
$end 'Graph2DsV2'
$begin

'PlotDisplayDataManager'

    NextUniqueID=33
    MoveBackwards=false
    $begin

'PlotHeaderDataSource'

    CompanyName='Ansoft Corporation'

    ShowDesignName=true

    ProjectFileName=''

    $end

'PlotHeaderDataSource'

    StockNameIDMap(AxisX=4, AxisY1=5, AxisY2=6, AxisY3=7, AxisY4=8,
Grid=9, Header=0, Legend=2)

    $begin 'SourceList'
    $end 'SourceList'
    $begin

'PlotAttributeStoreMap'

    $begin

'MainMapItem'

    $begin

'SubMapItem'

    DataSourceID=9

    $begin 'CartesianGridDescAttribute'

    ShowXMinor=true

    ShowYMinor=true

    ShowXMajor=true

    ShowYMajor=true

    $end

'CartesianGridDescAttribute'

    $end

'SubMapItem'

    $end

'MainMapItem'

    $begin

'MainMapItem'

    $begin

'SubMapItem'

    DataSourceID=19

```

```

        $begin 'CurveCartesianAttribute'
            YAxis='Y1'
        $end
    'CurveCartesianAttribute'
    $end
    'SubMapItem'
    $end
    'MainMapItem'
    $begin
    'MainMapItem'
        $begin
    'SubMapItem'
        DataSourceID=19
        $begin 'CurveRenderAttribute'
            $begin 'LineRenderAttribute'
                LineStyle='Solid'
                LineWidth=2
                LineColor(R=255, G=0, B=0)
            $end 'LineRenderAttribute'
            TraceType='Continuous'
            SymbolType='HorizontalLeftTriangle'
            SymbolColor(R=0, G=25, B=185)
            ShowSymbols=false
            SymbolFrequency=15
            ShowArrows=false
        $end
    'CurveRenderAttribute'
    $end
    'SubMapItem'
    $end
    'MainMapItem'
    $begin
    'MainMapItem'
        $begin
    'SubMapItem'
        DataSourceID=4
        $begin 'LineAxisRenderAttribute'
            DecimalFieldWidth=3
            DecimalFieldPrecision=2

```

```

ManualTitle=''

AxisColor(R=0, G=0, B=0)

MinScale=0

MaxScale=1

TickSpacing=1

ManualUnits=false

Units='mm'

AxisScale='Linear'

NumberFormat='Auto'

0, 19)

'TraceCharacteristicsMgr'
'TraceCharacteristicsMgr'
'CartesianXMarkerManager'
'ReferenceCurves'
'ReferenceCurves'
'CartesianXMarkerManager'
'PlotDisplayDataManager'

ViewID=-1
$begin 'SourceIDMap'
    IDMapItem(332,

$end 'SourceIDMap'
$begin

$end

$begin

    RefMarkerID=-1
$begin

$end

$end

$end

$end 'Report2D'
$end 'XY Plot 4'
$begin 'XY Plot 5'
    ReportID=335
    $begin 'Report2D'
        name='XY Plot 5'
        ReportID=335
        ReportType=0
        DisplayType=1
        Title=''
        Domain=''
        $begin 'Graph2DsV2'
            $begin 'Graph2D'
                TraceDefID=334

Type='Continuous'

        Axis='Y1'
        $end 'Graph2D'
    $end 'Graph2DsV2'

```

```

PlotDisplayDataManager'
    $begin
        NextUniqueID=33
        MoveBackwards=false
    $begin
PlotHeaderDataSource'
    CompanyName='Ansoft Corporation'
    ShowDesignName=true
    ProjectFileName=''
    $send
PlotHeaderDataSource'
    StockNameIDMap(AxisX=4, AxisY1=5, AxisY2=6, AxisY3=7, AxisY4=8,
Grid=9, Header=0, Legend=2)
    $begin 'SourceList'
    $send 'SourceList'
    $begin
PlotAttributeStoreMap'
    $begin
MainMapItem'
    $begin
SubMapItem'
    DataSourceID=9
    $begin 'CartesianGridDescAttribute'
    ShowXMinor=true
    ShowYMinor=true
    ShowXMajor=true
    ShowYMajor=true
    $send
'CartesianGridDescAttribute'
    $send
SubMapItem'
    $send
MainMapItem'
    $begin
MainMapItem'
    $begin
SubMapItem'
    DataSourceID=19
    $begin 'CurveCartesianAttribute'
    YAxis='Y1'
    $send
'CurveCartesianAttribute'
    $send
SubMapItem'

```

```

'MainMapItem'
'MainMapItem'
'SubMapItem'
    DataSourceID=19
    $begin 'CurveRenderAttribute'
    $begin 'LineRenderAttribute'
        LineStyle='Solid'
        LineWidth=2
        LineColor(R=255, G=0, B=0)
    $end 'LineRenderAttribute'
    TraceType='Continuous'
    SymbolType='HorizontalLeftTriangle'
    SymbolColor(R=0, G=25, B=185)
    ShowSymbols=false
    SymbolFrequency=15
    ShowArrows=false
    $end
'CurveRenderAttribute'
'SubMapItem'
'MainMapItem'
'MainMapItem'
'SubMapItem'
    DataSourceID=4
    $begin 'LineAxisRenderAttribute'
    DecimalFieldWidth=3
    DecimalFieldPrecision=2
    ManualTitle=''
    AxisColor(R=0, G=0, B=0)
    MinScale=0
    MaxScale=1

```

```

TickSpacing=1
ManualUnits=false
Units='mm'
AxisScale='Linear'
NumberFormat='Auto'
$begin 'TextFont'
    $begin 'FontAttribute'
        $begin 'Font'
            Height=-12
            Width=0
            Escapement=0
            Orientation=0
            Weight=400
            Italic=0
            Underline=0
            StrikeOut=0
            CharSet=0
            OutPrecision=7
            ClipPrecision=48
            Quality=6
            PitchAndFamily=0
            FaceName='Arial'
        $end 'Font'
        Color(R=0, G=0, B=0)
    $end 'FontAttribute'
$end 'TextFont'
InfMapMode=false
InfMapValue=1.79769313486232e+306
AutoRangeMin=true

```



```

        AutoRangeMax=true

        AutoSpacing=true

        kNumMinorDivisions=5
                                                    $end
'LineAxisRenderAttribute'
                                                    $end
'SubMapItem'
                                                    $begin
'SubMapItem'

        DataSourceID=5

        $begin 'LineAxisRenderAttribute'

        DecimalFieldWidth=3

        DecimalFieldPrecision=2

        ManualTitle=''

        AxisColor(R=0, G=0, B=0)

        MinScale=0

        MaxScale=1

        TickSpacing=1

        ManualUnits=false

        Units='mm'

        AxisScale='Linear'

        NumberFormat='Auto'

        $begin 'TextFont'

                $begin 'FontAttribute'

                        $begin 'Font'

                                Height=-12

                                Width=0

                                Escapement=0

                                Orientation=0

                                Weight=400

                                Italic=0

                                Underline=0

```

```

        StrikeOut=0
        CharSet=0
        OutPrecision=7
        ClipPrecision=48
        Quality=6
        PitchAndFamily=0
        FaceName='Arial'
    $end 'Font'
    Color(R=0, G=0, B=0)
    $end 'FontAttribute'
    $end 'TextFont'
    InfMapMode=false
    InfMapValue=1.79769313486232e+306
    AutoRangeMin=true
    AutoRangeMax=true
    AutoSpacing=true
    kNumMinorDivisions=5
    $end
'LineAxisRenderAttribute'
$end
'SubMapItem'
$begin
'SubMapItem'
    DataSourceID=6
    $begin 'LineAxisRenderAttribute'
        DecimalFieldWidth=3
        DecimalFieldPrecision=2
        ManualTitle=''
        AxisColor(R=0, G=0, B=0)
        MinScale=0
        MaxScale=1
        TickSpacing=1

```

```

ManualUnits=false

Units='mm'

AxisScale='Linear'

NumberFormat='Auto'

$begin 'TextFont'

    $begin 'FontAttribute'

        $begin 'Font'

            Height=-12

            Width=0

            Escapement=0

            Orientation=0

            Weight=400

            Italic=0

            Underline=0

            StrikeOut=0

            CharSet=0

            OutPrecision=7

            ClipPrecision=48

            Quality=6

            PitchAndFamily=0

            FaceName='Arial'

        $end 'Font'

        Color(R=0, G=0, B=0)

    $end 'FontAttribute'

$end 'TextFont'

InfMapMode=false

InfMapValue=1.79769313486232e+306

AutoRangeMin=true

AutoRangeMax=true

```

```

        AutoSpacing=true
        kNumMinorDivisions=5
                                                    $end
'LineAxisRenderAttribute'
                                                    $end
'SubMapItem'
                                                    $begin
'SubMapItem'
        DataSourceID=7
        $begin 'LineAxisRenderAttribute'
        DecimalFieldWidth=3
        DecimalFieldPrecision=2
        ManualTitle=''
        AxisColor(R=0, G=0, B=0)
        MinScale=0
        MaxScale=1
        TickSpacing=1
        ManualUnits=false
        Units='mm'
        AxisScale='Linear'
        NumberFormat='Auto'
        $begin 'TextFont'
                $begin 'FontAttribute'
                        $begin 'Font'
                                Height=-12
                                Width=0
                                Escapement=0
                                Orientation=0
                                Weight=400
                                Italic=0
                                Underline=0
                                StrikeOut=0

```

```

CharSet=0
OutPrecision=7
ClipPrecision=48
Quality=6
PitchAndFamily=0
FaceName='Arial'

$end 'Font'

Color(R=0, G=0, B=0)

$end 'FontAttribute'

$end 'TextFont'

InfMapMode=false
InfMapValue=1.79769313486232e+306
AutoRangeMin=true
AutoRangeMax=true
AutoSpacing=true
kNumMinorDivisions=5

'LineAxisRenderAttribute'
'SubMapItem'
'SubMapItem'

DataSourceID=8
$begin 'LineAxisRenderAttribute'
DecimalFieldWidth=3
DecimalFieldPrecision=2
ManualTitle=''
AxisColor(R=0, G=0, B=0)
MinScale=0
MaxScale=1
TickSpacing=1
ManualUnits=false

```

```

Units='mm'

AxisScale='Linear'

NumberFormat='Auto'

$begin 'TextFont'
    $begin 'FontAttribute'
        $begin 'Font'
            Height=-12
            Width=0
            Escapement=0
            Orientation=0
            Weight=400
            Italic=0
            Underline=0
            StrikeOut=0
            CharSet=0
            OutPrecision=7
            ClipPrecision=48
            Quality=6
            PitchAndFamily=0
            FaceName='Arial'
        $end 'Font'
        Color(R=0, G=0, B=0)
    $end 'FontAttribute'
$end 'TextFont'

InfMapMode=false

InfMapValue=1.79769313486232e+306

AutoRangeMin=true

AutoRangeMax=true

AutoSpacing=true

```

```

        kNumMinorDivisions=5
                                                                    $end
'LineAxisRenderAttribute'
                                                                    $end
'SubMapItem'
                                                                    $end
'MainMapItem'
                                                                    $end
'PlotAttributeStoreMap'
                                                                    $begin
'PerViewPlotAttributeStoreMap'
                                                                    $begin 'MapItem'
                                                                    $begin
'PlotAttributeStoreMap'
        $begin 'MainMapItem'
        $begin 'SubMapItem'
                DataSourceID=1
                $begin 'BasicLayoutAttribute'
                        $begin 'LayoutRect'
                                Top=883
                                Left=1091
                                Bottom=9749
                                Right=8968
                        $end 'LayoutRect'
                $end 'BasicLayoutAttribute'
        $end 'SubMapItem'
        $begin 'SubMapItem'
                DataSourceID=10
                $begin 'BasicLayoutAttribute'
                        $begin 'LayoutRect'
                                Top=883
                                Left=1091
                                Bottom=9749
                                Right=8968
                        $end 'LayoutRect'

```

```

        $end 'BasicLayoutAttribute'
    $end 'SubMapItem'
    $begin 'SubMapItem'
        DataSourceID=17
        $begin 'BasicLayoutAttribute'
            $begin 'LayoutRect'
                Top=75
                Left=75
                Bottom=9925
                Right=916
            $end 'LayoutRect'
        $end 'BasicLayoutAttribute'
    $end 'SubMapItem'
$end
'MainMapItem'
    $begin 'MainMapItem'
        $begin 'SubMapItem'
            DataSourceID=13
            $begin 'CartesianAxisLayoutAttribute'
                FontScale=1
                $begin 'AxisRect'
                    Top=75
                    Left=8968
                    Bottom=9925
                    Right=9925
                $end 'AxisRect'
                $begin 'GridRect'
                    Top=883
                    Left=1091
                    Bottom=9749

```



```

        Right=8968
        $end 'GridRect'
        $end 'CartesianAxisLayoutAttribute'
    $end 'SubMapItem'
    $begin 'SubMapItem'
        DataSourceID=14
        $begin 'CartesianAxisLayoutAttribute'
            FontScale=1
            $begin 'AxisRect'
                Top=75
                Left=916
                Bottom=882
                Right=8968
            $end 'AxisRect'
            $begin 'GridRect'
                Top=883
                Left=1091
                Bottom=9749
                Right=8968
            $end 'GridRect'
        $end 'CartesianAxisLayoutAttribute'
    $end 'SubMapItem'
    $end 'MainMapItem'
    $begin 'MainMapItem'
        $begin 'SubMapItem'
            DataSourceID=3
            $begin 'OverlayLayoutAttribute'
                $begin 'BoundingRect'
                    Top=8528

```

```

        Left=3399
        Bottom=9509
        Right=4597
        $Send 'BoundingRect'
        ModifySize=false
        ModifyPosition=true
        $Send 'OverlayLayoutAttribute'
    $Send 'SubMapItem'
$Send
'MainMapItem'
$Send
'PlotAttributeStoreMap'
$Send 'MapItem'
$begin 'MapItem'
$begin
'PlotAttributeStoreMap'
$begin 'MainMapItem'
$begin 'SubMapItem'
    DataSourceID=21
    $begin 'BasicLayoutAttribute'
        $begin 'LayoutRect'
            Top=883
            Left=1091
            Bottom=9749
            Right=8968
        $end 'LayoutRect'
    $end 'BasicLayoutAttribute'
$end 'SubMapItem'
$begin 'SubMapItem'
    DataSourceID=23
    $begin 'BasicLayoutAttribute'
        $begin 'LayoutRect'
            Top=883

```

```

        Left=1091
        Bottom=9749
        Right=8968
        $end 'LayoutRect'
        $end 'BasicLayoutAttribute'
    $end 'SubMapItem'
    $begin 'SubMapItem'
        DataSourceID=30
        $begin 'BasicLayoutAttribute'
            $begin 'LayoutRect'
                Top=75
                Left=75
                Bottom=9925
                Right=916
            $end 'LayoutRect'
            $end 'BasicLayoutAttribute'
        $end 'SubMapItem'
    $end 'MainMapItem'
    $begin 'MainMapItem'
        $begin 'SubMapItem'
            DataSourceID=26
            $begin 'CartesianAxisLayoutAttribute'
                FontScale=1
                $begin 'AxisRect'
                    Top=75
                    Left=8968
                    Bottom=9925
                    Right=9925
                $end 'AxisRect'
            $end 'CartesianAxisLayoutAttribute'
        $end 'SubMapItem'
    $end 'MainMapItem'

```

```

        $begin 'GridRect'
            Top=883
            Left=1091
            Bottom=9749
            Right=8968
        $end 'GridRect'
    $end 'CartesianAxisLayoutAttribute'
$end 'SubMapItem'
$begin 'SubMapItem'
    DataSourceID=27
    $begin 'CartesianAxisLayoutAttribute'
        FontScale=1
        $begin 'AxisRect'
            Top=75
            Left=916
            Bottom=882
            Right=8968
        $end 'AxisRect'
        $begin 'GridRect'
            Top=883
            Left=1091
            Bottom=9749
            Right=8968
        $end 'GridRect'
    $end 'CartesianAxisLayoutAttribute'
$end 'SubMapItem'
$end
'MainMapItem'
    $begin 'MainMapItem'
        $begin 'SubMapItem'

```

```

DataSourceID=22
$begin 'OverlayLayoutAttribute'
    $begin 'BoundingRect'
        Top=8736
        Left=2070
        Bottom=9717
        Right=3268
    $end 'BoundingRect'
    ModifySize=false
    ModifyPosition=true
$end 'OverlayLayoutAttribute'

$end 'SubMapItem'
$end
'MainMapItem'
$end
'PlotAttributeStoreMap'
$end 'MapItem'
$end
'PerViewPlotAttributeStoreMap'
    IsViewAttribServer=false
    ViewID=-1
    $begin 'SourceIDMap'
        IDMapItem(334,
0, 19)
$end 'SourceIDMap'
$begin
'MTraceCharacteristicsMgr'
$end
'MTraceCharacteristicsMgr'
$begin
'CartesianXMarkerManager'
    RefMarkerID=-1
$begin
'ReferenceCurves'
$end
'ReferenceCurves'
$end
'CartesianXMarkerManager'
$end
'PlotDisplayDataManager'
    $end 'Report2D'
    $end 'XY Plot 5'
$end 'Reports'
$begin 'ReportsWindowPositions'
    $begin 'XY Plot 1'

```

```

ReportID=327

WindowPositions(Report2D(View(WindowPos(5, -1, -1, -8, -28, 138,
138, 1064, 463))))

    $send 'XY Plot 1'
    $begin 'XY Plot 2'
        ReportID=329

WindowPositions(Report2D(View(WindowPos(5, -1, -1, -8, -28, 46, 46,
949, 378))))

    $send 'XY Plot 2'
    $begin 'XY Plot 3'
        ReportID=331

WindowPositions(Report2D(View(WindowPos(5, -1, -1, -8, -28, 69, 69,
995, 394))))

    $send 'XY Plot 3'
    $begin 'XY Plot 4'
        ReportID=333

WindowPositions(Report2D(View(WindowPos(5, -1, -1, -8, -28, 92, 92,
1018, 417))))

    $send 'XY Plot 4'
    $begin 'XY Plot 5'
        ReportID=335

WindowPositions(Report2D(View(WindowPos(5, -1, -1, -8, -28, 115,
115, 1041, 440))))

    $send 'XY Plot 5'
    $send 'ReportsWindowPositions'
    $send 'ReportSetup'
    $send 'HfssDesignInstance'
    $send 'Instance'
    $send 'DataInstances'
$send 'AnsoftProject'

```

## Appendix C

### Release recipe for the Single pole triple through (SP3T) switch

Pr: pressure, O<sub>2</sub> : Oxygen, ICP: Inductive coupling plasma

1	Pr 12, Read: 10, O2 30, ICP 200, time 15min	15min cool time	run this for 15 min Pressure: 100, O2: 50, RF 0, ICP 0
2	Pr 12, Read: 10, O2 30, ICP 200, time 15min	15min cool time	run this for 15 min Pressure: 100, O2: 50, RF 0, ICP 0
3	Pr 12, Read: 10, O2 30, ICP 200, time 15min	15min cool time	run this for 15 min Pressure: 100, O2: 50, RF 0, ICP 0
4	Pr 12, Read: 10, O2 30, ICP 200, time 15min	15min cool time	run this for 15 min Pressure: 100, O2: 50, RF 0, ICP 0
5	Pr 12, Read: 10, O2 30, ICP 250, time 15min	15min cool time	run this for 15 min Pressure: 100, O2: 50, RF 0, ICP 0
6	Pr 12, Read: 10, O2 30, ICP 250, time 15min	15min cool time	run this for 15 min Pressure: 100, O2: 50, RF 0, ICP 0
7	Pr 12, Read: 10, O2 30, ICP 300, time 15min	15min cool time	run this for 15 min Pressure: 100, O2: 50, RF 0, ICP 0
8	Pr 12, Read: 10, O2 30, ICP 300, time 15min	15min cool time	run this for 15 min Pressure: 100, O2: 50, RF 0, ICP 0
9	Pr 12, Read: 10, O2 30, ICP 300, time 15min	15min cool time	run this for 15 min Pressure: 100, O2: 50, RF 0, ICP 0
10	Pr 12, Read: 10, O2 30, ICP 300, time 15min	15 min cool time	run this for 15 min Pressure: 100, O2: 50, RF 0, ICP 0
11	Pr 12, Read: 10, O2 30, ICP 300, time 15min	15min cool time	run this for 15 min Pressure: 100, O2: 50, RF 0, ICP 0
12	Pr 12, Read: 10, O2 30, ICP 250, time 15min	15min cool time	run this for 15 min Pressure: 100, O2: 50, RF 0, ICP 0
13	Pr 12, Read: 10, O2 30, ICP 300, time 15min	15min cool time	run this for 15 min Pressure: 100, O2: 50, RF 0, ICP 0
14	Pr 12, Read: 10, O2 30, ICP 300, time 15min	15min cool time	run this for 15 min Pressure: 100, O2: 50, RF 0, ICP 0
15	Pr 12, Read: 10, O2 35, ICP 350, time 15min	15min cool time	run this for 15 min Pressure: 100, O2: 50, RF 0, ICP 0
16	Pr 12, Read: 10, O2 35, ICP 350, time 15min	15min cool time	run this for 15 min Pressure: 100, O2: 50, RF 0, ICP 0

## Appendix D

### Program code for microstrip antenna design

```
$begin 'AnsoftProject'
  Product='HFSS'
  NextUniqueID=0
  MoveBackwards=false
  $begin 'Desktop'
    Version(11, 0)
    InfrastructureVersion(1, 0)
  $end 'Desktop'
  $begin 'HFSSEnvironment'
    Version(1, 0)
  $end 'HFSSEnvironment'
  $begin 'geometry3deditor'
    Version(1, 0)
  $end 'geometry3deditor'
  $begin 'ProjectDatasets'
    NextUniqueID=0
    MoveBackwards=false
    DatasetType='ProjectDatasetType'
    $begin 'DatasetDefinitions'
      $end 'DatasetDefinitions'
    $end 'ProjectDatasets'
  $begin 'Definitions'
    $begin 'Folders'
      Definitions(1104, 10000, 1, 1, 0, false, false)
      Materials(1104, 9500, 9, 2, 1, false, false)
    $end 'Folders'
    $begin 'Materials'
      $begin 'vacuum'
        CoordinateSystemType='Cartesian'
        $begin 'AttachedData'
          $end 'AttachedData'
        $begin 'ModifierData'
          $end 'ModifierData'
        permittivity='1'
        ModTime=1028307964
        Library='Materials'
        LibLocation='SysLibrary '
      $end 'vacuum'
      $begin 'gold'
        CoordinateSystemType='Cartesian'
        $begin 'AttachedData'
          $end 'AttachedData'
        $begin 'ModifierData'
          $end 'ModifierData'
        permeability='0.99996'
        conductivity='41000000'
        thermal_conductivity='315'
        mass_density='19300'
        specific_heat='129'
        youngs_modulus='800000000000'
        poissons_ratio='0.4'
        thermal_expansion_coefficient='1.4e-005'
        ModTime=1132068239
        Library='Materials'
        LibLocation='SysLibrary '
```



```

$send 'gold'
$begin 'Al2_O3_ceramic'
    CoordinateSystemType='Cartesian'
    $begin 'AttachedData'
    $send 'AttachedData'
    $begin 'ModifierData'
    $send 'ModifierData'
    permittivity='9.8'
    thermal_conductivity='35'
    mass_density='3960'
    specific_heat='850'
    youngs_modulus='370000000000'
    poissons_ratio='0.22'
    thermal_expansion_coefficient='8.1e-006'
    ModTime=1132068239
    Library='Materials'
    LibLocation='SysLibrary '
$send 'Al2_O3_ceramic'
$begin 'Rogers RT/duroid 5880 (tm)'
    CoordinateSystemType='Cartesian'
    $begin 'AttachedData'
    $send 'AttachedData'
    $begin 'ModifierData'
    $send 'ModifierData'
    permittivity='2.2'
    dielectric_loss_tangent='0.0009'
    ModTime=1028307964
    Library='Materials'
    LibLocation='SysLibrary '
$send 'Rogers RT/duroid 5880 (tm)'
$begin 'air'
    CoordinateSystemType='Cartesian'
    $begin 'AttachedData'
    $send 'AttachedData'
    $begin 'ModifierData'
    $send 'ModifierData'
    permittivity='1.0006'
    permeability='1.0000004'
    thermal_conductivity='0.026'
    mass_density='1.1614'
    specific_heat='1007'
    ModTime=1132068239
    Library='Materials'
    LibLocation='SysLibrary '
    $send 'air'
$send 'Materials'
$begin 'Scripts'
$send 'Scripts'
$send 'Definitions'
DesignIDServer=2
MoveBackwards=false
$begin 'HFSSModel'
    RepRewriteV2=true
    Name='HFSSDesign1'
    DesignID=0
    'Allow Material Override'=false
    SolutionType='DrivenModal'
    MaterialDensity=1

```

```

MassOfTissue=1
$begin 'OutputVariable'
    NextUniqueID=0
    MoveBackwards=false
$end 'OutputVariable'
$begin 'ModelSetup'
    $begin 'Editor3D Doc Preferences'
        'Plane Background'=true
        BackgroundColor1=16777215
        BackgroundColor2=0
        'Need Lights'=true
        'Ambient Light'=8355711
        'Num Lights'=2
        Light0[4: 8289918, 0.200000002980232,
0.400000005960464, 1]
        Light1[4: 8289918, -0.200000002980232, -
0.400000005960464, -1]
    $end 'Editor3D Doc Preferences'
    $begin 'DesignDatasets'
        NextUniqueID=0
        MoveBackwards=false
        DatasetType='DesignDatasetType'
        $begin 'DatasetDefinitions'
            $end 'DatasetDefinitions'
        $end 'DesignDatasets'
        $begin 'Properties'
            VariableProp('subs_length', 'UD', 'substrate
length', '1.129mm')
            VariableProp('subs_height', 'UD', 'substrate
height', '125um')
            VariableProp('wpwidth', 'UD', 'wave port width',
'2mm')
            VariableProp('wpheight', 'UD', 'wave port height',
'900um')
            VariableProp('airboxh', 'UD', 'air box height',
'1800um')
            VariableProp('w', 'UD', 'Patch width', '1.54mm')
            VariableProp('l', 'UD', 'Patch length (it was
1.3133763 mm)', '1.26mm')
            VariableProp('insetl', 'UD', 'Inset length it was
0.702316', '1mm')
            VariableProp('insetw', 'UD', 'Inset width',
'0.395822mm')
            VariableProp('wg', 'UD', 'Ground plane width',
'3.08mm')
            VariableProp('lg', 'UD', 'Ground plane length',
'9.328mm')
            VariableProp('iftw', 'UD',
'inset_feed_test_width_cut', '0.593733mm')
            VariableProp('iftl', 'UD',
'inset_feed_test_length_cut', '0.4mm')
        $end 'Properties'
        SnapMode=2
        GroupByMaterial=true
        GroupSheetByMaterial=false
        $begin 'GeometryCore'
            BlockVersionID=3
            NativeKernel='ACIS'

```

```

NativeKernelVersionID=1
Units='um'
InstanceID=-1
ExternalNativeGeometryAllowed=false
$begin 'ValidationOptions'
    EntityCheckLevel='Strict'
$end 'ValidationOptions'
$begin 'GeometryOperations'
    BlockVersionID=2
    $begin 'AnsoftRangedIDServerManager'
        $begin 'AnsoftRangedIDServer'
            IDServerObjectTypeID=0
            IDServerRangeMin=0
            IDServerRangeMax=2146483647
            NextUniqueID=12303
            MoveBackwards=false
        $end 'AnsoftRangedIDServer'
        $begin 'AnsoftRangedIDServer'
            IDServerObjectTypeID=1
            IDServerRangeMin=2146483648
            IDServerRangeMax=2146485547
            NextUniqueID=2146483654
            MoveBackwards=false
        $end 'AnsoftRangedIDServer'
    $end 'AnsoftRangedIDServerManager'
    StartBackGroundFaceID=2146483648
    $begin 'CoordinateSystems'
    $end 'CoordinateSystems'
    $begin 'ToplevelParts'
        $begin 'GeometryPart'
            $begin 'Attributes'
                Name='wp1'
                Flags=''
                Color='(132 132 193)'
            $end 'Attributes'
        $end 'GeometryPart'
    $end 'ToplevelParts'
    $begin 'Operation'
        PartCoordinateSystem=1
        MaterialName='vacuum'
        SolveInside=true
    $end 'Operation'
$end 'GeometryOperations'

Transparency=0.400000005960464

OperationType='Rectangle'
ID=9279

ReferenceCoordSystemID=1
$begin
'RectangleParameters'
    KernelVersion=1

CoordinateSystemID=-1
XStart='0um'

YStart='354.213856605453um'

ZStart='216.902774953817um'
Width='wpwidth'

```

Height='wpheight'	WhichAxis='X'
'RectangleParameters'	\$end
	ParentPartID=9280
'OperationIdentity'	\$begin
'Topology'	\$begin
	NumLumps=1
NumShells=1	
	NumFaces=0
	NumWires=1
	NumLoops=0
NumCoedges=4	
	NumEdges=4
NumVertices=4	
	\$end 'Topology'
	BodyID=9280
	StartFaceID=-1
	StartEdgeID=9281
StartVertexID=9285	
	NumNewFaces=0
	NumNewEdges=4
	NumNewVertices=4
FaceNameAndIDMap()	
EdgeNameAndIDMap()	
VertexNameAndIDMap()	
'OperationIdentity'	\$end
	\$end 'Operation'
	\$begin 'Operation'
OperationType='CoverLines'	
	ID=9289
'LocalOperationParameters'	\$begin
	KernelVersion=1
CoordinateSystemID=-1	
	LocalOpPart=9280
'LocalOperationParameters'	\$end
	ParentPartID=9280
'OperationIdentity'	\$begin
'Topology'	\$begin
	NumLumps=1

```

NumShells=1
NumFaces=1
NumWires=0
NumLoops=1

NumCoedges=4
NumEdges=4

NumVertices=4
$end 'Topology'
BodyID=-1
StartFaceID=9290
StartEdgeID=-1
StartVertexID=-1
NumNewFaces=1
NumNewEdges=0
NumNewVertices=0

FaceNameAndIDMap()

EdgeNameAndIDMap()

VertexNameAndIDMap()

$begin
'GeomTopolBasedOperationIdentityHelper'
$begin
'NewFaces'

$begin 'Face'

NormalizedSerialNum=0

ID=9290

$begin 'FaceGeomTopol'

FaceTopol(1, 4, 4, 4)

$begin 'FaceGeometry'

Area=1800000

FcUVMid(1.33597859192816e-013, 1354.21385660545,
666.902774953817)

$begin 'FcTolVts'

TolVt(0, 354.213856605453, 216.902774953817, 0)

TolVt(1.22464679914735e-013, 2354.21385660545,
216.902774953817, 0)

TolVt(2.67195718385633e-013, 2354.21385660545,
1116.90277495382, 0)

TolVt(1.44731038470897e-013, 354.213856605453,
1116.90277495382, 0)

```

```

        $end 'FcTolVts'

    $end 'FaceGeometry'

    $end 'FaceGeomTopol'

    $end
'Face'
    $end
'NewFaces'
    $begin
'NewEdges'
    $end
'NewEdges'
    $begin
'NewVertices'
    $end
'NewVertices'
    $end
'GeomTopolBasedOperationIdentityHelper'
    $end
'OperationIdentity'
    $end
    ParentOperationID=9279
    $end 'Operation'
    $begin 'Operation'
        OperationType='Move'
        ID=9505

    ReferenceCoordSystemID=1
    $begin
'TranslateParameters'
        KernelVersion=1

    CoordinateSystemID=-1
        PartID=9280

    TranslateVectorX='1323.27073277155um'
    TranslateVectorY='-1104.31382006404um'
    TranslateVectorZ='-660.152774953817um'
    $end
'TranslateParameters'
    ParentPartID=9280
    $begin
'OperationIdentity'
    $begin
'Topology'
        NumLumps=1

    NumShells=1
        NumFaces=1
        NumWires=0
        NumLoops=1

    NumCoedges=4
        NumEdges=4

```

```

NumVertices=4

FaceNameAndIDMap()

EdgeNameAndIDMap()

VertexNameAndIDMap()

'OperationIdentity'

TransformBaseOperationID=9289

ReferenceCoordSystemID=1

'TranslateParameters'

CoordinateSystemID=-1

TranslateVectorX='3.63797880709171e-012um'

TranslateVectorY='-250.000000000006um'

TranslateVectorZ='0.999999999999802um'

'TranslateParameters'

'OperationIdentity'

'Topology'

NumShells=1

NumCoedges=4

NumVertices=4

$end 'Topology'
BodyID=-1
StartFaceID=-1
StartEdgeID=-1
StartVertexID=-1
NumNewFaces=0
NumNewEdges=0
NumNewVertices=0

$end

$begin 'Operation'
$begin 'Operation'
OperationType='Move'
ID=9806

$begin

KernelVersion=1

PartID=9280

$end

ParentPartID=9280
$begin

$begin

NumLumps=1

NumFaces=1
NumWires=0
NumLoops=1

NumEdges=4

$end 'Topology'
BodyID=-1

```

```

StartFaceID=-1
StartEdgeID=-1
StartVertexID=-1
NumNewFaces=0
NumNewEdges=0
NumNewVertices=0

FaceNameAndIDMap()

EdgeNameAndIDMap()

VertexNameAndIDMap()

$send
'OperationIdentity'

TranformBaseOperationID=9505

$send 'Operation'
$send 'Operations'
$send 'GeometryPart'
$begin 'GeometryPart'
$begin 'Attributes'
Name='Substrate'
Flags=''
Color=(132 132 193)'

Transparency=0.4000000005960464

PartCoordinateSystem=1
MaterialName='Rogers

RT/duroid 5880 (tm)'

SolveInside=true
$send 'Attributes'
$begin 'Operations'
$begin 'Operation'

OperationType='Rectangle'

ID=9446

ReferenceCoordSystemID=1

$begin
'RectangleParameters'

KernelVersion=1

CoordinateSystemID=-1

XStart='-
1981.27640649117um'

YStart='2423.28260944205um'

ZStart='0um'
Width='wg'
Height='lg'
WhichAxis='Z'

$send
'RectangleParameters'

ParentPartID=9447
$begin
'OperationIdentity'

$begin
'Topology'

```



	NumLumps=1
NumShells=1	NumFaces=0
	NumWires=1
	NumLoops=0
NumCoedges=4	
	NumEdges=4
NumVertices=4	
	\$end 'Topology'
	BodyID=9447
	StartFaceID=-1
	StartEdgeID=9448
StartVertexID=9452	
	NumNewFaces=0
	NumNewEdges=4
	NumNewVertices=4
FaceNameAndIDMap()	
EdgeNameAndIDMap()	
VertexNameAndIDMap()	
'OperationIdentity'	\$end
	\$end 'Operation'
	\$begin 'Operation'
OperationType='CoverLines'	
	ID=9456
'LocalOperationParameters'	\$begin
	KernelVersion=1
CoordinateSystemID=-1	
	LocalOpPart=9447
'LocalOperationParameters'	\$end
	ParentPartID=9447
'OperationIdentity'	\$begin
'Topology'	\$begin
	NumLumps=1
NumShells=1	
	NumFaces=1
	NumWires=0
	NumLoops=1
NumCoedges=4	
	NumEdges=4
NumVertices=4	
	\$end 'Topology'

```

BodyID=-1
StartFaceID=9457
StartEdgeID=-1
StartVertexID=-1
NumNewFaces=1
NumNewEdges=0
NumNewVertices=0

FaceNameAndIDMap()

EdgeNameAndIDMap()

VertexNameAndIDMap()

GeomTopolBasedOperationIdentityHelper
$begin
'NewFaces'
$begin 'Face'
NormalizedSerialNum=0
ID=9457
$begin 'FaceGeomTopol'
FaceTopol(1, 4, 4, 4)
$begin 'FaceGeometry'
Area=28730240
FcUVMid(-441.27640649117, 7087.28260944205, 0)
$begin 'FcTolVts'
TolVt(-1981.27640649117, 2423.28260944205, 0, 0)
TolVt(1098.72359350883, 2423.28260944205, 0, 0)
TolVt(1098.72359350883, 11751.2826094421, 0, 0)
TolVt(-1981.27640649117, 11751.2826094421, 0, 0)
$end 'FcTolVts'
$end 'FaceGeometry'
$end 'FaceGeomTopol'
$end
'Face'
$end
'NewFaces'
$begin
'NewEdges'
$end
'NewEdges'

```

```

'NewVertices'
'NewVertices'
'GeomTopolBasedOperationIdentityHelper'
'OperationIdentity'
    ParentOperationID=9446
    OperationType='Rotate'
    ReferenceCoordSystemID=1
'RotateParameters'
    CoordinateSystemID=-1
    RotateAngle='90deg'
'RotateParameters'
'OperationIdentity'
'Topology'
    NumShells=1
    NumCoedges=4
    NumVertices=4
    NumLumps=1
    NumFaces=1
    NumWires=0
    NumLoops=1
    NumEdges=4
    $begin
    $end 'Operation'
    $begin 'Operation'
        ID=9460
    $begin
        KernelVersion=1
        PartID=9447
        RotateAxis='Z'
    $end
    ParentPartID=9447
    $begin
    $begin
        NumLumps=1
        NumFaces=1
        NumWires=0
        NumLoops=1
        NumEdges=4
    $end 'Topology'
    BodyID=-1
    StartFaceID=-1
    StartEdgeID=-1
    StartVertexID=-1
    NumNewFaces=0
    NumNewEdges=0
    NumNewVertices=0
    FaceNameAndIDMap()
    EdgeNameAndIDMap()
    VertexNameAndIDMap()

```

```

                                $end
                                $begin 'DependencyInformation'
                                    NumParents=1

DependencyObject('GeometryBodyOperation', 9289)

DependencyObject('GeometryBodyOperation', 9279)
                                $end 'DependencyInformation'
                                $begin 'DependencyInformation'
                                    NumParents=2

DependencyObject('GeometryBodyOperation', 9505)
                                DependencyObject('CoordinateSystem',
1)

DependencyObject('GeometryBodyOperation', 9289)
                                $end 'DependencyInformation'
                                $begin 'DependencyInformation'
                                    NumParents=2

DependencyObject('GeometryBodyOperation', 9806)
                                DependencyObject('CoordinateSystem',
1)

DependencyObject('GeometryBodyOperation', 9505)
                                $end 'DependencyInformation'
                                $begin 'DependencyInformation'
                                    NumParents=1

DependencyObject('GeometryBodyOperation', 9446)
                                DependencyObject('CoordinateSystem',
1)

                                $end 'DependencyInformation'
                                $begin 'DependencyInformation'
                                    NumParents=1

DependencyObject('GeometryBodyOperation', 9456)

DependencyObject('GeometryBodyOperation', 9446)
                                $end 'DependencyInformation'
                                $begin 'DependencyInformation'
                                    NumParents=2

DependencyObject('GeometryBodyOperation', 9460)
                                DependencyObject('CoordinateSystem',
1)

DependencyObject('GeometryBodyOperation', 9456)
                                $end 'DependencyInformation'
                                $begin 'DependencyInformation'
                                    NumParents=2

DependencyObject('GeometryBodyOperation', 9461)
                                DependencyObject('CoordinateSystem',
1)

DependencyObject('GeometryBodyOperation', 9460)
                                $end 'DependencyInformation'

```

```

                                $begin 'DependencyInformation'
                                NumParents=2

DependencyObject('GeometryBodyOperation', 9462)
                                DependencyObject('CoordinateSystem',
1)

DependencyObject('GeometryBodyOperation', 9461)
                                $send 'DependencyInformation'
                                $begin 'DependencyInformation'
                                NumParents=2

DependencyObject('GeometryBodyOperation', 9537)
                                DependencyObject('CoordinateSystem',
1)

DependencyObject('GeometryBodyOperation', 9462)
                                $send 'DependencyInformation'
                                $begin 'DependencyInformation'
                                NumParents=1

DependencyObject('GeometryBodyOperation', 10953)
                                DependencyObject('CoordinateSystem',
1)

                                $send 'DependencyInformation'
                                $begin 'DependencyInformation'
                                NumParents=1

DependencyObject('GeometryBodyOperation', 10963)

DependencyObject('GeometryBodyOperation', 10953)
                                $send 'DependencyInformation'
                                $begin 'DependencyInformation'
                                NumParents=2

DependencyObject('GeometryBodyOperation', 10965)
                                DependencyObject('CoordinateSystem',
1)

DependencyObject('GeometryBodyOperation', 10963)
                                $send 'DependencyInformation'
                                $begin 'DependencyInformation'
                                NumParents=2

DependencyObject('GeometryBodyOperation', 10984)
                                DependencyObject('CoordinateSystem',
1)

DependencyObject('GeometryBodyOperation', 10965)
                                $send 'DependencyInformation'
                                $begin 'DependencyInformation'
                                NumParents=2

DependencyObject('GeometryBodyOperation', 11420)
                                DependencyObject('CoordinateSystem',
1)

DependencyObject('GeometryBodyOperation', 10984)

```

```

                                $end 'DependencyInformation'
                                $begin 'DependencyInformation'
                                    NumParents=2

DependencyObject('GeometryBodyOperation', 11421)
                                DependencyObject('CoordinateSystem',
1)

DependencyObject('GeometryBodyOperation', 11420)
                                $end 'DependencyInformation'
                                $begin 'DependencyInformation'
                                    NumParents=2

DependencyObject('GeometryBodyOperation', 12302)
                                DependencyObject('CoordinateSystem',
1)

DependencyObject('GeometryBodyOperation', 11421)
                                $end 'DependencyInformation'
                                $begin 'DependencyInformation'
                                    NumParents=1

DependencyObject('GeometryBodyOperation', 11041)
                                DependencyObject('CoordinateSystem',
1)

                                $end 'DependencyInformation'
                                $begin 'DependencyInformation'
                                    NumParents=2

DependencyObject('GeometryBodyOperation', 11417)
                                DependencyObject('CoordinateSystem',
1)

DependencyObject('GeometryBodyOperation', 11041)
                                $end 'DependencyInformation'
                                $begin 'DependencyInformation'
                                    NumParents=2

DependencyObject('GeometryBodyOperation', 11418)
                                DependencyObject('CoordinateSystem',
1)

DependencyObject('GeometryBodyOperation', 11417)
                                $end 'DependencyInformation'
                                $begin 'DependencyInformation'
                                    NumParents=2

DependencyObject('GeometryBodyOperation', 11419)
                                DependencyObject('CoordinateSystem',
1)

DependencyObject('GeometryBodyOperation', 11418)
                                $end 'DependencyInformation'
                                $begin 'DependencyInformation'
                                    NumParents=2

DependencyObject('GeometryBodyOperation', 12301)

```

```

DependencyObject('CoordinateSystem',
1)
DependencyObject('GeometryBodyOperation', 11419)
    $send 'DependencyInformation'
    $begin 'DependencyInformation'
        NumParents=1

DependencyObject('GeometryBodyOperation', 12028)
    DependencyObject('CoordinateSystem',
1)
        $send 'DependencyInformation'
        $begin 'DependencyInformation'
            NumParents=1

DependencyObject('GeometryBodyOperation', 12038)

DependencyObject('GeometryBodyOperation', 12028)
    $send 'DependencyInformation'
    $begin 'DependencyInformation'
        NumParents=2

DependencyObject('GeometryBodyOperation', 12040)

DependencyObject('GeometryBodyOperation', 12038)
    DependencyObject('CoordinateSystem',
1)
        $send 'DependencyInformation'
        $begin 'DependencyInformation'
            NumParents=2

DependencyObject('GeometryBodyOperation', 12058)

DependencyObject('GeometryBodyOperation', 12040)

DependencyObject('GeometryBodyOperation', 12291)
    $send 'DependencyInformation'
    $begin 'DependencyInformation'
        NumParents=2

DependencyObject('GeometryBodyOperation', 12086)

DependencyObject('GeometryBodyOperation', 12058)

DependencyObject('GeometryBodyOperation', 12260)
    $send 'DependencyInformation'
    $begin 'DependencyInformation'
        NumParents=2

DependencyObject('GeometryBodyOperation', 12093)

DependencyObject('GeometryBodyOperation', 12086)
    DependencyObject('CoordinateSystem',
1)
        $send 'DependencyInformation'
        $begin 'DependencyInformation'
            NumParents=2

```

```

DependencyObject('GeometryBodyOperation', 12094)

DependencyObject('GeometryBodyOperation', 12093)
DependencyObject('CoordinateSystem',
1)
    $Send 'DependencyInformation'
    $begin 'DependencyInformation'
        NumParents=2

DependencyObject('GeometryBodyOperation', 12095)

DependencyObject('GeometryBodyOperation', 12094)

DependencyObject('GeometryBodyOperation', 12167)
    $Send 'DependencyInformation'
    $begin 'DependencyInformation'
        NumParents=2

DependencyObject('GeometryBodyOperation', 12293)
DependencyObject('CoordinateSystem',
1)

DependencyObject('GeometryBodyOperation', 12095)
    $Send 'DependencyInformation'
    $begin 'DependencyInformation'
        NumParents=2

DependencyObject('GeometryBodyOperation', 12294)

DependencyObject('GeometryBodyOperation', 12293)

DependencyObject('GeometryBodyOperation', 12021)
    $Send 'DependencyInformation'
    $begin 'DependencyInformation'
        NumParents=1

DependencyObject('GeometryBodyOperation', 11764)
DependencyObject('CoordinateSystem',
1)
    $Send 'DependencyInformation'
    $begin 'DependencyInformation'
        NumParents=1

DependencyObject('GeometryBodyOperation', 11774)

DependencyObject('GeometryBodyOperation', 11764)
    $Send 'DependencyInformation'
    $begin 'DependencyInformation'
        NumParents=2

DependencyObject('GeometryBodyOperation', 11776)

DependencyObject('GeometryBodyOperation', 11774)
DependencyObject('CoordinateSystem',
1)
    $Send 'DependencyInformation'
    $begin 'DependencyInformation'

```



```

                                NumParents=2

DependencyObject('GeometryBodyOperation', 11794)

DependencyObject('GeometryBodyOperation', 11776)

DependencyObject('GeometryBodyOperation', 11891)
                                $Send 'DependencyInformation'
                                $begin 'DependencyInformation'
                                    NumParents=2

DependencyObject('GeometryBodyOperation', 11822)

DependencyObject('GeometryBodyOperation', 11794)

DependencyObject('GeometryBodyOperation', 11860)
                                $Send 'DependencyInformation'
                                $begin 'DependencyInformation'
                                    NumParents=2

DependencyObject('GeometryBodyOperation', 11829)

DependencyObject('GeometryBodyOperation', 11822)
                                DependencyObject('CoordinateSystem',
1)
                                    $Send 'DependencyInformation'
                                    $begin 'DependencyInformation'
                                        NumParents=1

DependencyObject('GeometryBodyOperation', 11830)
                                DependencyObject('CoordinateSystem',
1)
                                    $Send 'DependencyInformation'
                                    $begin 'DependencyInformation'
                                        NumParents=1

DependencyObject('GeometryBodyOperation', 11840)

DependencyObject('GeometryBodyOperation', 11830)
                                $Send 'DependencyInformation'
                                $begin 'DependencyInformation'
                                    NumParents=2

DependencyObject('GeometryBodyOperation', 11842)

DependencyObject('GeometryBodyOperation', 11840)
                                DependencyObject('CoordinateSystem',
1)
                                    $Send 'DependencyInformation'
                                    $begin 'DependencyInformation'
                                        NumParents=2

DependencyObject('GeometryBodyOperation', 11860)

DependencyObject('GeometryBodyOperation', 11842)
                                DependencyObject('CoordinateSystem',
1)
                                    $Send 'DependencyInformation'

```

```

                                $begin 'DependencyInformation'
                                    NumParents=1
DependencyObject('GeometryBodyOperation', 11861)
                                DependencyObject('CoordinateSystem',
1)
                                    $send 'DependencyInformation'
                                    $begin 'DependencyInformation'
                                        NumParents=1

DependencyObject('GeometryBodyOperation', 11871)

DependencyObject('GeometryBodyOperation', 11861)
                                $send 'DependencyInformation'
                                $begin 'DependencyInformation'
                                    NumParents=2

DependencyObject('GeometryBodyOperation', 11873)

DependencyObject('GeometryBodyOperation', 11871)
                                DependencyObject('CoordinateSystem',
1)
                                    $send 'DependencyInformation'
                                    $begin 'DependencyInformation'
                                        NumParents=2

DependencyObject('GeometryBodyOperation', 11891)

DependencyObject('GeometryBodyOperation', 11873)
                                DependencyObject('CoordinateSystem',
1)
                                    $send 'DependencyInformation'
                                    $begin 'DependencyInformation'
                                        NumParents=1

DependencyObject('GeometryBodyOperation', 11892)
                                DependencyObject('CoordinateSystem',
1)
                                    $send 'DependencyInformation'
                                    $begin 'DependencyInformation'
                                        NumParents=1

DependencyObject('GeometryBodyOperation', 11902)

DependencyObject('GeometryBodyOperation', 11892)
                                $send 'DependencyInformation'
                                $begin 'DependencyInformation'
                                    NumParents=2

DependencyObject('GeometryBodyOperation', 11904)

DependencyObject('GeometryBodyOperation', 11902)
                                DependencyObject('CoordinateSystem',
1)
                                    $send 'DependencyInformation'
                                    $begin 'DependencyInformation'
                                        NumParents=2

```

```

DependencyObject('GeometryBodyOperation', 11922)
DependencyObject('GeometryBodyOperation', 11904)
DependencyObject('GeometryBodyOperation', 12019)
    $send 'DependencyInformation'
    $begin 'DependencyInformation'
        NumParents=2
DependencyObject('GeometryBodyOperation', 11950)
DependencyObject('GeometryBodyOperation', 11922)
DependencyObject('GeometryBodyOperation', 11988)
    $send 'DependencyInformation'
    $begin 'DependencyInformation'
        NumParents=2
DependencyObject('GeometryBodyOperation', 11957)
DependencyObject('GeometryBodyOperation', 11950)
    DependencyObject('CoordinateSystem',
1)
        $send 'DependencyInformation'
        $begin 'DependencyInformation'
            NumParents=2
DependencyObject('GeometryBodyOperation', 12020)
    DependencyObject('CoordinateSystem',
1)
DependencyObject('GeometryBodyOperation', 11957)
    $send 'DependencyInformation'
    $begin 'DependencyInformation'
        NumParents=2
DependencyObject('GeometryBodyOperation', 12021)
DependencyObject('GeometryBodyOperation', 12020)
DependencyObject('GeometryBodyOperation', 11829)
    $send 'DependencyInformation'
    $begin 'DependencyInformation'
        NumParents=1
DependencyObject('GeometryBodyOperation', 11958)
    DependencyObject('CoordinateSystem',
1)
        $send 'DependencyInformation'
        $begin 'DependencyInformation'
            NumParents=1
DependencyObject('GeometryBodyOperation', 11968)
DependencyObject('GeometryBodyOperation', 11958)
    $send 'DependencyInformation'
    $begin 'DependencyInformation'

```

```

                                NumParents=2

DependencyObject('GeometryBodyOperation', 11970)

DependencyObject('GeometryBodyOperation', 11968)
                                DependencyObject('CoordinateSystem',
1)
                                $send 'DependencyInformation'
                                $begin 'DependencyInformation'
                                NumParents=2

DependencyObject('GeometryBodyOperation', 11988)

DependencyObject('GeometryBodyOperation', 11970)
                                DependencyObject('CoordinateSystem',
1)
                                $send 'DependencyInformation'
                                $begin 'DependencyInformation'
                                NumParents=1

DependencyObject('GeometryBodyOperation', 11989)
                                DependencyObject('CoordinateSystem',
1)
                                $send 'DependencyInformation'
                                $begin 'DependencyInformation'
                                NumParents=1

DependencyObject('GeometryBodyOperation', 11999)

DependencyObject('GeometryBodyOperation', 11989)
                                $send 'DependencyInformation'
                                $begin 'DependencyInformation'
                                NumParents=2

DependencyObject('GeometryBodyOperation', 12001)

DependencyObject('GeometryBodyOperation', 11999)
                                DependencyObject('CoordinateSystem',
1)
                                $send 'DependencyInformation'
                                $begin 'DependencyInformation'
                                NumParents=2

DependencyObject('GeometryBodyOperation', 12019)

DependencyObject('GeometryBodyOperation', 12001)
                                DependencyObject('CoordinateSystem',
1)
                                $send 'DependencyInformation'
                                $begin 'DependencyInformation'
                                NumParents=1

DependencyObject('GeometryBodyOperation', 12102)
                                DependencyObject('CoordinateSystem',
1)
                                $send 'DependencyInformation'
                                $begin 'DependencyInformation'
                                NumParents=1

```

```

DependencyObject('GeometryBodyOperation', 12112)

DependencyObject('GeometryBodyOperation', 12102)
    $send 'DependencyInformation'
    $begin 'DependencyInformation'
        NumParents=2

DependencyObject('GeometryBodyOperation', 12114)

DependencyObject('GeometryBodyOperation', 12112)
    DependencyObject('CoordinateSystem',
1)
        $send 'DependencyInformation'
        $begin 'DependencyInformation'
            NumParents=2

DependencyObject('GeometryBodyOperation', 12132)

DependencyObject('GeometryBodyOperation', 12114)

DependencyObject('GeometryBodyOperation', 12229)
    $send 'DependencyInformation'
    $begin 'DependencyInformation'
        NumParents=2

DependencyObject('GeometryBodyOperation', 12160)

DependencyObject('GeometryBodyOperation', 12132)

DependencyObject('GeometryBodyOperation', 12198)
    $send 'DependencyInformation'
    $begin 'DependencyInformation'
        NumParents=2

DependencyObject('GeometryBodyOperation', 12167)

DependencyObject('GeometryBodyOperation', 12160)
    DependencyObject('CoordinateSystem',
1)
        $send 'DependencyInformation'
        $begin 'DependencyInformation'
            NumParents=1

DependencyObject('GeometryBodyOperation', 12168)
    DependencyObject('CoordinateSystem',
1)
        $send 'DependencyInformation'
        $begin 'DependencyInformation'
            NumParents=1

DependencyObject('GeometryBodyOperation', 12178)

DependencyObject('GeometryBodyOperation', 12168)
    $send 'DependencyInformation'
    $begin 'DependencyInformation'
        NumParents=2

```

```

DependencyObject('GeometryBodyOperation', 12180)
DependencyObject('GeometryBodyOperation', 12178)
1)      DependencyObject('CoordinateSystem',
          $send 'DependencyInformation'
          $begin 'DependencyInformation'
          NumParents=2

DependencyObject('GeometryBodyOperation', 12198)
DependencyObject('GeometryBodyOperation', 12180)
1)      DependencyObject('CoordinateSystem',
          $send 'DependencyInformation'
          $begin 'DependencyInformation'
          NumParents=1

DependencyObject('GeometryBodyOperation', 12199)
1)      DependencyObject('CoordinateSystem',
          $send 'DependencyInformation'
          $begin 'DependencyInformation'
          NumParents=1

DependencyObject('GeometryBodyOperation', 12209)
DependencyObject('GeometryBodyOperation', 12199)
          $send 'DependencyInformation'
          $begin 'DependencyInformation'
          NumParents=2

DependencyObject('GeometryBodyOperation', 12211)
DependencyObject('GeometryBodyOperation', 12209)
1)      DependencyObject('CoordinateSystem',
          $send 'DependencyInformation'
          $begin 'DependencyInformation'
          NumParents=2

DependencyObject('GeometryBodyOperation', 12229)
DependencyObject('GeometryBodyOperation', 12211)
1)      DependencyObject('CoordinateSystem',
          $send 'DependencyInformation'
          $begin 'DependencyInformation'
          NumParents=1

DependencyObject('GeometryBodyOperation', 12230)
1)      DependencyObject('CoordinateSystem',
          $send 'DependencyInformation'
          $begin 'DependencyInformation'
          NumParents=1

```

```

DependencyObject('GeometryBodyOperation', 12240)

DependencyObject('GeometryBodyOperation', 12230)
    $send 'DependencyInformation'
    $begin 'DependencyInformation'
        NumParents=2

DependencyObject('GeometryBodyOperation', 12242)

DependencyObject('GeometryBodyOperation', 12240)
    DependencyObject('CoordinateSystem',
1)
        $send 'DependencyInformation'
        $begin 'DependencyInformation'
            NumParents=2

DependencyObject('GeometryBodyOperation', 12260)

DependencyObject('GeometryBodyOperation', 12242)
    DependencyObject('CoordinateSystem',
1)
        $send 'DependencyInformation'
        $begin 'DependencyInformation'
            NumParents=1

DependencyObject('GeometryBodyOperation', 12261)
    DependencyObject('CoordinateSystem',
1)
        $send 'DependencyInformation'
        $begin 'DependencyInformation'
            NumParents=1

DependencyObject('GeometryBodyOperation', 12271)

DependencyObject('GeometryBodyOperation', 12261)
    $send 'DependencyInformation'
    $begin 'DependencyInformation'
        NumParents=2

DependencyObject('GeometryBodyOperation', 12273)

DependencyObject('GeometryBodyOperation', 12271)
    DependencyObject('CoordinateSystem',
1)
        $send 'DependencyInformation'
        $begin 'DependencyInformation'
            NumParents=2

DependencyObject('GeometryBodyOperation', 12291)

DependencyObject('GeometryBodyOperation', 12273)
    DependencyObject('CoordinateSystem',
1)
        $send 'DependencyInformation'
        $send 'GeometryDependencies'
        $send 'GeometryCore'
        $begin 'LastUserInputs'

```

```

        $send 'LastUserInputs'
    $send 'ModelSetup'
    $begin 'BoundarySetup'
        $begin 'GlobalBoundData'
            PortImpedance='1'
            GlobalMaterialEnv='vacuum'
        $end 'GlobalBoundData'
        $begin 'Boundaries'
            NextUniqueID=30
            MoveBackwards=false

            $begin 'Solution'
                ID=1644
                Name='LastAdaptive'
                $begin 'SimDataExtractor'
                    SimValue('GainTotal', 1, 90, true,
SimValueID=5776, 0, 0, 2, 0, false, false, 6, 1, 0, 1, 1, '', 0, 0)
                    SimValue('rETotal', 1, 67, false,
SimValueID=5812, 0, 0, 2, 0, false, false, 6, 1, 0, 1, 1, '', 0, 0)
                    SimValue('Mag_E', 1, 90, false,
SimValueID=5813, 3, 0, 2, 0, false, false, -2, 1, 0, 1, 1, '', 0, 0)
                $begin 'Sweeps'
                    $begin 'Sweep'
                        Variable='Freq'
                        Column='77GHz'
                        Units='GHz'
                    $end 'Sweep'
                    $begin 'PostprocessSweep'

Variable='NormalizedDistance'

                        RegularSweep=1
                        Units=''
                        Minimum=0
                        Maximum=1
                        Increment=0.01

CreateIndexedSubsweepFlag=false

                    $send 'PostprocessSweep'
                    $begin 'PostprocessSweep'
                        Variable='Phi'
                        RegularSweep=1
                        Units='deg'
                        Minimum=0
                        Maximum=6.28318530717959

Increment=0.0872664625997165

CreateIndexedSubsweepFlag=false

                    $send 'PostprocessSweep'
                    $begin 'PostprocessSweep'
                        Variable='Theta'
                        RegularSweep=1
                        Units='deg'
                        Minimum=0
                        Maximum=6.28318530717959

Increment=0.0872664625997165

```



```

CreateIndexedSubsweepFlag=false
$send 'PostprocessSweep'
$begin 'PostprocessSweep'
    Variable='Phase'
    RegularSweep=1
    Units='deg'
    Minimum=0
    Maximum=6.28318530717959

Increment=0.0872664625997165

CreateIndexedSubsweepFlag=false
$send 'PostprocessSweep'

$begin 'MainMapItem'
$begin 'SubMapItem'
    DataSourceID=3
    $begin 'OverlayLayoutAttribute'
        $begin 'BoundingRect'
            Top=4850
            Left=963
            Bottom=9850
            Right=8463
        $end 'BoundingRect'
        ModifySize=false
        ModifyPosition=false
    $end 'OverlayLayoutAttribute'
$end 'SubMapItem'
$end 'MainMapItem'

$begin 'MainMapItem'
$begin 'SubMapItem'
    DataSourceID=5
    $begin 'PolarLayoutAttribute'
        FontScale=1
    $begin 'PolarCircleRect'

```

```

        Top=1225
        Left=8368
        Bottom=8774
        Right=819
    $end 'PolarCircleRect'
    $begin 'AxisRect'
        Top=-993693061
        Left=-1005189397
        Bottom=88583552
        Right=-985551698
    $end 'AxisRect'
    $begin 'AxisLabelRect'
        Top=1136801480
        Left=0
        Bottom=460512
        Right=-1526660786
    $end 'AxisLabelRect'
    $end 'PolarLayoutAttribute'
$end 'SubMapItem'
$begin 'SubMapItem'
    DataSourceID=7
    $begin 'PolarLayoutAttribute'
        FontScale=1
    $begin 'PolarCircleRect'
        Top=1225
        Left=8368
        Bottom=8774
        Right=819
    $end 'PolarCircleRect'

```

```

$begin 'AxisRect'
    Top=-993693061
    Left=-1005189397
    Bottom=88583552
    Right=-985551698
$end 'AxisRect'
$begin 'AxisLabelRect'
    Top=1136801480
    Left=0
    Bottom=460512
    Right=-1526660786
$end 'AxisLabelRect'
$end 'PolarLayoutAttribute'
$end 'SubMapItem'
$begin 'SubMapItem'
    DataSourceID=11
    $begin 'PolarLayoutAttribute'
        FontScale=1
        $begin 'PolarCircleRect'
            Top=1225
            Left=8368
            Bottom=8774
            Right=819
        $end 'PolarCircleRect'
        $begin 'AxisRect'
            Top=-993693061
            Left=-1005189397
            Bottom=88583552
            Right=-985551698

```

```

$end 'AxisRect'

$begin 'AxisLabelRect'

    Top=1136801480

    Left=0

    Bottom=460512

    Right=-1526660786

$end 'AxisLabelRect'

$end 'PolarLayoutAttribute'

    $end 'SubMapItem'

'MainMapItem'

$end

'PlotAttributeStoreMap'

$end 'MapItem'

$end 'PerViewPlotAttributeStoreMap'

    IsViewAttribServer=false

    ViewID=-1
    $begin 'SourceIDMap'
        IDMapItem(481,
0, 10)

$end 'SourceIDMap'
$begin

$end

$begin

    RefMarkerID=-1
    $begin

$end

$end

'CartesianXMarkerManager'

$end

$end

$end

    $end 'Report2D'
$end 'Radiation Pattern 1'
$begin 'XY Plot 1'
    ReportID=484
    $begin 'Report2D'
        name='XY Plot 1'
        ReportID=484
        ReportType=3
        DisplayType=1
        Title=''
        Domain=''

```

```

$begin 'Graph2DsV2'
    $begin 'Graph2D'
        TraceDefID=483

        Type='Continuous'

        Axis='Y1'
    $end 'Graph2D'
$end 'Graph2DsV2'
$begin

'PlotDisplayDataManager'

    NextUniqueID=21
    MoveBackwards=false
    $begin

'PlotHeaderDataSource'

    CompanyName='Ansoft Corporation'

    ShowDesignName=true

    ProjectFileName=''

    $end

'PlotHeaderDataSource'

    StockNameIDMap(AxisX=4, AxisY1=5, AxisY2=6, AxisY3=7, AxisY4=8,
Grid=9, Header=0, Legend=2)

    $begin 'SourceList'
    $end 'SourceList'
    $begin

'PlotAttributeStoreMap'

    $begin

'MainMapItem'

    $begin

'SubMapItem'

    DataSourceID=9

    $begin 'CartesianGridDescAttribute'

    ShowXMinor=true

    ShowYMinor=true

    ShowXMajor=true

    ShowYMajor=true

    $end

'CartesianGridDescAttribute'

    $end

'SubMapItem'

    $end

'MainMapItem'

    $begin

'MainMapItem'

    $begin

'SubMapItem'

    DataSourceID=19

```

```

        $begin 'CurveCartesianAttribute'
            YAxis='Y1'
                                                    $end
        'CurveCartesianAttribute'
                                                    $end
        'SubMapItem'
                                                    $end
        'MainMapItem'
                                                    $begin
        'MainMapItem'
                                                    $begin
        'SubMapItem'
            DataSourceID=19
            $begin 'CurveRenderAttribute'
            $begin 'LineRenderAttribute'
                LineStyle='Solid'
                LineWidth=2
                LineColor(R=255, G=0, B=0)
            $end 'LineRenderAttribute'
            TraceType='Continuous'
            SymbolType='HorizontalLeftTriangle'
            SymbolColor(R=0, G=25, B=185)
            ShowSymbols=false
            SymbolFrequency=15
            ShowArrows=false
                                                    $end
        'CurveRenderAttribute'
                                                    $end
        'SubMapItem'
                                                    $end
        'MainMapItem'
                                                    $begin
        'MainMapItem'
                                                    $begin
                                                    $begin
        'PerViewPlotAttributeStoreMap'
                                                    $begin 'MapItem'
                                                    $begin
        'PlotAttributeStoreMap'
            $begin 'MainMapItem'
            $begin 'SubMapItem'

```

```

DataSourceID=1

$begin 'BasicLayoutAttribute'
    $begin 'LayoutRect'
        Top=809
        Left=702
        Bottom=9718
        Right=9256
    $end 'LayoutRect'
$end 'BasicLayoutAttribute'

$end 'SubMapItem'

$begin 'SubMapItem'
    DataSourceID=10
    $begin 'BasicLayoutAttribute'
        $begin 'LayoutRect'
            Top=809
            Left=702
            Bottom=9718
            Right=9256
        $end 'LayoutRect'
    $end 'BasicLayoutAttribute'
$end 'SubMapItem'

$begin 'SubMapItem'
    DataSourceID=17
    $begin 'BasicLayoutAttribute'
        $begin 'LayoutRect'
            Top=75
            Left=75
            Bottom=9925
            Right=594

```

```

        $end 'LayoutRect'

        $end 'BasicLayoutAttribute'

    $end 'SubMapItem'

'MainMapItem'
    $begin 'MainMapItem'
        $begin 'SubMapItem'
            DataSourceID=13

            $begin 'CartesianAxisLayoutAttribute'
                FontScale=1
                $begin 'AxisRect'
                    Top=75
                    Left=9256
                    Bottom=9925
                    Right=9925
                $end 'AxisRect'
                $begin 'GridRect'
                    Top=809
                    Left=702
                    Bottom=9718
                    Right=9256
                $end 'GridRect'
            $end 'CartesianAxisLayoutAttribute'
        $end 'SubMapItem'
        $begin 'SubMapItem'
            DataSourceID=14

            $begin 'CartesianAxisLayoutAttribute'
                FontScale=1
                $begin 'AxisRect'
                    Top=75

```



```

        Left=594
        Bottom=808
        Right=9256
    $end 'AxisRect'
    $begin 'GridRect'
        Top=809
        Left=702
        Bottom=9718
        Right=9256
    $end 'GridRect'
    $end 'CartesianAxisLayoutAttribute'
    $end 'SubMapItem'
'MainMapItem'
    $begin 'MainMapItem'
    $begin 'SubMapItem'
        DataSourceID=3
        $begin 'OverlayLayoutAttribute'
            $begin 'BoundingRect'
                Top=4850
                Left=669
                Bottom=9850
                Right=8169
            $end 'BoundingRect'
            ModifySize=false
            ModifyPosition=false
        $end 'OverlayLayoutAttribute'
    $end 'SubMapItem'
'MainMapItem'
'PlotAttributeStoreMap'

```

```

                                $Send 'MapItem'
                                $Send
'PerViewPlotAttributeStoreMap'
                                $Send
                                $Send 'SourceIDMap'
                                $begin 'SourceIDMap'
                                IDMapItem(483,
0, 19)
                                $Send 'SourceIDMap'
                                $begin
'TraceCharacteristicsMgr'
                                $Send
'TraceCharacteristicsMgr'
                                $begin
'CartesianXMarkerManager'
                                $begin
                                RefMarkerID=-1
                                $begin
'ReferenceCurves'
                                $Send
'ReferenceCurves'
                                $Send
'CartesianXMarkerManager'
                                $Send
'PlotDisplayDataManager'
                                $Send
                                $Send 'Report2D'
                                $Send 'XY Plot 1'
                                $Send 'Reports'
                                $begin 'ReportsWindowPositions'
                                $begin 'Radiation Pattern 1'
                                ReportID=482
                                WindowPositions(Report2D(View(WindowPos(5, -1, -1, -8, -28, 92, 92,
995, 427))))
                                $Send 'Radiation Pattern 1'
                                $begin 'XY Plot 1'
                                ReportID=484
                                WindowPositions(Report2D(View(WindowPos(3, -1, -1, -8, -28, 23, 23,
949, 351))))
                                $Send 'XY Plot 1'
                                $Send 'ReportsWindowPositions'
                                $Send 'ReportSetup'
                                $Send 'HfssDesignInstance'
                                $Send 'Instance'
                                $Send 'DataInstances'
$Send 'AnsoftProject'

```

---

## **VITA AUCTORIS**

---

Ahmad Sinjari was born in 1964 in Sinjar, Iraq. He completed his bachelor degree in Electrical Engineering from the University of Salahuddin, Iraq in 1987, and master in Electrical Engineering from University of Mosul, Iraq in 1993, had experience in University teaching of 5 years and automotive industry of 10 years in different positions in North America, got his own company in automation. His research interest includes microprocessor hardware, PLC and Microelectromechanical Systems (MEMS). At the time of writing this thesis Ahmad is a member of the MEMS Lab, and a candidate for the degree of Ph.D. in Electrical and Computer Engineering, at the University of Windsor (Ontario, Canada).